

# CONCRETE STRUCTURES

ANNUAL TECHNICAL JOURNAL

Károly Péter Juhász

**EFFECTS OF POURING TECHNIQUE ON ORIENTATION OF STEEL AND SYNTHETIC MACROFIBRES IN FIBRE REINFORCED CONCRETE**

2

Ahmed Maher Seyam - Samir Shihada - Rita Nemes

**EFFECTS OF POLYPROPYLENE FIBERS ON ULTRA HIGH PERFORMANCE CONCRETE AT ELEVATED TEMPERATURE**

11

Andor Windisch, PhD

**STEEL STRESS PATTERNS BETWEEN TWO PRIMARY CRACKS IN CONCRETE**

DEDICATED TO THE MEMORY OF PROF. GALLUS REHM (1924-2020)

17

Suha Ismail Ahmed Ali - Éva Lublóy

**RADIATION SHIELDING STRUCTURES: CONCEPTS, BEHAVIOUR AND THE ROLE OF THE HEAVY-WEIGHT CONCRETE AS A SHIELDING MATERIAL - REVIEW**

24

Ali Abdulhasan Khalaf - Katalin Kopecskó

**PROPOSED SIMPLIFIED METHOD OF GEOPOLYMER CONCRETE MIX DESIGN**

31

**FIB BULLETINS 91, 92, 93, 94, 95, 96**

38



# 2020

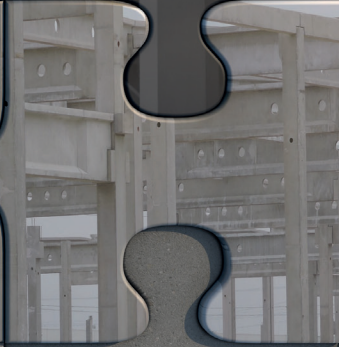
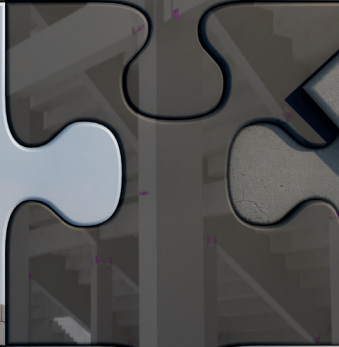
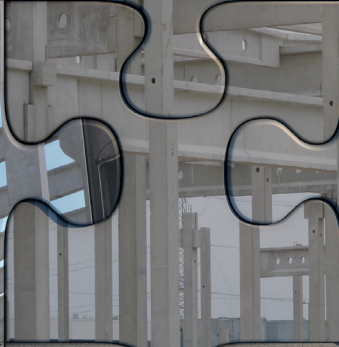
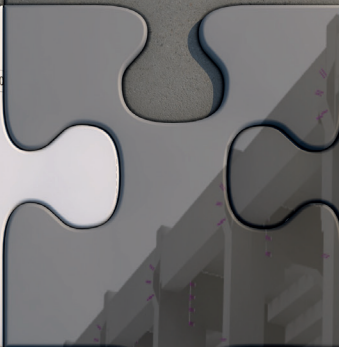
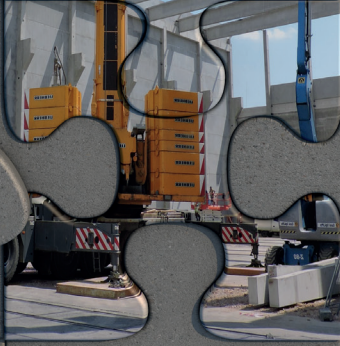
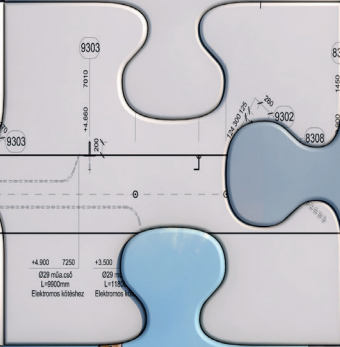
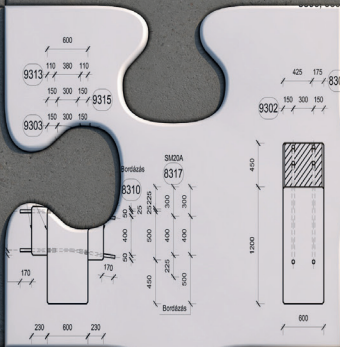
Vol. 21



# FERROBETON

A CRH COMPANY

safe basis provided by concrete



[www.ferrobeton.hu](http://www.ferrobeton.hu)

**Editor-in-chief:**

Prof. György L. Balázs

**Editors:**

Prof. Géza Tassi

Dr. Herbert Träger

**Editorial Board:**

János Barta

Dr. Béla Csíki

Dr. Olivér Czoboly

Assoc. Prof. Attila Erdélyi

Prof. György Farkas

Gyula Kolozsi

Assoc. Prof. Katalin Kopecskó

Assoc. Prof. Kálmán Koris

Assoc. Prof. Imre Kovács

Dr. Károly Kovács

Assoc. Prof. Tamás Kovács

Ervin Lakatos

Assoc. Prof. Éva Lublók

László Mátyássy

Assoc. Prof. Balázs Móczár

Assoc. Prof. Salem G. Nehme

Assoc. Prof. Zoltán Orbán

Zsuzsa Pisch

László Polgár

Assoc. Prof. István Sajtos

Antonia Teleki

Dr. László Tóth\*

Attila Várdai

Assoc. Prof. István Völgyi

József Vörös

**Board of Reviewers:**

Prof. Endre Dulácska

Antónia Királyföldi

Dr. Miklós Loykó

Botond Madaras

Dr. Gábor Madaras

Prof. Árpád Orosz

Prof. Robert Ratay

Prof. Kálmán Szalai

Dr. Ernő Tóth

Founded by: Hungarian Group of *fib*

Publisher: Hungarian Group of *fib*

(*fib* = International Federation for  
Structural Concrete)

**Editorial office:**

Budapest University of Technology

and Economics (BME)

Department of Construction Materials

and Engineering Geology

Műegyetem rkp. 3., H-1111 Budapest

Phone: +36-1-463 4068

Fax: +36-1-463 3450

WEB <http://www.fib.bme.hu>

WEB editor: András Bíró

Layout and print: Csaba Halmai,  
Navigar Ltd.

Price: 10 EUR, Printed in 1000 copies

© Hungarian Group of *fib*

HU ISSN 2062-7904

online ISSN: 1586-0361

Cover photo: The Transamerica Pyramid

- the tallest building in San Francisco

Photo by György L. Balázs

# CONTENT

- 2** Károly Péter Juhász  
**EFFECTS OF POURING TECHNIQUE ON  
ORIENTATION OF STEEL AND SYNTHETIC  
MACROFIBRES IN FIBRE-REINFORCED CONCRETE**
- 11** Ahmed Maher Seyam - Samir Shihada - Rita Nemes  
**EFFECTS OF POLYPROPYLENE FIBERS ON ULTRA  
HIGH PERFORMANCE CONCRETE AT ELEVATED  
TEMPERATURE**
- 17** Andor Windisch, PhD  
**STEEL STRESS PATTERNS BETWEEN  
TWO PRIMARY CRACKS IN CONCRETE**  
DEDICATED TO THE MEMORY OF PROF. GALLUS REHM (1924-2020)
- 24** Suha Ismail Ahmed Ali - Éva Lublók  
**RADIATION SHIELDING STRUCTURES: CONCEPTS,  
BEHAVIOUR AND THE ROLE OF THE HEAVY-  
WEIGHT CONCRETE AS A SHIELDING MATERIAL -  
REVIEW**
- 31** Ali Abdulhasan Khalaf - Katalin Kopecskó  
**PROPOSED SIMPLIFIED METHOD OF GEOPOLYMER  
CONCRETE MIX DESIGN**
- 38** **FIB BULLETINS 91**  
Floating concrete structures
- 38** **FIB BULLETINS 92**  
Serviceability Limit State of Concrete Structures
- 38** **FIB BULLETINS 93**  
Birth Certificate and Through-Life Management Documentation
- 39** **FIB BULLETINS 94**  
Precast concrete bridge continuity over piers
- 39** **FIB BULLETINS 95**  
Fibre Reinforced Concrete: From Design to Structural  
Applications
- 40** **FIB BULLETINS 96**  
Guidelines for Submerged Floating Tube Bridges

Sponsors:

Railway Bridges Foundation, ÉMI Nonprofit Ltd., HÍDÉPÍTŐ Co., Holcim Hungary Co.,  
MÁV Co., MSC Consulting Co., Lábatlani Vasbetonipari Co., Pont-*TERV* Co.,  
UVATERV Co., MÉLYÉPTEK KOMPLEX Engineering Co.,  
SW Umwelttechnik Hungary Ltd., Betonmix Consulting Ltd., BVM Épelem Ltd.,  
CAEC Ltd., Pannon Freyssinet Ltd., STABIL PLAN Ltd., UNION PLAN Ltd.,  
DCB Consulting Ltd., BME Dept. of Structural Engineering,  
BME Dept. of Construction Materials and Technologies

# EFFECTS OF POURING TECHNIQUE ON ORIENTATION OF STEEL AND SYNTHETIC MACROFIBRES IN FIBRE-REINFORCED CONCRETE



Károly Péter Juhász

<https://doi.org/10.32970/CS.2020.1.1>

*Fibre-reinforced concrete is a short-fibre composite material, whose properties are significantly dependent on the orientation of the mixed fibres. As a starting point, the fibres are assumed to be uniformly distributed and have a uniform orientation. However, in reality, they have a non-uniform distribution owing to various factors. Such deviations in the orientation may have a significant effect on the material parameters, both favourable and unfavourable. In this study, the orientation factors determined based on the mixing models reported in the literature are compared with the results of experimental tests performed in the laboratory, and the effects of the formwork and the pouring methods used on the orientation of both steel and synthetic macrofibres are investigated. Based on the results of the study, the orientation of the fibres (both, steel and macro synthetic) significantly depends on the pouring method, which considerably influences the material parameters of fibre-reinforced concrete.*

**Keywords:** fibre reinforced concrete, mixing model, steel fibre, synthetic macro fibre

## 1. INTRODUCTION

Fibres mixed in concrete, which is a quasibrittle material, can improve several properties such as the fracture energy and ductility, which must be taken into account during the design stage (Gopalaratnam et al., 1991; Balaguru and Shah, 1992). The residual flexural strength of materials is measured using the three-point or four-point bending beam test, such as the EN 14651 (EN 14651, 2007) or ASTM C-1609 test (ASTM C-1609, 2019), respectively. The size and cross-section of the beam used depends on the standard employed. However, the most common cross-sectional dimensions are  $150 \times 150 \text{ mm}^2$ . The residual flexural strength primarily depends on the number and locations of the fibres on the crack surfaces. However, other factors, such as the fibre content (i.e., number of fibres added), geometry of the fibres, and the homogeneity of the mix also have an effect. The number of fibres intersecting the cross-section is a key parameter. Romualdi and Mandel (1964) and later Naaman (1972) proposed expressions for determining this number while Krenchel (1975) introduced the orientation factor to characterize the fibre orientation. Assuming ideal mixing, the orientation factor should be 0.5 (Stroeven, 1978).

However, several factors can affect the fibre orientation, and the most important one is probably the wall effect. There have been several studies on the determination of the factors that affect the fibre orientation, including the wall effect (Kameswara Rao, 1979; Stroeven 1991, 1999; Soroushian and Lee, 1990; Hoy, 1998; Kooiman, 2000; Dupont and Vandewalle, 2005; Lee, Cho and Vecchio, 2011; Ng, Foster and Htut, 2012). During the vibration and compaction of

concrete, the fibre orientation will change (Soroushian and Lee, 1990; Edgington and Hannant, 1972; Stroeven, 1979; Toutanji and Bayasi, 1998; Stahli, Custer, and van Mier, 2008). Zerbino et al. (2012) investigated the orientation of steel fibres in self-compacted concrete elements, such as slabs, walls, and beams, and so did Sarmiento et al. (2012), who compared the results of numerical calculations with those of tests performed on fibre-reinforced concrete (FRC) beams. The wall effect in the case of synthetic macrofibres is different from that for steel fibres because of their higher stiffness; steel fibers rotate when they come into contact with the wall while synthetic ones bend. In contrast, Oh, Kim, and Choi (2007) did not take this effect into account in their model, while Alberti (2017) and Juhász (2018a, 2018b) suggested a method for considering it during modelling.

Because of these effects, the orientation of the fibres will not be uniform. Thus, the number of fibres that intersect the cross-section will also change. In the case of beam tests performed on a relatively small cross-sectional reference area, the residual flexural strength will exhibit a wide distribution, owing to which the values of the designed and actual parameters will be lower than required (Bernard, 2013). This can lead to exaggerated safety assessment results and uneconomical designs. Thus, the number of fibres intersecting the cross-section is an important parameter that must be determined with precision. However, few standards and guidelines exist on how to do so (Juhász, 2019).

The Italian CNR-DT guidelines (2006) consider the orientation in their introduction, drawing attention to the fact that the orientation of the fibres depends primarily on the pouring method used and has a determining effect on

the properties of the concrete. However, they do not take it into account while evaluating the material parameters. In contrast, the RILEM TC-162 (Vandewalle et al., 2003) guidelines do not consider the orientation at all. On the other hand, the Austrian ÖVBB Richtlinie Faserbeton guidelines (2008) for hybrid materials (FRC with conventional steel bar reinforcement) and slab-type elements (those with  $b > 5h$  and  $bh > 1.0 \text{ m}^2$ , where  $b$  is the width and  $h$  is the height of the elements) suggest that the residual flexural strength increases by a factor of  $\eta = 1.4$ . The reason for this increase is not discussed. However, based on the geometrical parameters, it is likely that this increase is due to the fibre orientation. Section 6.5.7 of the fib Model Code (2013) is devoted to the effects of the fibre orientation. Factor  $K$  is defined as the orientation factor, and its value is 1.0 in general. The code also states that whether the orientation of the fibres is uniform or not must be verified experimentally. If the orientation is favourable, its effects may be taken into consideration; in case of unfavourable orientation, the orientation factor must be applied in the calculation. However, no methods for doing so are suggested.

In this paper, the various analytical mixing models and the corresponding orientation factors reported in the literature are reviewed. The effects of these orientation factors are compared with the results of experimental tests. These tests were performed on FRC beams produced using different pouring techniques and different types of fibres (steel and synthetic macrofibres), and the number of fibres intersecting the cross-section and the corresponding orientation factors are determined. Finally, the effects of the different pouring methods are compared based on the results of numerical calculations and experimental tests.

## 2. ANALYTICAL MIXING MODELS

The number of fibres that intersect the unit-area cross-section is the basis for most material models that consider the fibres discretely. These models include the variable engagement model (Voo and Foster, 2003), the diverse embedment model (Lee, Cho, and Vecchio, 2011), the simplified diverse embedment model (Lee, Cho, and Vecchio, 2013), and the hybrid diverse embedment model (Chasioti, 2017). The orientation of the fibres is also a relevant parameter for evaluating experimental results. On the one hand, the quality of the mixing can be determined based on the fibre orientation (Dupont and Vandewalle, 2005), while on the other hand, the effect of the nonuniform distribution of the fibres on crack formation in the cross-section can also be considered (Juhász, 2013; Juhász, 2015). Numerous studies have examined the impact of mixing on the experimental results in the case of different types of elements (Zerbino et al., 2012; Sarmiento et al., 2012).

### 2.1. Method proposed by Romualdi and Mandel (1964)

Fibres parallel or nearly parallel to the tensile stress are effective in controlling cracks. Thus, corrections must be made for the fibres that are not oriented as desired. Romualdi and Mandel (1964) assumed that the ratio of the average of the projected lengths in a given direction to the total length is a suitable correction measure. The projection of a fibre in the  $x$ -direction such that the origin is the midpoint of the fibre and

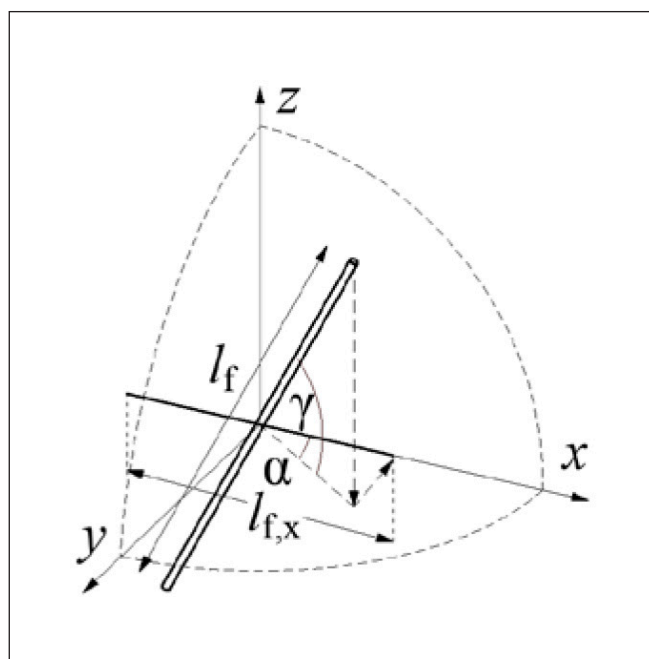


**Fig. 1:** Determining spatial distribution of fibres using polar coordinates  $\alpha$  and  $\gamma$

the orientation is defined using polar coordinates  $\alpha$  and  $\gamma$  can be given as follows:

$$l_{f,x} = l_f \cos \alpha \cos \gamma \quad (1)$$

where  $l_f$  is the length of the fibre and  $\alpha$  and  $\gamma$  are the polar coordinates, as shown in Fig. 1.

Based on this, if a midpoint and length  $l_f$  as projected on the  $x$ -axis are given, along with a uniform distribution of  $\alpha$  and  $\gamma$ , the average length of the fibres will be given by

$$l_{f,x,m,l} = \frac{\int_0^{\frac{\pi}{2}} \int_0^{\frac{\pi}{2}} l_f \cos \alpha \cos \gamma d\alpha d\gamma}{\left(\frac{\pi}{2}\right)^2} = 0.405 l_f \quad (2)$$

Romualdi and Mandel derived the number of fibres intersecting the unit-area cross-section from the average distance of the midpoints of the fibres, as follows:

$$n = \frac{l_{f,x,m,l} N}{V} = 0.405 l_f \frac{N}{V} \quad (3)$$

where  $n$  is the number of fibres intersecting the unit-area cross section [ $\text{m}^2$ ] and  $N$  is the total number of fibres in volume  $V$ .

### 2.2. Method proposed by Naaman (1972)

Naaman (1972) determined the number of fibres intersecting the cross-section based on a probability analysis. Consider a fibre whose midpoint lies on the  $x$ -axis (Fig. 2):

If the midpoint of the fibre is located at a distance smaller than  $0.5l_f$  then the fibre will intersect the crack plane. The probability of this is the quotient of the surface areas of spherical cap  $S_1$  and half-sphere  $S$  drawn around the midpoint

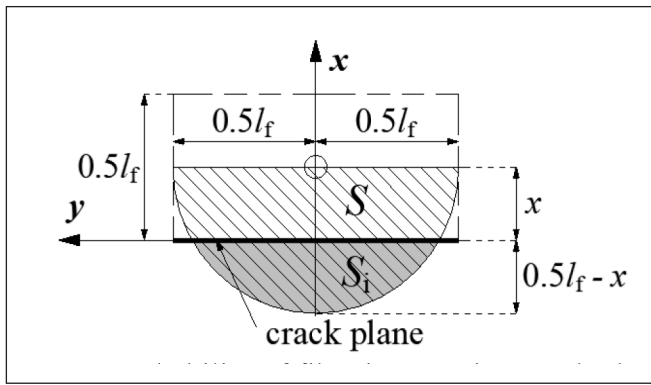


**Fig. 2:** Probability of fibre intersecting crack plane

of the fibre, as shown in *Fig. 2*.

$$q_{\text{Naaman}} = \frac{S_i}{S} = \frac{0.5l_f - x}{0.5l_f} = 1 - \frac{2x}{l_f} \quad (4)$$

Considering the unit volume on both sides of the crack plane, the number of fibres intersecting the unit-area cross-section will be similar to that obtained using the expression for a uniform distribution in a sphere (Eq. 3):

$$n = 2 \int_0^{\frac{l_f}{2}} \left(1 - \frac{2x}{l_f}\right) \frac{N}{V} dx = \frac{N}{V} 2 \int_0^{\frac{l_f}{2}} \left(1 - \frac{2x}{l_f}\right) dx = \frac{N}{V} 0.5l_f \quad (5)$$

### 2.3. Orientation factor proposed by Krenchel (1975)

Let us assume that, in the ideal state, each fibre is perpendicular to the crack plane. Then, in the current case, each fibre will be aligned along the  $x$ -axis. Based on the volume fraction of the fibres,  $V_p$  which is the weight of the fibres in concrete [kg/m<sup>3</sup>] divided by the bulk density of the fibres [kg/m<sup>3</sup>], and the cross-sectional area of a single fibre,  $A_f$ , the number of fibres intersecting cross-section  $A$  can be determined as:

$$n_i = \frac{V_f}{A_f} A \quad (6)$$

where  $n_i$  [-] represents the ideal number of fibres in cross-section  $A$ .

Given that the orientation of the fibres would not be perpendicular to the crack plane in reality, Krenchel (1975) introduced the orientation factor:

$$\theta_{\text{Krenchel}} = \frac{n_a}{n_i} = n_a \frac{A_f}{V_f A} \quad (7)$$

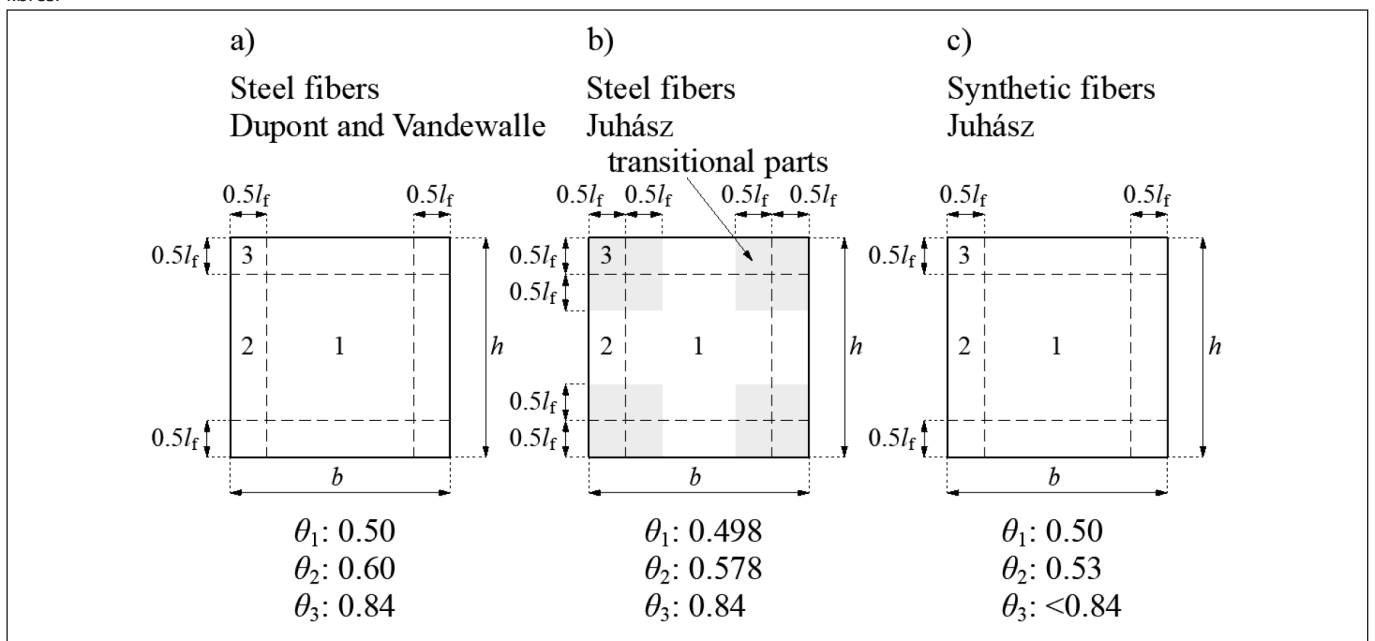
where  $n_a$  is the number [pc] of fibres intersecting cross-section  $A$ , as determined experimentally by counting the fibres in a cracked surface or sliced section.

Thus, it can be seen that the orientation factor proposed by Krenchel (1975) is similar to the factor for modifying the fibre length used by Romualdi and Mandel (1964) and Naaman (1972), whose value is 0.5 in case the fibre distribution is uniform (Stroeven, 1978).

### 2.4. Orientation factors suggested by Dupont and Vandewalle and proposed model

Dupont and Vandewalle (2005) used the cross-section dimensions recommended in RILEM TC-162 (Vandewalle et al., 2003) and investigated the influence of the wall effect on the orientation factors herein. They divided the cross-section of a beam into three zones in order to consider the effects of the formwork used: 1: undisturbed zone, 2: disturbed zone—one side of the mould, and 3: disturbed zone—two sides of the mould (corner) (Figure 3a). Steel fibres are rigid and thus would rotate when they come into contact with the formwork. The orientation factors proposed by Dupont and Vandewalle were subsequently modified by Juhász (2018b), who took into account the differences between rigid (steel) and flexible (synthetic) fibres. The different orientation factors are shown in *Fig. 3*.

**Fig. 3:** Cross-section zones and orientation factors proposed by (a) Dupont and Vandewalle for steel fibres and Juhász for (b) steel and (c) synthetic fibres.



The orientation factor for the entire cross-section can be calculated from the weighted mean:

$$\theta_T = \sum_{i=1}^n \frac{A_i}{A} \theta_i \quad (8)$$

where  $\theta_T$  is the orientation factor of the entire cross-section,  $A_i$  is the area of cross-section zone  $i$ ,  $A$  is the area of the entire cross-section, and  $\theta_i$  is the orientation factor of zone  $i$ .

In the rest of the study, the orientation factors proposed by Juhász (2018b) for steel and synthetic fibres (see Figures 3(b) and (c)) are used.

### 3. LABORATORY TESTS

FRC beams with steel and synthetic macrofibres were produced using different pouring techniques. The contents of the two types of fibers were kept the same to allow for a comparison of the numbers of fibres intersecting the beam cross-sections. In the case of a high steel fibre content, the fibres would have a significant effect on each other's movement; this, in turn, would affect their orientation as well (Juhász, 2018b; Kang et al., 2011; Czoboly, 2016). Thus, their content was limited to  $\sim 30 \text{ kg/m}^3$ . The composition of the concrete mix is listed in Table 1, while the fibre types used and their properties are listed in Table 2. The water/cement ratio was kept at 0.5, and the consistency of the concrete was F5.

**Table 1:** Composition of concrete mix

Component	Quantity (kg/m <sup>3</sup> )
Aggregate (4–8 mm)	629
Sand (0–4)	997
Microsilica	40
Cement (CEM I 42,5 R)	400
Water	200
Superplasticizer (Mapei SR1)	3

**Table 2:** Material properties of fibres used

Property	Steel fibres (ST)	Synthetic fibres (SY)
Base material	Steel	Polypropylene
Tensile strength [MPa]	700	550
Elastic modulus [GPa]	200	10
Diameter/length [mm]	1/50	0.7/48
Anchorage	Hooked end	Continuous embossing
Fibres/kg	3 181	35 714
Content [kg/m <sup>3</sup> ]	33.73	3
Content [fibre/m <sup>3</sup> ]	107 346	107 346

The dimensions of the beams were  $150 \times 150 \times 1000 \text{ mm}^3$ , and they were produced using two different pouring methods. The first method (P1) was the one recommended in RILEM TC-162 (Vandewalle et al., 2003), while in the case of the second method (P2), the formwork was tilted at an angle of  $45^\circ$  during pouring and then set in the vertical position until the concrete had hardened. In addition, for the two pouring methods, the flow directions of the poured concrete were also different. For P1, it was perpendicular to the longitudinal axis of the beam while for P2, it was parallel to the axis. The two flow directions are denoted by arrows in Fig. 4. The formworks used were made from plastic-covered plywood, and form

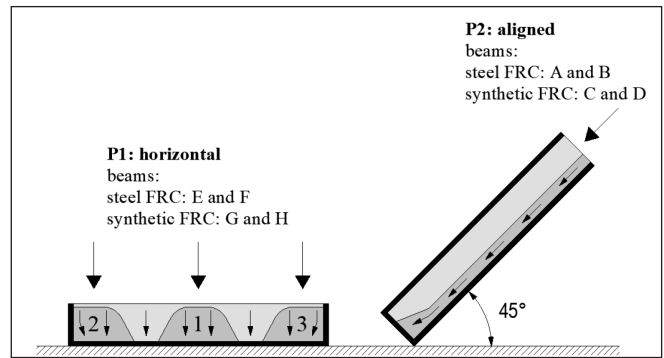


**Fig. 4:** Pouring methods P1 (formwork was horizontal) and P2 (formwork was inclined).

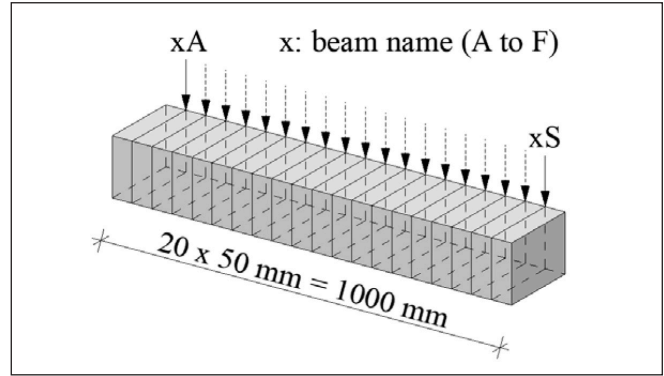


**Fig. 5:** Investigated cross-sections.

oil was applied prior to pouring of the concrete. In the case of pouring method P1, the formwork was open on one side along its length, while in the case of P2, the formwork was open at the endplate. After the pouring process, there was no need to subject the formworks to vibrations for compaction.

After the hardening of the concrete, the beams were cut into 50-mm slices, as shown in Fig. 5, and their surfaces were investigated.

Fibres could be seen intersecting the cross-sections in the case of all the beams. As stated previously, the cross-sections were divided into different zones (see Fig. 3), and the numbers of intersecting fibres in these zones were determined. The research matrix is shown in Table 3. A typical cross-section of a steel-fibre-reinforced concrete beam is shown in Fig. 6.

**Table 3:** Research matrix

Fibre type	Pouring method	Beam label	Section labels
Steel	(P1) Horizontal	E, F	EA...ES; FA...FS
Steel	(P2) Inclined	A, B	AA...AS; BA...BS
Synthetic macrofibres	(P1) Horizontal	G, H	GA...GS; HA...HS
Synthetic macrofibres	(P2) Inclined	C, D	CA...CS; DA...DS

### 4. RESULTS

The results of the statistical analysis are listed in Table 4. During the analysis, the mean value of the number of intersecting fibres, its standard deviation, and coefficient of variation (CV) were determined. Then, the sample averages were analysed using Tukey's biweight M-estimator and the Shapiro-Wilk normality test in order to determine whether the data were normally distributed.

The histograms of the numbers of fibres intersecting the

**Table 4:** Results of statistical analysis

Sample name	Mean value	SD	CV (%)	M-estimator <sup>1</sup>	Normality <sup>2</sup>
P1-ST-Z1	33.526	15.485	46.19	29.264	0.011
P1-ST-Z2	31.894	10.159	31.85	31.526	<b>0.673</b>
P1-ST-Z3	5.907	2.683	45.42	5.484	<b>0.097</b>
P1-ST-TOT	71.328	23.102	32.39	67.756	0.045
P2-ST-Z1	24.842	11.117	44.75	21.052	0.000
P2-ST-Z2	18.618	8.306	44.62	16.763	0.003
P2-ST-Z3	3.407	1.930	56.65	3.281	<b>0.149</b>
P2-ST-TOT	46.868	16.542	35.29	40.515	0.001
P1-SY-Z1	37.157	8.958	24.11	35.859	0.033
P1-SY-Z2	32.671	6.237	19.09	34.310	0.02
P1-SY-Z3	8.000	4.170	52.13	6.875	0.001
P1-SY-TOT	77.828	11.493	14.77	76.661	<b>0.211</b>
P2-SY-Z1	16.657	7.213	43.30	16.035	<b>0.27</b>
P2-SY-Z2	23.921	6.085	25.44	23.613	<b>0.96</b>
P2-SY-Z3	6.263	2.409	38.48	6.059	<b>0.534</b>
P2-SY-TOT	46.842	11.336	24.20	47.194	<b>0.309</b>

1: Tukey's biweight M-estimator

2: Shapiro-Wilk test of normality (null hypothesis accepted if  $p > 0.05$ ; shown in bold)**Table 5:** Comparison of test and analytical results

Steel FRC beams						
Pouring method	Zone	Test		Analytical		
		$\theta$ mean	$\theta$ M-est	$\theta$	Difference mean	Difference M-est
P1	Z1	0.625	0.545	0.498	-20.27	-8.66
	Z2	0.594	0.587	0.578	-2.73	-1.60
	Z3	0.440	0.409	0.84	+90.78	+105.53
	TOT	0.591	0.561	0.57	-3.50	+1.59
P2	Z1	0.463	0.392	0.498	+7.60	+26.97
	Z2	0.347	0.312	0.578	+66.63	+85.07
	Z3	0.254	0.245	0.84	+230.83	+243.53
	TOT	0.388	0.335	0.57	+46.87	+69.90
Total	Z1	0.544	-	0.498	-8.41	-
	Z2	0.471	-	0.578	+22.83	-
	Z3	0.347	-	0.84	+142.01	-
	TOT	0.489	-	0.57	+16.48	-
Synthetic FRC beams						
Pouring method	Zone	Test		Analytical		
		$\theta$ mean	$\theta$ M-est	$\theta$	Difference mean	Difference M-est
P1	Z1	0.693	0.668	0.5	-27.86	-25.16
	Z2	0.648	0.639	0.53	-18.15	-17.09
	Z3	0.674	0.512	0.84	+24.65	+63.95
	TOT	0.671	0.635	0.55	-18.07	-13.36
P2	Z1	0.311	0.299	0.5	+60.92	+67.36
	Z2	0.474	0.440	0.53	+11.79	+20.47
	Z3	0.528	0.452	0.84	+59.22	+86.03
	TOT	0.404	0.391	0.55	+36.12	+40.74
Total	Z1	0.502	-	0.5	-0.38	-
	Z2	0.561	-	0.53	-5.50	-
	Z3	0.601	-	0.84	+39.83	-
	TOT	0.538	-	0.55	+2.29	-

various cross-section zones as well as for the entire cross-section and the corresponding distributions are shown in Fig. 7. The data for the different pouring methods are shown in

the same graphs for ease of comparison. The distribution was narrower in the case of larger surfaces. Thus, the CV was the smallest in the case of the entire cross-section. The distribution

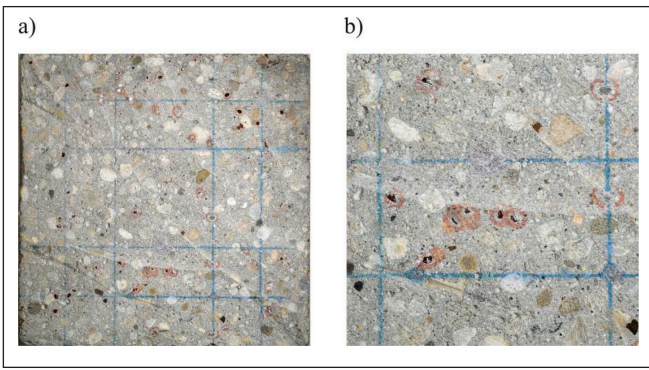
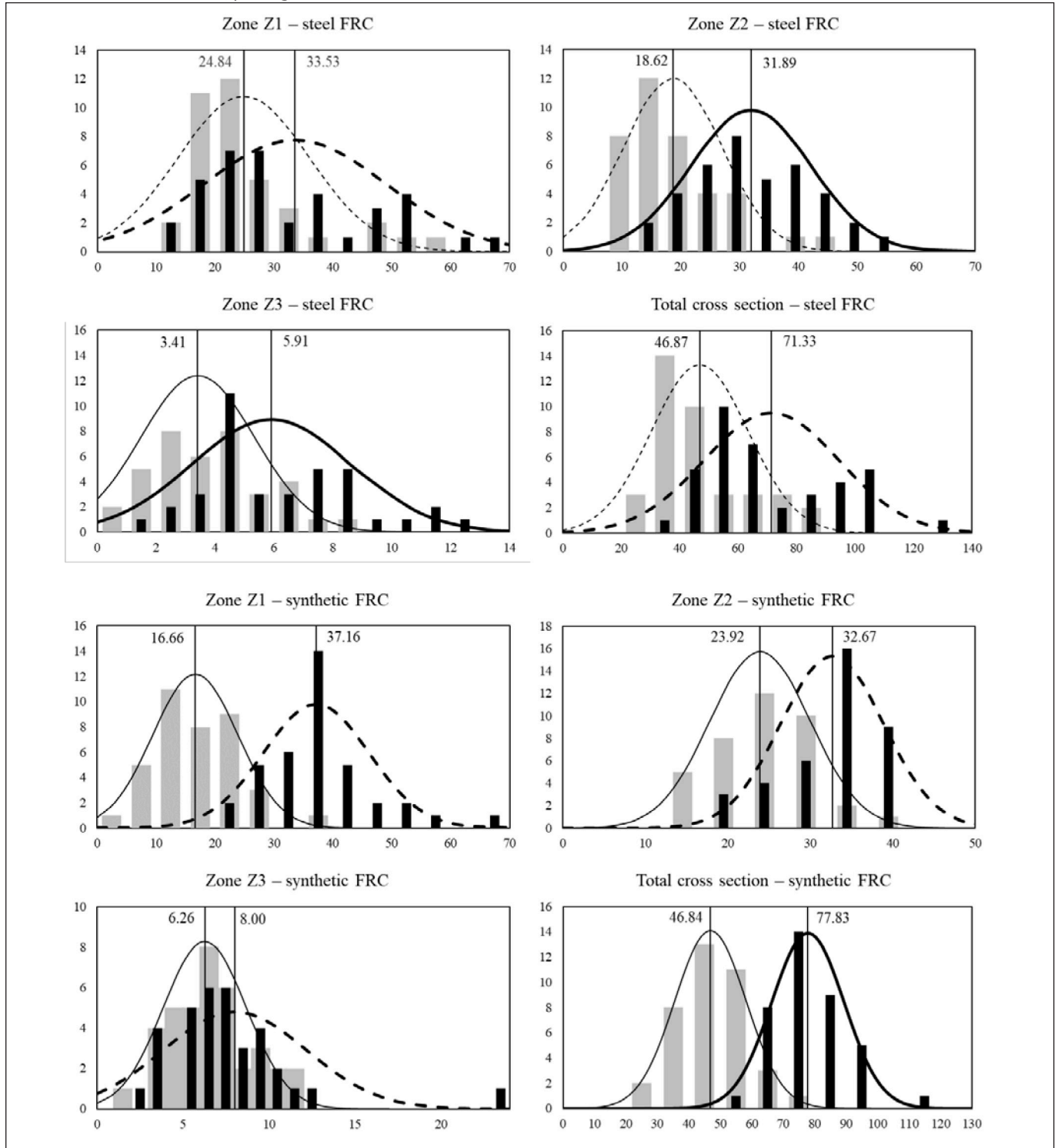


**Fig. 6:** Typical cross-section of steel FRC beam: (a) complete cross-section with various zones marked and (b) higher-magnification image of cross-section.

**Fig. 7:** Histograms and corresponding distribution curves for numbers of fibres intersecting various cross-section zones and entire cross-section in case of steel and synthetic macrofibres (black columns and bold distribution curve: P1 (horizontal) pouring method and grey columns and thin distribution curves: P2 (inclined) pouring method).



curves that passed the normality test are represented by solid lines while those that did not are represented by dashed lines.

The orientation factors were calculated from the mean values and the results of the M-estimator test. The values of the orientation factors were then compared with the analytical results. The orientation factors for all the beams (those fabricated using both the P1 method and the P2 method) were also determined and compared with the analytical results. These results are listed in *Table 5*.

Near the end plate of the formwork, the flow direction of the concrete changes, and the wall effect becomes more pronounced. To highlight this, the number of fibres intersecting the cross-section are shown along the longitudinal

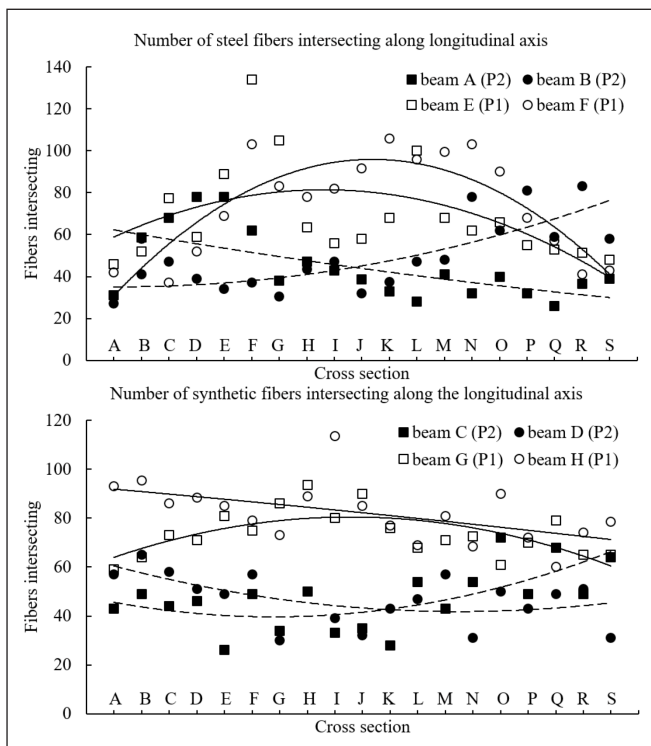


**Fig. 8:** Changes in number of fibres intersecting cross-section along longitudinal axis of beams (solid line: pouring method P1 and dashed line: pouring method P2).

axis of the beam in *Fig. 8*. The results for the two pouring methods and two fibre types are shown in the same diagrams. A second-order polynomial regression curve was fitted to the data to illustrate the changes in the number of fibres along the longitudinal axis.

## 5. DISCUSSION

It can be seen clearly that the choice of the pouring method used has a significant effect on the number of fibres intersecting the cross-sections. This was true for both steel and synthetic macrofibres. The numbers of steel and synthetic fibres that intersected the cross-sections of the beams formed by method P2 were 34% and 39% lower, respectively, than those in the case of the beams formed using method P1. A similar difference was also observed in the case of the different cross-section zones as well as between the zones and the total cross-section. Therefore, it can be assumed that the pouring method has a determining effect on the orientation of the incorporated fibres.

The flow of the concrete can explain these differences. In the flowing concrete matrix, the fibres are oriented perpendicular to the direction of the flow (Toutanji and Bayasi, 1998; Stahl, Custer, and van Mier, 2008; Stahl, and van Mier, 2007). In the case of the horizontal pouring method (P1), the flow direction of the concrete is vertical. Thus, the orientation of the fibres is horizontal. The vibration of these beams may cause the fibres to become even more aligned horizontally (Soroushian and Lee, 1990; Toutanji and Bayasi, 1998; Barragán et al., 2000). In contrast, in the case of the inclined pouring method (P2), the concrete flow direction is parallel to the longitudinal axis of the beam. Thus, the orientation of the fibres is perpendicular to the longitudinal axis. At the ends of the beams, this effect is not as strong, owing to the end plates of the formwork (*Fig. 8*).

In the case of method P1, the mean value (of the number

of intersecting fibres) for the synthetic fibres was 9.1% higher than that for the steel fibres while for method P2, the values were almost similar. The M-estimator values for the synthetic fibres for P1 and P2 were 13.1% and 16.4% higher, respectively, than those for the steel fibres. Moreover, for the same pouring method, in almost all the cases, more synthetic fibres were observed in the cross-section than the steel fibres. This is in contradiction to the results of the proposed analytical model, since according to the model, the total orientation factor is higher in the case of the steel fibres and would result in more steel fibres intersecting the cross-section.

The normality test results suggested that the following data for the synthetic fibres exhibited a normal distribution: method P1 and the entire cross-section and method P2 and all the zones as well as the entire cross-section. In contrast, for the steel fibres, only the data for zone Z3 for both pouring methods and those for zone Z2 and method P1 exhibited a normal distribution. However, the number of samples in the corner zone, that is, Z3, is not as relevant, given the small area of the zone. Thus, if the data for the entire cross-section were not normal, the normality of the data for Z3 was probably incorrect. In summary, the null hypothesis, namely, that the distribution of the data were normal, was accepted only in the case of the synthetic fibres. This conclusion can be confirmed through a visual inspection of the histograms: in case of the steel fibres, the distributions were either asymmetrical or bimodal.

The CV values for the different cross-section zones lay between 31.8% and 56.6% in the case of the steel fibres and between 14.7 and 52.1% in the case of the synthetic fibres. Further, the CV values for the entire cross-section lay between 32.3% and 35.2% in the case of the steel fibres and between 14.7% and 24.2% in the case of the synthetic fibres, meaning that the distributions of the synthetic fibres in the beams were slightly more uniform.

On comparing the results of the proposed analytical model with those of the laboratory tests, the following conclusions could be drawn. The orientation factors obtained using the analytical model closely approximated the M-estimator values for the steel fibres and method P1, while in the case of the synthetic fibres, the closest estimates were the mean values in the case of method P2. The orientation factor of the analytical model for the corner zone (Z3) yielded the worst estimates in all the cases: in the case of the steel fibres, the orientation factors for zone Z3 were the lowest, in contrast to the predictions of the model. On the other hand, in the case of the steel fibres, the analytical model results differed significantly from the test results: the undisturbed zone (Z1) exhibited the highest orientation factor, while the zones with the wall effect (Z2 and Z3) exhibited smaller values. Although, in the case of the steel fibres, there is an upper limit for fibre content. Above this limit, the effect of the fibres on their respective movements should also be taken into account, as this would result in more of the fibres being located in the middle zone than in the edge and corner zones (Juhász, 2018b; Czoboly, 2016). The actual concentration of 33.73 kg/m<sup>3</sup> was higher than this limit. With respect to this steel fibre concentration, which is used widely in the industry, the standard cross-section dimensions of 150 × 150 mm<sup>2</sup> seem to be insufficient for the steel fibres in question.

Based on the results of the statistical analysis and after comparing the test and analytical results, the following conclusions can be drawn. In case of steel fibres, the use

of the M-estimator is recommended, given the significant divergence of the data from a normal distribution. Further, the analytical model is suitable in the case of pouring method P1. In case of synthetic fibres, the analytical model underestimates the orientation factors for P1 and overestimates them for P2. However, it yields good estimates of the average values for the two pouring methods. According to the analytical model, there is no significant difference between the orientation factors of the undisturbed zone (Z1) and the edge zone (Z2). This was confirmed in the case of pouring method P1 but not in the case of pouring method P2.

According to the obtained results, the wall effect affects the orientation factors to a lesser degree than the flow type and direction of the concrete. Consequently, knowing the flow type and direction of the concrete and taking these factors into account during the modelling of FRC is of greater importance.

As per this study, the mean value of the orientation factors related to the different flow directions will lie between 0.3 and 0.6. Thus, 0.5 seems to be a good value to assume. Finally, the assumption of the existence of different cross-section zones seems to be invalid in most cases. This is true for both steel and synthetic fibres.

## 6. CONCLUSIONS

The residual tensile strength of FRC depends primarily on the number of fibres that intersect the cracked cross-section of the structure in question. While the mixing of the fibres should ideally be uniform, this is not the case in reality, owing to various factors. In this study, the effects of the pouring method on the orientation factors of steel and synthetic fibres were investigated. Beams were produced using two different pouring methods, and the orientation factors in the different zones of sections of these beams were investigated. The obtained results were compared with the orientation factors reported in the literature.

The study examined two types of fibres: steel and synthetic. The dosage of these fibres was chosen so that the number of mixed fibres was the same. In this study, the matrix of fibre-reinforced concrete was kept constant, while the pouring method varied. Moreover, the orientation of the fibres can be affected by a number of parameters, which were not detailed in this study, e.g., fibre length and shape, aggregate type and size, paste saturation, etc. These parameters may have varying degrees of influence on the orientation factors, which can be elucidated in future studies.

According to the results obtained in this study, there is a difference of 34–40% in the orientations, based on the pouring method used. This difference is significant and must be taken into account during the engineering design stage. In the case of the standard beams used for tests, owing to the vibrations that occur during the manufacturing of the test specimens, the fibres are oriented along the longitudinal axis of the beams. As a result, more fibres intersect the cross-section than would be the case for a uniform distribution. In the case of flowable concrete, the fibres are oriented perpendicular to the flow direction. Thus, fewer fibres intersect the cross-section that would be the case if the flow were parallel to the longitudinal axis of the beam. Thus, the error may be magnified in that the material parameters may be overestimated, although in the sections of actual structures, the number of fibres intersecting the cross-section may also be overestimated if

their orientation is unsuitable. Thus, there can be a significant difference between the tension or moment capacities as calculated based on the overestimated material parameters and the actual capacity of the structure.

Thus, in the case of precast elements and structures that are functionally important, the orientation of the reinforcing fibres added to the concrete must be considered during the design stage.

## 7. REFERENCES

- Alberti, M.G., Enfedaque, A. and Gálvez, J.C. (2017), „On the prediction of the orientation factor and fibre distribution of steel and macro-synthetic fibres for fibre-reinforced concrete”, *Cement and Concrete Composites* 77, pp. 29–48, <https://doi.org/10.1016/j.cemconcomp.2016.11.008>
- ASTM C1609 (2019), „Standard test method for flexural performance of fiber-reinforced concrete (Using beam with third-point loading)”, ASTM International, West Conshohocken, PA, 2019, [www.astm.org, https://doi.org/10.1520/C1609\\_C1609M-19](https://doi.org/10.1520/C1609_C1609M-19)
- Balaguru, P.N. and Shah, S.P. (1992), „Fiber reinforced cement composites”, *McGraw-Hill International Editions, Civil Engineering Series*
- Barragán, B.E., Gardner, D., Gettu, R. and Ferreira, L.E.T. (2000), „Study of the distribution and orientation of fibers in cast cylinders”, Report for Test and Design Methods for Steel Fibre Reinforced Concrete, EU Contract–BRPR–CT98-813.
- Bernard, E.S. (2013), „Development of a 1200-mm-diameter round panel test for post-crack assessment of fiber-reinforced concrete,” *Advances in Civil Engineering Materials* 2(1), pp. 457–471, <https://doi.org/10.1520/ACEM20120021>
- Chasioti, S. (2017), „Hybrid steel fibre reinforced concrete in shear: from the material to the structural level”, Doctoral thesis, University of Toronto, Toronto, 2017.
- CNR-DT 204/2006 (2006), „Guide for the Design and Construction of Fiber-Reinforced Concrete Structures”, design recommendation, Advisory Committee on Technical Recommendations for Construction, CNR, Rome
- Czoboly O. (2016), „A keverési idő és a keverési mód hatása a szálak és a szálerősítésű betonok jellemzőire (The effect of mixing time and mixing mode on the characteristics of fibres and fibre reinforced concrete, in Hungarian)”, Doctoral thesis, Budapest University of Technology and Economics, Budapest.
- Dupont, D. and Vandewalle, L. (2005), „Distribution of steel fibres in rectangular sections”, *Cement & Concrete Composites* 27, pp. 391–398, <https://doi.org/10.1016/j.cemconcomp.2004.03.005>
- Edgington, J. and Hannant, D. J. (1972), „Steel Fibre Reinforced Concrete. The effect on fibre orientation of compaction by vibration”, *Materials and Structures* 5(25), pp. 41–44, <https://doi.org/10.1007/BF02479076>
- EN 14651 (2007), „Test method for metallic fibre concrete – measuring the flexural tensile strength (limit of proportionality (LOP), residual)”, European Committee for Standardization, <https://doi.org/10.3403/30092475>
- fib (2013), „Model Code for Concrete Structure 2010”, *Wiley Ernst & Sohn*.
- Gopalratnam, V.S., Shah, S.P., Batson, G.B., Criswell, M.E., Ramakrishnan, V. and Wecharatana, M. (1991), „Fracture toughness of fiber reinforced concrete”, *ACI Materials Journal* 88(4), pp. 339–353, <https://doi.org/10.14359/1840>
- Hoy, C.W. (1998), „Mixing and mix proportioning of fibre reinforced concrete”, Doctoral thesis, Department of Civil, Structural and Environmental Engineering, University of Paisley, Scotland, 284 p.
- Juhász K.P. (2013), „Szintetikus makro szálerősítendő beton gerendavizsgálatok kiértékelése a valós száleloszlás vizsgálata alapján (Evaluation of synthetic macro fibre reinforced concrete beam test results based on the examination of the real fibre distribution, in Hungarian)”, *Anyagvizsgáló Lapja* 23, pp. 93–97.
- Juhász, K.P. (2015), „Evaluation of fibre reinforced concrete beam test results based on the examination of the real fibre distribution”, in: A. Kohoutková et al. (Eds.), *Proceedings of Fibre Concrete 2015*. Prague, Czech Republic.
- Juhász K. P. (2018a), „Acél and szintetikus szálak orientációjának meghatározása szálerősítésű betonban (Determining the orientation of steel and synthetic fibres in fibre reinforced concrete, in Hungarian)”, *Építés-Építészettudomány* 46(1–2), pp. 221–238, <https://doi.org/10.1556/096.2017.007>
- Juhász K. P. (2018b) „The effect of synthetic fibre reinforcement on the fracture energy of the concrete”, Doctoral thesis, Budapest University of Technology and Economics, Budapest, <https://perma.cc/4JMY-HN5C>
- Juhász K.P. (2019), „Analytical model for rigid (steel) and flexible (synthetic) fibre mixing in concrete”, *IOP Conference Series: Materials Science and Engineering* 596, <https://doi.org/10.1088/1757-899X/596/1/012003>

- Kameswara Rao, C.V.S. (1979), „Effectiveness of random fibres in composites”, *Cement and Concrete Research* 9, pp. 685-693, [https://doi.org/10.1016/0008-8846\(79\)90063-2](https://doi.org/10.1016/0008-8846(79)90063-2)
- Kang, S.T., Lee, B.Y., Kim, J-K., Kim, Y.Y. (2011), „The effect of fibre distribution characteristics on the flexural strength of steel fibre-reinforced ultra high strength concrete”, *Construction and Building Materials* 25(5), pp. 2450–245, <https://doi.org/10.1016/j.conbuildmat.2010.11.057>
- Kooiman, A.G. (2000), „Modelling steel fibre reinforced concrete for structural design”, Doctoral thesis, Technical University of Delft (The Netherlands), pp. 87–106.
- Krenchel, H. (1975), „Fibre spacing and specific fibre surface”, A. Neville, (ed.) *Fibre reinforced cement and concrete*, London: The Construction Press, pp. 67–75.
- Lee, S.C., Cho, J.Y., and Vecchio, F. J. (2011), „Diverse Embedment Model for Steel Fiber-Reinforced Concrete in Tension: Model Development”, *ACI Materials Journal* 108(5), pp. 516–525, <https://doi.org/10.14359/51683261>
- Lee, S.C., Cho, J.Y., Vecchio, F.J. (2013) „Simplified diverse embedment model for steel fiber-reinforced concrete elements in tension”, *ACI Materials Journal* 110, pp. 403–412.
- Naaman, A. E. (1972), „A statistical theory of strength for fiber reinforced concrete”, Doctoral thesis, Massachusetts Institute of Technology.
- Ng, T.S., Foster, S.J. and Htut T.N.S. (2012), „Fracture of Steel Fibre Reinforced Concrete – the Unified Variable Engagement Model”, UNICIV Report R–460, School of Civil and Environmental Engineering, The University of New South Wales.
- Oh, B.H., Kim, J.C. and Choi, Y.C. (2007), „Fracture behavior of concrete members reinforced with structural synthetic fibers”, *Engineering Fracture Mechanics* 74, pp. 243–257, <https://doi.org/10.1016/j.engfracmech.2006.01.032>
- Österreichische Vereinigung für Beton- und Bautechnik (2008), „Richtlinie Faserbeton”, Vienna.
- Romualdi, J.P. and Mandel, J.A. (1964), „Tensile strength of concrete affected by uniformly distributed and closely spaced short lengths of wire reinforcement”, *Journal of the American Concrete Institute* 61(6), pp. 657–671, <https://doi.org/10.14359/7801>
- Sarmiento, E. V., Zirgulis, G., Sandbakk, S., Geiker, M. R. and Kanstad, T. (2012), „Influence of concrete flow on fibre distribution, orientation and mechanical properties of fibre reinforced concrete”, in J. Barros (ed) *BEFIB2012 – Fibre reinforced concrete*
- Stahli, P. and van Mier, J.G.M. (2007), „Effect of Manufacturing Methods on Tensile Properties of Fibre Concrete”, in *Proceedings of Fracture Mechanics for Concrete and Concrete Structures (FraMCo)6*, Catania, Italy.
- Stahli, P., Custer, R. and van Mier, J.G.M., (2008), „On flow properties, fibre distribution, fibre orientation and flexural behaviour of FRC”, *Materials and Structures* 41(1), pp. 189–196, <https://doi.org/10.1617/s11527-007-9229-x>
- Stroeven, P. (1978), „Morphometry of fiber reinforced cementitious materials”, *Materials and Structures* 11(61), pp. 31–37, <https://doi.org/10.1007/BF02478701>
- Stroeven, P. (1979), „Morphometry of Fibre Reinforced Cementitious Materials, Part II: Inhomogeneity, segregation and anisometry of partially oriented fibre structures”, *Materials and Structures* 12(67) pp. 9–20, <https://doi.org/10.1007/BF02473994>
- Stroeven, P. (1991), „Effectiveness of steel wire reinforcement in a boundary layer of concrete”, *Acta Stereol* 10(1), pp.113–22.
- Stroeven, P. (1999), „Steel fibre reinforcement at boundaries in concrete elements”, in *Proceedings of the Third International Workshop on High Performance Fiber Reinforced Cement Composites (HPFRCC3)*, Mainz (Germany), pp. 413–421.
- Soroshian, P. and Lee, C. (1990), „Distribution and orientation of fibers in steel fiber reinforced concrete”, *ACI Mater Journal* 87(5), pp. 433–439, <https://doi.org/10.14359/1803>
- Toutanji, H. and Bayasi, Z. (1998), „Effects of Manufacturing Techniques on the Flexural Behavior of Steel Fiber-Reinforced Concrete”, *Cement and Concrete Research* 28(1), pp. 115–124, [https://doi.org/10.1016/S0008-8846\(97\)00213-5](https://doi.org/10.1016/S0008-8846(97)00213-5)
- Vandewalle, L. et al. (2003), „RILEM TC 162-TDF: Test and design methods for steel fibre reinforced concrete –  $\sigma$ - $\epsilon$  design method”, *Materials and Structures* 36(8), pp. 560–567, <https://doi.org/10.1617/14007>
- Voo, J. Y. L.; Foster, J.S. (2003), „Variable engagement model for the design of fibre reinforced concrete structures”, in: V. Mistry et al., (Eds.) *Advanced Materials for Construction of Bridges, Buildings, and Other Structures III*. Davos, Switzerland, 2003, pp. 1–10.
- Zerbino, R., Tobes J. M., Bossio M. E. and Giaccio G. (2012), „On the orientation of fibres in structural members fabricated with self compacting fibre reinforced concrete”, *Cement & Concrete Composites* 34, pp. 191–200, <https://doi.org/10.1016/j.cemconcomp.2011.09.005>

**Károly Péter Juhász** (1980), Structural Engineer MSc., PhD, owner and chief engineer of JKP Static Ltd. His main fields of activities are experimental investigation and modelling of synthetic fibre reinforced concrete, finite element modelling of concrete structures. He is a member of the Hungarian Group of *fib* and the *fib* Working Group 2.4.2. email: [office@jkp.hu](mailto:office@jkp.hu)

# EFFECTS OF POLYPROPYLENE FIBERS ON ULTRA HIGH PERFORMANCE CONCRETE AT ELEVATED TEMPERATURE



Ahmed Maher Seyam, Samir Shihada, Rita Nemes

<https://doi.org/10.32970/CS.2020.1.2>

*This paper presents an experimental study to evaluate the influence of polypropylene on fire resistance of ultra-high performance concrete (UHPC). Concrete mixtures are prepared by using different percentages of polypropylene fibres 0%, 0.75% and 1.5%, by volume. Samples are heated to 250 or 500 °C, for exposures 2.5 or 5 hours, and tested after cooling for compressive strength and flexural tensile strength. The research includes the use of mineral admixture of a recognized, polypropylene fibre, quartz sand, superplasticizers and without using any type of aggregates other than the quartz sand.*

*The effect on subjected samples to elevated temperature up to 250 °C and 500 °C for durations 2.5 hours and 5 hours was studied for each mix and comparing the results of compressive strength and tensile strength among the mixes.*

*Results obtained, showed that adding 0.75% of polypropylenes fibres only to a concrete mixture, improved the fire resistance of the concrete by 27% and 72% when the samples exposed to 250 °C and 500 °C for 2.5 hours respectively, compared with concrete mixes without fibres. In addition, the residual strength was improved by 39% and 14% when the samples exposed to 250 °C and 500 °C for 5 hours, respectively.*

**Keywords:** concrete, fibres, polypropylene, UHPC, FRC, fire, elevated temperature

## 1. INTRODUCTION

Reinforced concrete is the most commonly used construction material worldwide. High performance concrete (HPC) is a novel material with improved properties like higher strength, longer durability and higher workability, than conventional concretes (Aitcin 1998). Concrete with high strength and durability has been primarily used in special constructions such as military buildings, nuclear power plants, infrastructures and high rise buildings since it became commercially available (Akca and Zihnioğlu 2013).

Ultra high performance concrete (UHPC) is a newly developed material that has gained more interest in the concrete construction industry. Fibres added to concrete improve its mechanical properties, reduce its plastic shrinkage, improves its resistance to fire, to abrasion and to impact and decrease its permeability. With such material, engineers are able to design new structures, original in their design or their ability to resist severe conditions.

Since the strength development, mechanical properties and durability characteristics of high-performance concrete may be different from ordinary concrete, moreover high-performance concrete is a relatively new class of concrete, so additional research is needed to understand more fully the factors affecting the development of its physical and mechanical characteristics, it follows that actual performance of ultra-high performance concrete (UHPC) under elevated temperature is also different and it should be studied.

### 1.1 Statement of the problem

The damage caused by fire is one of the most serious problems that face civil engineers, especially in countries that are susceptible to wars and enemy fighting such as Gaza Strip. During the last war (2014) perpetrated by the Israelis on Gaza Strip, large number of buildings were subjected to fires lasting for long periods of time. Some of these buildings were repairable, while others are beyond repair and need to be demolished and reconstructed. The activity of concrete rehabilitation or reconstruction usually takes place in areas which are more exposed to fire risk. In these cases, special types of concrete should be used.

The usage of ultra-high strength concrete with high compressive strength in construction applications has been increasing worldwide and it will make an impact construction industry due to the limited land area available and the fast growing population. High-rise multistory buildings have increasingly used, where the large loads in high rise buildings lead to the design of large sections when ordinary concretes are used. But when ultra-high performance concrete is used small cross sections can be designed. Also, this type of concrete will be used in rehabilitation techniques.

### 1.2 Research objectives

The main goal of this research is to study the effect of polypropylene fibres on improving fire resistance of Ultra High Performance Concrete and to produce Ultra High Performance

Fire Resistant Concrete (UHPFRC) using available materials. This will open new possibilities for the production of a new material.

## 2. LITERATURE REVIEW

Shihada S. (2011) investigated the effects of using polypropylene fibres (PP) on fire resistance of normal strength concrete. Concrete mixtures were prepared by using different percentages of polypropylene fibres (PP) 0%, 0.5% and 1%, by volume. Samples subjected to elevated temperatures 200 °C, 400 °C and 600 °C, for exposures duration up to 2, 4 and 6 hours, and tested for compressive strength. Results showed that, the relative compressive strengths of concretes containing polypropylene fibres were higher than those of concretes without polypropylene fibres. Furthermore, the researcher concluded that concrete mixes which are prepared using 0.5% polypropylene fibres, by volume, can significantly promote the residual compressive strength during the heating, lower and higher contents of fibres generally showed worse performance due to the more deterioration and higher volumes of voids, respectively.

Dharan and Lal (2016) studied the effects of adding polypropylene fibres of 0.5%, 1%, 1.5%, and 2% to concrete. Tests on workability, modulus of elasticity, compressive strength, split tensile strength and flexural resistance were conducted on specimens obtained that compressive strength of concrete contains 1.5% of polypropylene fibre was increased by 17% of the strength of conventional concrete. Moreover, strength enhancement in split tensile strength is 22%, flexural strength is 24% and modulus of elasticity is 11% compared to that of conventional concrete.

Tanyildizi and Çevik (2009) studied the effect of using polypropylene fibre and silica fume on the mechanical properties of lightweight concrete exposed to high temperatures. Mixes containing polypropylene fibres with 0%, 0.5%, 1% and 2% and silica fumes with 0% and 10% were prepared. The flexural and compressive strength for lightweight concrete samples were determined after being exposed to high temperatures (400 °C, 600 °C and 800 °C). Three control factors (silica fume percentage, polypropylene fibre percentage and high temperature degree) were used for this study. They demonstrated that the compressive and flexural strength of polypropylene fibre reinforced lightweight concrete drops with temperature starting from 400 °C. The test results indicated that each temperature range had a distinct pattern of strength loss.

Sohaib et. al. (2018) studied the using polypropylene fibres in concrete to achieve maximum strength, and they observed the significant improvement in ultimate compressive strength, and the inclusion of polypropylene fibres increases the compressive strength by 20% after 7 days and 16 % after 28 days, compared to the control samples, moreover, 11% and 17% increment was observed in split tensile strength after 7 days and 28 days respectively. They have been concluded that the optimum percentage of polypropylene fibres was obtained both in compressive and split tensile strength as 1.5% of cement contents.

Komonen and Penttala (2003) investigated the effect of high temperature on the residual properties of plain and polypropylene fibre reinforced Portland cement paste. Plain Portland cement paste with w/c ratio of 0.32 exposed to elevated temperatures up to 1000 °C. Paste with polypropylene

fibres was exposed to elevated temperatures up to 700 °C. The residual flexural and compressive strengths were measured. The gradual heating coarsened the pore structure. At 600 °C, the residual compressive capacity ( $f_{c_{600^{\circ}\text{C}}}/f_{c_{20^{\circ}\text{C}}}$ ) was still over 50% of the original. Strength loss due to increasing of temperature was not linear. Polypropylene fibres produced a finer residual capillary pore structure, decreased compressive strengths, and improved residual flexural strengths at low temperatures. According to the tests, it seems that exposure temperatures from 50 °C to 120 °C can be influence as exposure temperatures 400–500 °C to the residual strength of cement paste produced by a low water cement ratio.

## 3. CONSTITUENT MATERIALS & EXPERIMENTAL PROGRAM

### 3.1 General overview

The experimental program and the constituent materials used to produce ultra-high performance fire resistant concrete associated with this research work.

The laboratory investigation consisted of tests on hardened concrete. The tests for hardened concrete included compressive and flexural strengths.

The influence of the polypropylene fibres “PP” was studied in order to obtain the optimum percentage for the mix and to reduce the loss in compressive strength due to high temperature by preparing different mixes with different percentages of “PP”.

The influence of silica fume dosages, cement/ultra-fine ratio, superplasticizer, steel fibres and polypropylene fibres amounts on the compressive strength concrete that’s subjected to high temperatures together with the workability and density of UHPFRC were studied by preparing several concrete mixes.

The properties of the different constituent materials used to produce UHPFRC were also discussed such as moisture content, unit weight, specific gravity and the grain size distribution. The test procedures, details and equipment used to assess concrete properties are also shown.

### 3.2 Characterizations of constituent materials

Constituent materials used in this research included ordinary Portland cement, silica fume, quartz sand, polypropylene fibres. In addition, superplasticizer was used to ensure suitable workability. Proportions of these constituent materials have been chosen carefully in order to optimize the packing density of the mixture.

Cement paste is the binder in UHPFRC, it holds the aggregate (fine, micron fine) together and reacts with mineral materials in hardened mass. The property of UHPFRC depends on the quantities and the quality of its constituents. Because cement is the most active component of UHPFRC and usually has the greatest unit cost, its selection and proper use is important in obtaining most economically the balance of properties desired of UHPFRC mixture.

The cement used throughout the experiments is ordinary Portland cement (OPC) 52.5. The results of mechanical and physical tests of the cements are summarized in *Table 1*. along with the requirements of ASTM C150 specifications for comparison purposes.

**Table 1:** Cement characteristics according to manufacturer data sheet

Test type		Ordinary Portland Cement	
		Results	ASTM C 150
Setting time (Vicat test) [min]	Initial	90 min.	>60 min.
	Final	192 min.	<375 min.
Mortar comp. strength [MPa]	3 days	18 MPa	min. 12 MPa
	7 days	34 MPa	min. 19 MPa
	28 days	52 MPa	no limits
Fineness (cm <sup>2</sup> /g)		3390	> 2800
Water demand		27.5 %	no limits

Silica fume is a by-product resulting from the reduction of high-purity quartz with coke or coal and wood chips in an electric furnace during the production of silicon metal or ferrosilicon alloys. The silica fume, which condenses from the gases escaping from the furnaces, has a very high content of amorphous silicon dioxide and consists of very fine spherical particles (ACI 548.6R-96). Silica fume is extremely fine with particle size of 0.1 µm. It exists in grey powder. The dry bulk density is 0.65 ±0.1 kg. The silica fume was supplied by SIKA Company.

Aggregate is relatively inexpensive and strong making material for concrete. It is treated customarily as inert filler. The primary concerns of aggregate in mix design for Ultra High Performance Fibre Reinforced Concrete are grain size distribution, maximum size and strength. Providing that concrete is workable, the large particles of aggregate are undesirable for producing UHPFRC. For producing UHPFRC, the nominal size ranges from 0.15 to 0.6 mm for quartz sand (fine aggregate) which are locally available in Gaza. In addition, it is important to ensure that the aggregates are clean, since a layer of mud or clay will reduce the cement aggregate bond strength, in addition to increasing the water demand.

Tap water of the laboratory at Islamic University of Gaza was used in all concrete mixtures and in the curing all of the tests specimens. Polypropylene is a plastic polymer that was developed in the middle of the 20th century.

Polypropylene fibres (PP) were first suggested for use in 1965 as an admixture in concrete material for blast resistant buildings at USA.

Subsequently, the polypropylene fibre has been improved further and now, used as short discontinuous fibrillated material for production of fibre reinforced concrete or as a continuous mat for production of thin sheet components. Moreover, the application of using PP fibres in construction was largely increased because addition of fibres in concrete mix improves the flexural strength, tensile strength, toughness, impact strength and the failure mode of concrete.

Micro cracks develop in concrete with curing and these cracks propagate rapidly under applied stress resulting in low tensile strength of concrete. Hence addition of fibres improves the strength of concrete and these problems can be overcome by use of polypropylene fibres in concrete (Madhavi et al. 2014).

Application of polypropylene fibres provides strength to the concrete while the matrix protects the fibres. The primary role of fibres in a cementitious composite is to control cracks, increase the tensile strength, toughness and to improve the deformation characteristics of the composite, recently become widely used in the construction industry in order to enhance fire resistance of concrete. Table 2. shows property of the used polypropylene in this research work.

**Table 2:** Polypropylene fibres properties

Property	Polypropylene
Density (g/cm <sup>3</sup> )	0.9 – 0.91
Reaction with water	hydrophobic
Tensile strength (MPa)	300 – 400
Elongation at break (%)	100 – 600
Melting point (°C)	175
Thermal conductivity (W/mK)	0.12
Length of fibres (mm)	15

The chemical admixture used is superplasticizer which is manufactured to conform to ASTM-C-494 specification types G and F. This plasticizing effect can be used to increase the workability of fresh concrete, extremely powerful water reduction, excellent flowability, reduced placing and compacting efforts, reduce energy cost for steam cured precast elements, improve shrinkage and creep behaviour, also it reduces the rate of carbonatisation of the concrete and finally improves water impermeability. This type is known as Sika ViscoCrete-10, some technical data shown in Table 3.

**Table 3:** The technical data for the superplasticizer

Type	Property
Appearance	Turbid liquid
Density	1.08 kg/l ±0.005
PH value	7.5
Basis	Aqueous solution of modified polycarboxylate
Toxicity	Non-Toxic under relevant health and safety codes

In all trial mixtures, where the w/c was constant and equal to 0.24, no segregation was observed and all mixtures were homogenous and fibres were well distributed through every batch.

### 3.3 Preparation of UHPFRC

After selection of all needed constituent materials and amounts to be used (mix designs); all materials are weighed properly. Then mixing with a power-driven tilting revolving drum mixer, started to ensure that all particles are surrounded with cement paste, silica fume and all other materials furthermore fibres should be distributed homogeneously in the concrete mass.

All mixes and tests were conducted in Soil & Materials Laboratory at the Islamic University of Gaza, Palestine.

Mixing procedure was carried out according following steps: (Arafa et.al. 2010)

1. Placing all dry materials (cement, silica fume, quartz sand and polypropylene fibres) in the mixer pan, and mixing for 2 minutes.
2. Adding 40% of superplasticizer to the mixing water.
3. Adding water (with 40% of superplasticizer) to the dry materials, slowly for 2 minutes.
4. Waiting 1 minute then adding the remaining superplasticizer to the dry materials for 30 seconds.
5. Continuation of mixing as the UHPFRC changes from a dry powder to a thick paste.
6. After final mixing, the mixer is stopped, turned up with its end right down, and the fresh homogeneous concrete is poured into a clean plastic pan.

The casting of all UHPFRC specimens used in this research was completed within 20 minutes after being mixed. All specimens were cast, cured and covered to prevent evaporation.

All mixtures were subjected to hardened concrete tests in

order to be classified as UHPFRC. Some mixing ingredients were fixed and the others were variable. Table 4. summarizes the different mix proportions. The percentage of silica fume, quartz sand, superplasticizer and water was used was the same percentage obtained by Madhoun A. (2013) in his research at Islamic University.

Each result listed in the search is an average of three examined specimens with the same properties and under the same conditions at least.

**Table 4:** Different mix proportions of UHPFRC by weight of cement

Mix No.	Mix-1	Mix-2	Mix-3
Cement	1	1	1
Silica fume	15%	15%	15%
Quartz sand	125%	125%	125%
Superplasticizer	3%	3%	3%
PP fibre	0%	0.75%	1.50%
Water	24%	24%	24%

## 4. RESULTS AND DISCUSSION

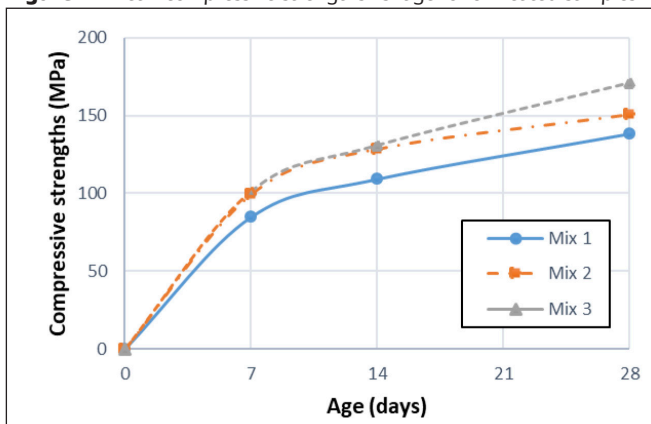
### 4.1 Hardened properties results

Laboratory tests were conducted to evaluate and study the hardened properties of UHPFRC. Results are the unit weight, compressive strength and tensile strength tests. Mean results for concrete mixtures at several ages are summarized in Table 5 and Figures 1 through 3. These results are the base line in comparing the strength reduction of the samples after being subjected to the heating tests.

**Table 5:** Compressive and tensile strengths for samples without heating

Mix No.	Density kg/m <sup>3</sup>	Compressive strengths MPa			Flexural strengths at 28 days, MPa
		7 days	14 days	28 days	
Mix1	2335	84.8	109.1	138.2	14.2
Mix2	2320	99.2	128.5	150.6	16.7
Mix3	2315	101.5	130.9	171.4	19.2

**Figure 1:** Mean compressive strengths vs. age for unheated samples



Results shown in Table 5 and Figure 1 demonstrate that it is possible to develop UHPFRC with different polypropylene amounts.

It can be observed that increasing the polypropylene content from 0.75% to 1.5% effectively increases the compressive strength of concrete when it was used alone.

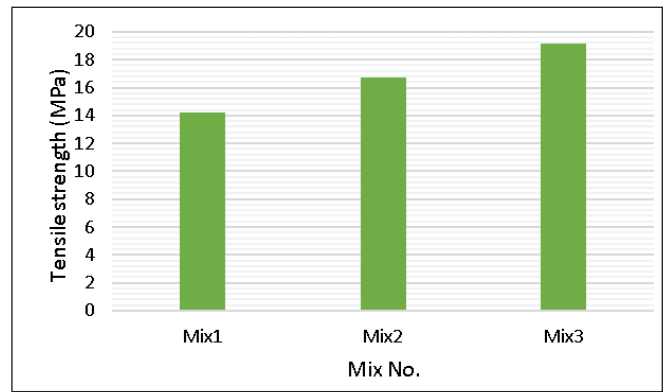


**Figure 2:** Mean tensile strengths for unheated samples

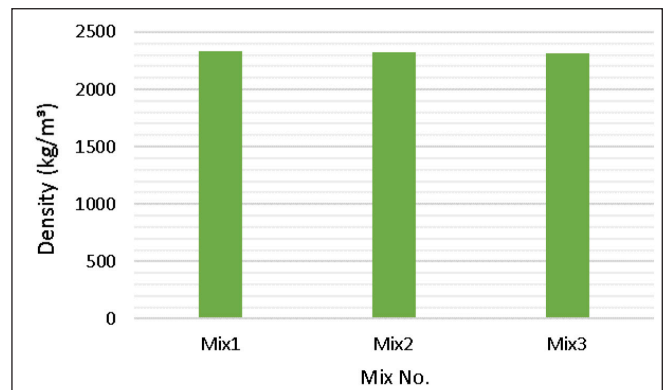


**Figure 3:** Mean density for unheated samples

### 4.2 Compressive strength test results of heated samples

Results of the compressive strength tests are shown in Table 6, Table 6 and Figures 5 through 6 for different percentages of polypropylene (0%, 0.75% and 1.5%), different heating temperatures (room temperature, 250 °C and 500 °C) and heating durations (0, 2.5 and 5 hours).

**Table 6:** Compressive strengths for heated samples

2.5-hour heating				
Mix No.	Mix-1	Mix-2	Mix-3	
% of PP fibre	0.00%	0.75%	1.50%	
Average compressive strength (MPa)	room temp.	138.2	150.6	171.4
	250 °C	113.3	145.0	168.7
	500 °C	40.1	69.3	63.6

**Table 7:** Compressive strengths for heated samples

5-hour heating				
Mix No.	Mix-1	Mix-2	Mix-3	
% of PP fibre	0.00%	0.75%	1.50%	
Average compressive strength (MPa)	room temp.	138.2	150.6	171.4
	250 °C	92.6	128.7	140.9
	500 °C	21.8	34.9	37.8

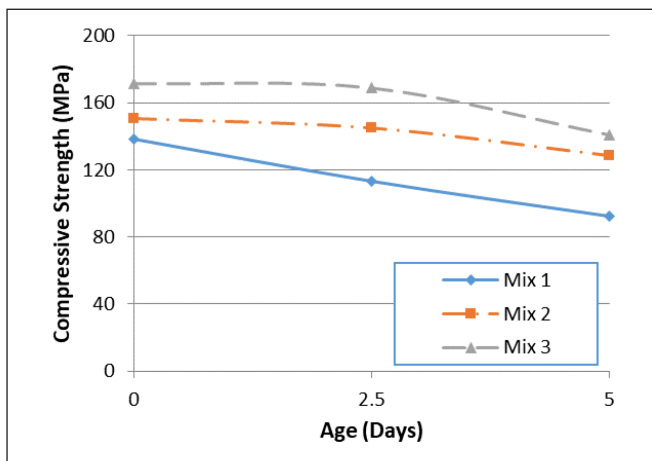


**Figure 4:** Compressive strength results for samples heated to 250 °C

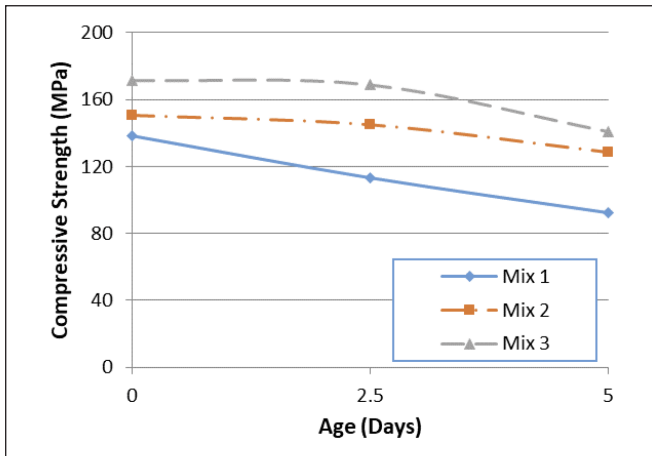


**Figure 5:** Compressive strength results for samples heated at 500 °C

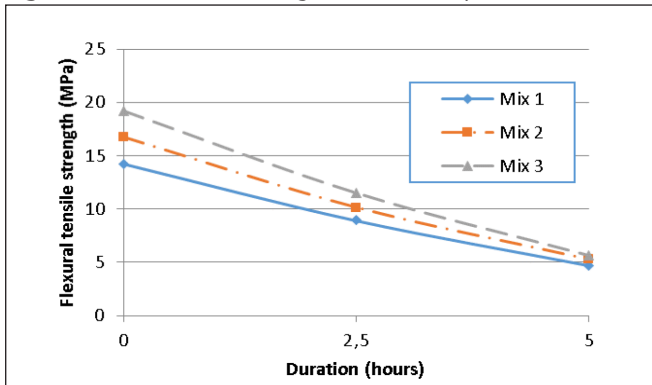
### 4.3 Flexural strengths test results after heating tests

Results of the flexural tensile strength tests are shown in Table 8 and Figures 6, for different percentages of PP (0%, 0.75% and 1.5%), different heating temperatures (room temperature and 250 °C) and heating durations (0, 2.5 and 5 hours).

**Table 8:** Flexural tensile strength for heated samples

Mix No.	% of PP fibre	Average flexural tensile strength, MPa		
		0 hour	2.5 hours	5 hours
Mix-1	0.00%	14.2	8.9	4.7
Mix-2	0.75%	16.7	10.1	5.3
Mix-3	1.50%	19.2	11.5	5.7

**Figure 6:** Flexural tensile strength results for samples heated at 250 °C



From Table 8 and Figure 6, it is noticed that for samples without polypropylene, the reductions in flexural tensile strengths are larger than at those with polypropylene. For example, the percentage of strength losses for samples without PP fibres heated at 250 °C for 2.5 hours was 37.7%, and when heated to 5 hours at the same temperature was 66.8%. On the other hand, the loss in tensile strength for samples with 0.75% PP fibres heated at 250 °C for 5 hours the loss was 68.5%. So from these results, one may conclude that the addition of polypropylene is highly decreasing the loss of concrete tensile strength when it was heated up to 2.5 hours at 250 °C but its not significant when the samples heating to 250 °C for 5 hours.

### 4.4 Results discussion

It is noticed that PP fibres not only improve the concrete resistance at elevated temperatures, but also improve samples initial strength before heating.

Results showed that the optimum percentage of polypropylene fibre is 1.5%, and this percentage complies with both Sohaib et. al. (2018) and Dharan and Lal (2016) they conclude that the optimum percentage of polypropylene fibres to improve the strength of concrete is 1.5%, and after 1.5% the decrease is gradual. The optimum percentage of polypropylene fibres was changed in other researchers, whose studying different type of concrete, fibres or additional materials in the concrete mix, for example 1.5% PP was not comply with the optimum percentage of Shihada (2011), Komonen and Penttala (2003); the different results comes from the difference of the type of concrete, in ultra-high performance concrete we have a high density mix without aggregate so the polypropylene fibres working as an internal reinforcement to confine the structural core of concrete, in addition the difference of polypropylene length, shape and diameter will lead to difference behaviour of the concrete mixture.

To conclude, all of researchers agreed that adding polypropylene fibres to the concrete mix improves their performance and increases strength, but in different proportions depending on the type of concrete mixture.

The masses of the different groups of concretes decrease with temperature. An additional mass decrease is noticed with the concrete incorporating polypropylene fibres, after the heating at 250 °C and 500 °C, the mass loss of fibres (PP fibres) concretes is lower than that of concretes with polypropylene fibres,

## 5. CONCLUSION

In this research, specimens of various concrete compositions were made and subjected to different heating periods. Three concrete groups were formulated without or with polypropylene fibres. Concrete mass loss and residual mechanical properties were studied. The following conclusions can be drawn from the experimental results:

1. All of concrete mixes prepared in this research achieved high workability and flowability, and may be used it as a self-compacting concrete the compressive strength of reference mixture was higher than 138 MPa.
2. The masses of the different groups of concretes decrease with temperature. An additional mass decrease is noticed with the concrete incorporating polypropylene fibres. After the heating at 250 °C and 500 °C, the mass loss of fibres (PP fibres) concretes is lower than that of concretes with PP fibres.

3. The 0.75 and 1.5% of PP fibre addition increased the compressive and the flexural tensile strength, too. The compressive strength for mix without fibres (Mix 1) was increased by 34.8% when polypropylene fibres were added as in (Mix 3).
4. The residual compressive strength of fibre reinforced concrete was relative and absolute higher than reference mixture. Comparing with concretes without fibres (Mix 1), reduction of relative residual strength was observed at 250 °C for 5 hours was 33%, and when heated at 500 °C for 5 hours was 84.2%. On the other hand, for concrete (Mix 2) heated at 250 °C for 5 hours, the loss was 14.5% and when heated to 500 °C for 5 hours the loss was 76.8%.
5. The relative residual flexural strength of mixtures with fibres are lower than the reference mixture, but the flexural strength increasing in room temperature were so high, than the absolute value of flexural strength is higher after heating. Comparing with concrete without fibres (Mix 1), it is noticed that the reductions in flexural tensile strengths are larger than at those with polypropylene fibres. The percentage of strength losses for Mix 1 heated at 250 °C for 2.5 hours was 37.7%, and when heated to 5 hours at the same temperature was 66.8%.

The optimum amount of polypropylene fibres on Ultra High Performance Concrete (UHPC) improves the fire resistance properties, by decreasing the rate of compressive strength loss as well as increasing the time of exposure before occurrence of failure.

## 6. REFERENCES

- ACI Committee 548.6R-96 (2003). Guide for the Use of Silica Fume in Concrete *ACI Manual of Concrete Practice part 2*.
- Aitcin, P. C. (1998). *High performance concrete*. CRC press. <https://doi.org/10.4324/9780203475034>
- Akca, A. H., & Zihnioglu, N. Ö. (2013). High performance concrete under elevated temperatures. *Construction and building materials*, 44, 317-328. <https://doi.org/10.1016/j.conbuildmat.2013.03.005>
- Arafa, M., Shihada, S., & Karmout, M. (2010). Mechanical properties of ultra high performance concrete produced in the Gaza Strip. *Asian Journal of Materials Science*, 2(1), 1-12. <https://doi.org/10.3923/ajmskr.2010.1.12>
- Dharan, D. S., & Lal, A. (2016). Study the effect of polypropylene fiber in concrete. *International Research Journal of Engineering and Technology*, 3(6), 616-619. <https://doi.org/10.21275/v5i5.nov163750>
- Komonen, J., & Penttala, V. (2003). Effects of high temperature on the pore structure and strength of plain and polypropylene fiber reinforced cement pastes. *Fire technology*, 39(1), 23-34. <https://doi.org/10.1023/A:1021723126005>
- Madhavi, T. C., Raju, L. S., & Mathur, D. (2014). Polypropylene fiber reinforced concrete-a review. *International journal of emerging technology and advanced engineering*, 4(4), 114-119.
- Al Madhoun, A. T. (2013). Mechanical Properties of Ultra High Performance Fiber Reinforced Self-Compacting Concrete. *Mechanical Properties of Ultra High Performance Fiber Reinforced Self-Compacting Concrete*. <http://hdl.handle.net/20.500.12358/19187>
- Noumowe, A. (2005). Mechanical properties and microstructure of high strength concrete containing polypropylene fibres exposed to temperatures up to 200 C. *Cement and concrete research*, 35(11), 2192-2198. <https://doi.org/10.1016/j.cemconres.2005.03.007>
- Shihada, S. (2011). Effect of polypropylene fibers on concrete fire resistance. *Journal of civil engineering and management*, 17(2), 259-264. <https://doi.org/10.3846/13923730.2011.574454>
- Sohaib, N., Seemab, F., Sana, G., & Mamoon, R. (2018). Using Polypropylene Fibers in Concrete to achieve maximum strength. In *Proc. of the Eighth International Conference on Advances in Civil and Structural Engineering* (pp. 36-42). <https://doi.org/10.15224/978-1-63248-145-0-36>
- Tanyildizi, H., & Çevik, A. (2010). Modeling mechanical performance of lightweight concrete containing silica fume exposed to high temperature using genetic programming. *Construction and Building Materials*, 24(12), 2612-2618. <https://doi.org/10.1016/j.conbuildmat.2010.05.001>
- Ahmed Maher Seyam**, (1989), civil engineer (M.Sc) in design and rehabilitation of structures, Ph.D. student at department of construction materials and technologies, Budapest University of Technology and Economics. Main field of interest: concrete technology, fibre reinforced concrete, fire design and improving construction materials. Member of the Palestinian association of engineers and the Hungarian Group of *fib*. [aseyam@edu.bme.hu](mailto:aseyam@edu.bme.hu).
- Samir Shihada, Ph.D.** professor in structural engineering at the department of civil engineering in the Islamic University of Gaza. He has extensive experience in teaching and practicing structural concrete design where he has published a refereed book entitled "Reinforced Concrete Design". His research interests include structural concrete design codes, seismic design, ultra-high performance concrete. Furthermore, he has served on several government committees dealing with building damage evaluation and engineering education. [sshihada@iugaza.edu.ps](mailto:sshihada@iugaza.edu.ps)
- Rita Nemes, Ph.D.** (1978) civil engineer (MSc), postgraduate degree in concrete technology, associate professor at the Department of Construction Materials and Technologies, Budapest University of Technology and Economics (Műegyetem rkp 3. Budapest H-1111, Hungary). Main field of interest: non destructive testing of concrete, fibre reinforced concrete, lightweight concrete, shrinkage of concrete, durability measurement, waste materials as aggregate and supplementary materials. Member of the Hungarian Group of *fib* and the Scientific Sociate of silicate Industry. [nemes.rita@epito.bme.hu](mailto:nemes.rita@epito.bme.hu)

# STEEL STRESS PATTERNS BETWEEN TWO PRIMARY CRACKS IN CONCRETE

DEDICATED TO THE MEMORY OF PROF. GALLUS REHM (1924-2020)



Andor Windisch, PhD

<https://doi.org/10.32970/CS.2020.1.3>

## SUMMARY

The national and international codes and standards and the literature consider the stress patterns either in case of a single crack or of equidistant primary cracks which developed at the same load level. Moreover, most FE models consider smeared cracks which do not allow for any insight in the real inner behavior of structural concrete. This paper considers the stochastic character of the concrete tensile strength's distribution along the reinforced concrete element and a realistic local bond stress vs. slip relationship with its hysteretic character when the sign of local slip changes due to the occurrence of a new primary crack.

**Keywords:** primary crack, local bond stress, slip, hysteretic characteristics, members in tension,

## NOTATIONS

a, b, c	coefficients of a local bond stress-slip function
a	crack spacing
$c_s$	rib spacing on the rebar surface
$d_s$	rebar diameter
$f_{cti}^*$ , $f_{ctk}^*$ , $f_{ct i+1}$	( $\beta_{bz}$ ) concrete tensile strengths
$f_{ctm}$	mean concrete tensile strength
$f_R$	relative rib area
$\ell_{bi}$	transfer length
u	perimeter of a rebar
v	slip
$x_i$	coordinates along the axis x
w	crack width
$A_c$	cross section area of concrete
$A_s$	cross section area of the rebars in the cross section
$A_0$	uncracked ideal concrete cross section
$E_c$	Young's Modulus of concrete
$E_s$	Young's Modulus of steel (rebar)
N	axial tensile force
$\alpha_E$	$E_s / E_c$
$\beta_w$	concrete cube strength
$\rho$	geometrical rate of reinforcement
$\sigma_c$	concrete stress
$\sigma_c$	concrete tensile stress
$\sigma_s$	steel (rebar) stress
$\tau_v(x)$	local bond stress
Lower case letters	
I, II	uncracked and cracked cross sections (state I and II), resp.

## 1. INTRODUCTION

This paper discusses the steel stress distribution between two primary cracks which develop at different load levels one after another in different distances from each other. This treatise was

part of an article which was first published in 1989 in German in a festive collection of articles published on the occasion of Professor Rehm's 65<sup>th</sup> birthday. Nevertheless, as a German language paper published in a local occasional publication, it was not available to the professional public. Until now no similar results have been published in the literature, while the stress distribution between the two primary cracks provides an important insight into the behavior of reinforced concrete structures. The common FEM models for members in tension and bending consider smeared cracks which develop at the same load level.

In this article a continuous crack theory is explained, which considers

- the stochastic character of the concrete tensile strength's distribution along the reinforced concrete element and
- a realistic local bond stress vs. slip relationship, with the influence of a change in sign of the relative slip between reinforcing steel and concrete.

Note: in this paper Goto-cracks and secondary cracks are not treated. Details see in Windisch (2016, 2017)

## 2. CONTINUOUS CRACK FORMATION IN MEMBERS IN TENSION

This section describes the development of the crack pattern in a prismatic r.c. member in centric tension with a known distribution of the concrete tensile strength. It is shown that the terms "crack formation stage" and "stabilized cracking stage" and the like always appear in reality side by side and the stochastic character of the crack formation that can be observed in the experiments can be easily explained.

Figure 1a shows a simplified distribution of the concrete tensile strength along an r.c. member.

The tensile force N is increased monotonically. In the non-

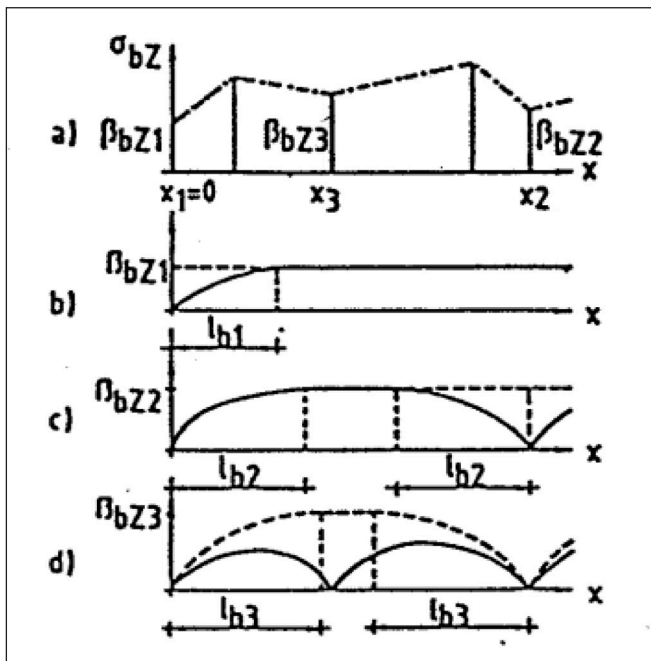


**Figure 1:** Crack development in a member in tension: Distribution of a) the concrete tensile strength, b) the concrete tensile stresses before and after the development of the first, c) the second, and d) the third primary crack

cracked state, the concrete and steel stresses are constant - apart from the transfer lengths at the member's ends

$$\sigma_c = \sigma_{ct} = N / A_0 \quad \sigma_s = \alpha_E \cdot \sigma_{ct}$$

(Note: in the original figures the concrete tensile stresses are marked as  $\beta_{bZi}$ .)

At the tensile force level:

$$N_1 = A_0 \cdot f_{ct1}$$

the concrete tensile stress reaches the lowest actual concrete tensile strength, then primary cracks appear in one or more cross-sections. The size of the smallest concrete tensile strength and its distribution along the tension rod are random variables. In *Figure 1a* it was assumed that the weakest cross-section is at  $x_1 = 0$ .

If the concrete tensile strength of this member would be uniform, then infinitely many, infinitely narrow cracks would appear at infinitely small intervals. The cross-sections with the same lowest concrete tensile strength are at different distances from one another: in some areas they can be so close to one another that the transfer lengths extend into one another.

The steel stress in the cracked section is

$$\sigma_{sII} = N_1 / A_s = (1 + \alpha_E \cdot \rho) / \rho \cdot f_{ct1}$$

The concrete stress in the crack sinks to zero and increases on both sides of the crack, along the transfer lengths according to the bond forces: a crack unloads the concrete on both sides. *Figure 1b* shows the course of the concrete tensile stresses along the bar axis  $x > 0$  (with a dashed line shortly before, with a full line shortly after the occurrence of the first crack in the cross-section  $x_1 = 0$ ). The transfer length is  $l_{b1}$ .

If the tensile force is increased further, the stresses in the steel and in the concrete and the transfer lengths increase in the crack/on both sides of the cracks. When the tensile force  $N_2 = A_0 \cdot f_{ct2}$  is reached, a new crack will appear in the cross-

section at  $x_2$  which can be anywhere outside the transmission length  $l_{b2}$ . *Figure 1c* shows the distribution of the concrete stresses before and after the appearance of the 2<sup>nd</sup> crack.

It is quite possible that cross-sections with a concrete tensile strength

$$f_{cti} < f_{ctk} < f_{cti+1}$$

initially remain uncracked if they are in the transfer length of a crack. With the increase in the tensile force and the bond forces, it can happen that, due to the relieving influence of the adjacent primary crack, primary cracks will nevertheless occur in some of these cross-sections at a higher tensile force  $N > A_0 \cdot f_{ctk}$ .

This means that the smallest possible primary crack distance can also be smaller than the transfer length. At the tensile force  $N_3 = A_0 \cdot f_{ct3}$  a new crack will appear in cross-section  $x_3$  (see *Figure 1d*).

In our example, the transfer lengths that belong to the tensile force  $N_3$  overlap on both sides of the 3<sup>rd</sup> crack. Between the cracks No.1 and No.2, along the transfer lengths, there are no areas without any slip between concrete and steel. This still does not mean that the stabilized crack pattern is achieved.

In *Figure 2*, the phases of crack formation shown in *Figure 1* are shown axonometrically as a function of the tensile force  $N$ . The relieving effect of the neighboring cracks on the concrete stress, e.g. in cross-sections A and B, or the increase in the transfer lengths during the monotonically increasing load can be followed.

The loading process locates the "weak points" with the lowest concrete tensile strength of the concrete tension member. Of two otherwise identical reinforced concrete tensile members that are reinforced with reinforcing bars of different bond characteristics, the one with the better bond characteristics will have a denser crack pattern: the transfer lengths are shorter, so that shorter zones between the cracks that have already occurred are relieved, higher number of "weak points" will be loaded several beyond their current tensile strength.

### 3. FORCE- AND DEFORMATION PATTERNS BETWEEN TWO PRIMARY CRACKS

In this section, the patterns of the concrete-, steel- and bond stresses between two primary cracks whose transfer lengths overlap, are examined in more detail.

#### 3.1 Differential equation of the cracked tension member

From the equilibrium condition of a  $dx$ -long cracked tension member the relationship

$$d\sigma_s A_s = -d\sigma_c A_c \quad (1)$$

and the differential equation

$$d\sigma_s(x) A_s = \tau_v(x) u dx \quad (2)$$

can be derived

When deriving Eq. (1) it was assumed that the concrete

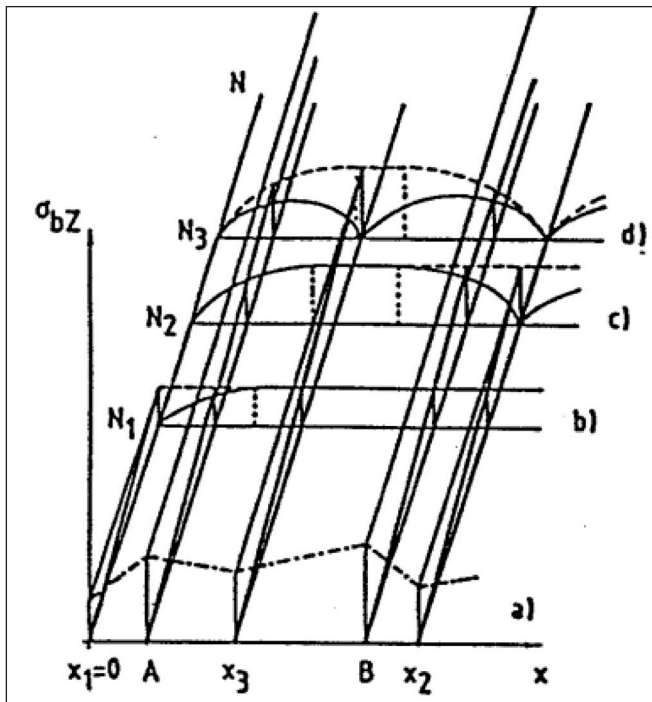


Figure 2: Phases of continuous crack development process

cross-sections would remain plain. This assumption is only permissible in case of limited cross-sectional dimensions - and there, too, only with reservations - because a constant transfer of force into the concrete takes place along the transfer lengths, so these concrete cross-sections are in the de Saint Venant- interference areas, where this assumption is inadmissible.

The Eq. (1) is not valid in the case of beams with flexure, because the eccentric compressive stresses in the cracked cross-sections, too, cause tensile stresses in the concrete tensile zone between the primary cracks.

Eq. (3) describes the compatibility condition:

$$dv/dx = (\sigma_s - \alpha_E \cdot \sigma_c) / E_s \quad (3)$$

This equation is also only valid under the assumption that cross sections remain plane.

From Eqs. (2) and (3) the differential equation

$$dv / d^2x = 4 \tau_v (1 + \alpha_E \rho) / (E_s d_s) \quad (4)$$

can be derived. When deriving Eq. (4) an elastic behavior of the reinforcing steel was assumed.

The bond-slip relationship is to be used in its most general form, whereby the influence of the hysteresis effect - a reversal of the initial relative displacements - is also taken into account.

### 3.2 Local bond stress-slip relationship

The local bond stress-slip relationship is of fundamental importance in the cracking process.

Rehm (1961) referred for the first time to the role of the relative displacement (slip) between reinforcing steel and concrete in the interaction of the two building materials and introduced the relationships between the local bond stress and the slip as a material law.

The local bond stress-slip relationship was determined using different embedded lengths and almost always under monotonically increasing tensile forces.

Experiments with cyclic tensile forces by Windisch et

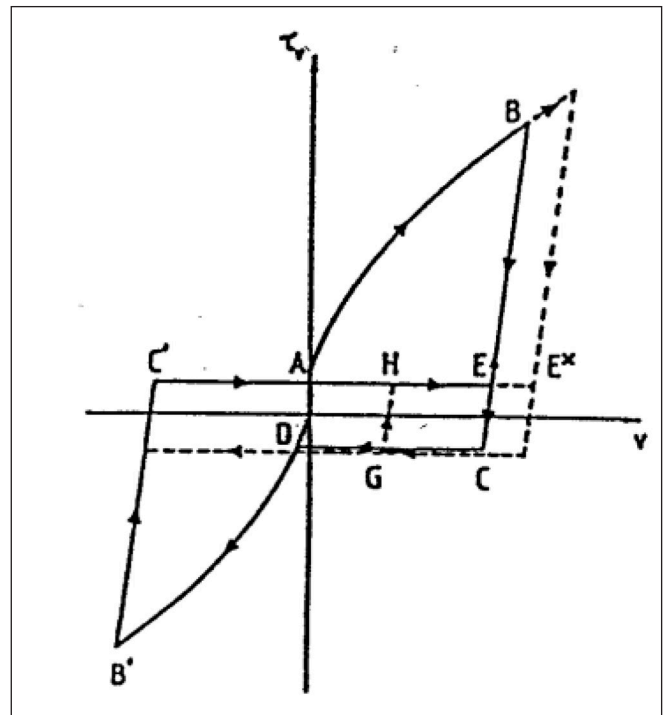


Figure 3: Local bond stress-slip relationship under generalized displacement states

al. (1983), Eligehausen et al. (1983) showed that when the sign of the slip is reversed, there are very steep unloading characteristics and very low bond stresses when there are slight opposite slips.

From more than hundred pull-out tests with cyclical loading (Windisch et al. 1983), using a refined evaluation method (Windisch 1985) the simplified local bond stress-slip relationship shown in Figure 3 was derived.

During the first loading phase (line OAB) the bond behavior can be described with the formula

$$\tau_v = \beta_w \cdot (a + b \cdot v^c) \quad (5)$$

This assumption corresponds to the formulas of Rehm (1961) and Martin (1973).

In the case of unloading, the law follows a straight line (line BC) with an inclination of 250 N/mm<sup>3</sup>. Hawkins et al. (1982) have given a similar value.

The remaining slip after an unloading can only be canceled by an opposing bond stress with the intensity of

$$\tau_v = -0.1 \tau_v(B).$$

If the tensile force or the slip is increased in the opposite direction (-v), the law follows the line DB' according to the formula

$$\tau_v = \beta_w \cdot (b \cdot v^c) \quad (6)$$

If the load is further reduced, the relationship between local bond stress and slip follows a straight line again with an incline of 250 N / mm<sup>3</sup> (line B'C'). Along the line C'E

$$\tau_v = -0.1 \tau_v(B')$$

applies.

If the slip reaches the line BE, the local bond force (bond stress) necessary to increase the slip increases according to the line BC. Eq. (5) is valid again beyond point B.

In the case of a new unloading, the bond stress-slip relationship follows the law shown with a dashed line.

If the sign of the slip changes at point G, the bond stress first follows the line GH with an inclination of 250 N/mm<sup>3</sup> and then the line HE\* etc.

Similar local bond-slip relationships have been proposed by Morita and Kaku (1975) and Tassios (1979), respectively.

In the following calculations, the “deterioration” of the bond in the vicinity of the crack and the scatter of bond strength are not taken into account.

### 3.3 Solution of the differential equation

When solving the differential equation (4), the corresponding boundary conditions must be taken into account. These boundary conditions change in part during the loading process.

The following applies to all primary cracks

$$\sigma_s = \sigma_{sII} = N / A_s \text{ and } \sigma_{ct} = 0 \quad (7)$$

and in the case of single cracks, at the other end of the transfer length ( $x = \ell_b$ )

$$\sigma_s = n \cdot \sigma_{ct} \text{ and } v = 0 \quad (8)$$

For tension rod areas between two primary cracks whose distance is smaller than twice the current transfer length,  $2 \ell_b$ , only the boundary conditions for both cracks are taken into account.

In view of the very complicated form of the composite law, a closed solution of the differential equation (4) is only possible for individual cracks (Noakowski, 1978, Krips, 1984). For all other cases a numerical solution is sought.

The algorithm is similar to the one used for beams on elastic subgrade.

Starting from a crack, the equilibrium and compatibility conditions are met in the end points of integration sections  $\Delta x$

$$\sigma_{s,i+1} = \sigma_{si} - 4 \cdot \Delta x \cdot \tau_{vi} / d_s \quad (9a)$$

$$v_{i+1} = v_i - \sigma_{s,i+1} \cdot \Delta x / E_s \quad (9b)$$

$$\sigma_{c,i+1} = \rho / (1 - \rho) \cdot (N / A_s - \sigma_{s,i+1}) \quad (9c)$$

In the case of the relative displacements (Eq. (9b)), the influence of the concrete deformations was neglected.

The rib spacing  $c_s$  is recommended as  $\Delta x$ .

The progressive approximation method was used to solve this algorithm. The principle of this method is that the actual boundary value problem is transformed into an initial value problem, whereby a variable in the starting point - here the relative displacement in crack No. 1 - is increased until the boundary conditions (7) or (8) for the other crack or are met at the other end of the transfer length.

### 3.4 The behavior of a tension member between two primary cracks

With the method described above, the behavior of a tension rod between two primary cracks was investigated.

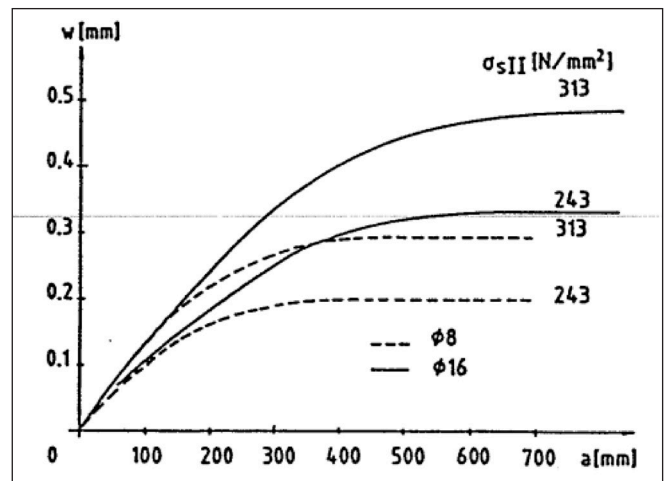


Figure 4: Crack width - crack spacing relationships as a function of the steel stress in the crack and the rebar diameter

As reinforcement, Ø8 mm or Ø16 mm deformed bars (rib spacing 5 mm or 8 mm) with a related rib area of  $f_{Rk} = 0.075$  were selected.

The two adjacent cracks at distance  $a$  may have occurred at the same load level or one after the other.

First, the course of the steel stresses and the crack widths as a function of the crack spacing and the steel stress in the crack for the case of two cracks occurring “simultaneously” are examined.

The courses of the concrete- and steel stresses are mirror-symmetrical, those of the bond stresses or the relative displacements (slips) are antimetric to the center of the crack spacing.

On the basis of the crack width - crack spacing relationships (concrete class B25, which roughly corresponds to C20) shown in Figure 4 the following can be observed:

At the beginning the crack widths increase disproportionately with the crack spacing, but are independent of this above a certain limit distance - it is twice the transfer length for the tensile force in the reinforcement bar in the crack

- for smaller ( $a \leq 150$  mm) crack spacings, the crack widths calculated for Ø16 mm rebars are hardly wider than those for Ø8 mm rebars
- The ratio of the largest crack widths for Ø16 mm and Ø8 mm rebars is only about 1.65: 1, i.e. the largest (critical) crack widths do not depend linearly on the rebar diameter.

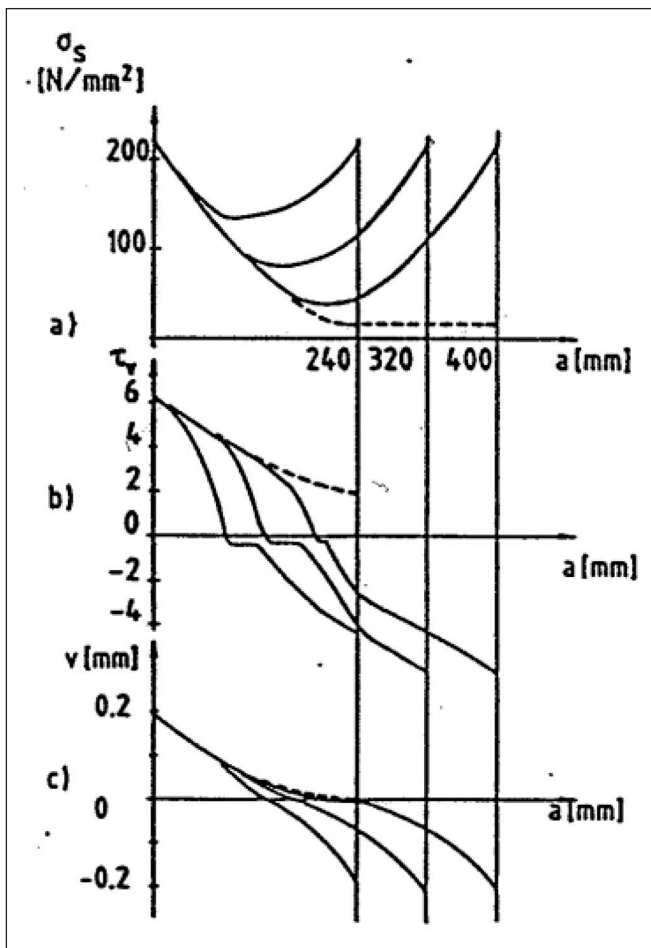
Between two cracks that occurred at different load levels, the stress or slip curves show completely different properties: there is no symmetry or antimetry more.

Figure 5 a - c show the courses of the steel- and bond stresses and the relative displacements (slips) shortly before (with a dashed line) and immediately after the appearance of the 2nd (right) crack as a function of the crack spacing.

The strong influence of the occurrence of the second primary crack and the crack spacing on all three courses is obvious. The contribution of the concrete increases as the distance between the cracks increases (see Figure 5a).

The following can also be assessed from the calculation results:

- When the second crack occurs, the width of the first decreases a bit, the more the “closer” the second crack is to the first,
- If the crack spacing is only slightly greater than the transfer length belonging to the tensile force which caused the second crack, then the width of this second crack is at



**Figure 5:** Courses of the steel stresses, slips and bond stresses in the case of cracks that do not occur simultaneously ( $\varnothing 16$  mm,  $\sigma_{sII} = 215$  N/mm<sup>2</sup>, concrete class B25, which roughly corresponds to C20)

the beginning smaller than that of the first. However, as the tensile force increases, the second crack becomes wider than the first one.

- Neither the steel-, nor the concrete stresses have their extreme (min. and max. resp.) at the middle of the crack distance. From this it follows that the crack spacing does not try to „halve“ itself regardless of the distribution of the concrete tensile strength. König and Fehling (1988) came to the same conclusion in a completely different way.
- The „closer“ the cracks are to one another, the longer will be the zone with the smallest bond stresses, the flatter are the steel- and concrete stresses around their extreme values.
- The smaller is the concrete tensile strength in the cross section of the second crack, the greater is the likelihood of another crack occurring between the two.
- The further the two cracks are apart, the more the crack width increases with the tensile force.

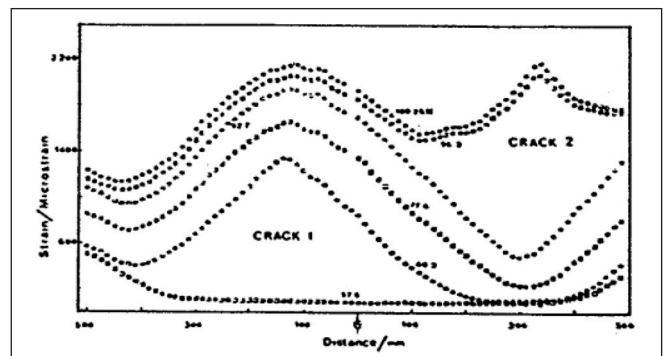
Figure 6 shows the steel strains measured along a r.c. tension member with  $\varnothing 20$  mm reinforcement according to Scott and Gill (1987). The similarity to the stress curve in Figure 5a is obvious.

Figure 7 shows the calculated crack widths as a function of the crack spacing. The straight lines correspond to

$$w = a \cdot \sigma_{sII} / E_s$$

i.e. the pure steel expansion without the contribution of the concrete. The following conclusions can be drawn:

- The relatively small crack distances include several crack



**Figure 6:** Measured steel strains in tensile reinforcement according to Scott and Gill (1987)

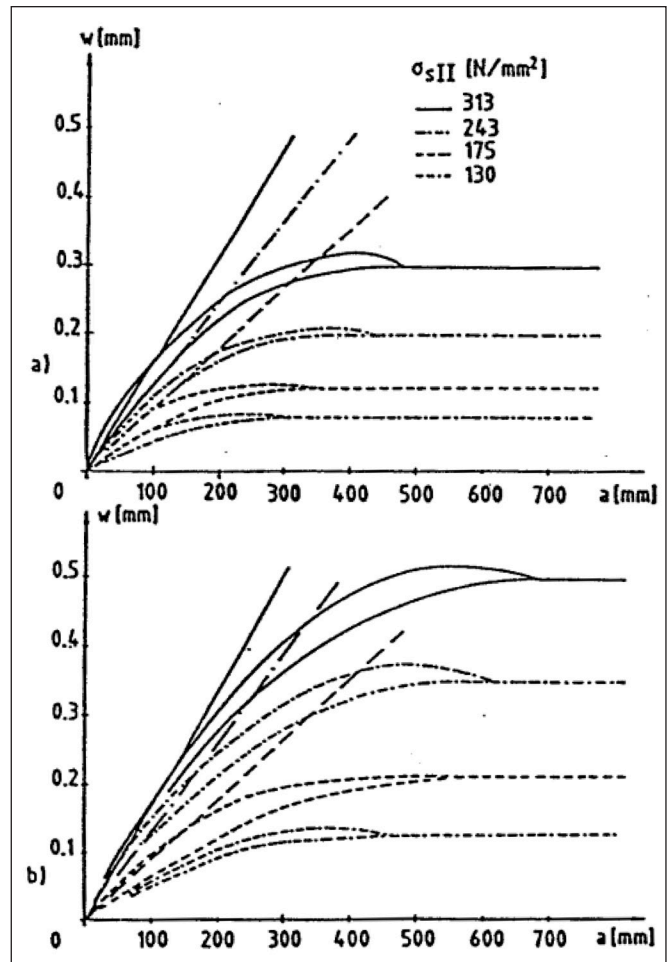


**Figure 7:** Calculated crack widths for a)  $\varnothing 8$  mm, b)  $\varnothing 16$  mm rebars

widths, the size of which depends on whether the adjacent cracks occurred at the same or different tensile forces.

- The crack widths first increase with the crack spacing, above a crack spacing which corresponds to twice the transfer length for  $N = \sigma_{sII} \cdot A_s$ , the function becomes monovalent.
- The transfer lengths are not linear, neither on the bar diameter nor on the steel stress.

All calculation results discussed so far have been determined for concrete class B25, (which roughly corresponds to C20).

Figure 8 shows the influence of the concrete quality on the crack width for a tension member with  $\epsilon = 1$  ‰, reinforced with  $\varnothing 8$  mm or  $\varnothing 16$  mm rebars. For this numerical example, 300 mm or 480 mm crack spacings and the tensile force at the appearance of the first crack  $N = A_0 \cdot f_{ctm}$  were assumed. The following could be concluded:

- The steel stress at the crack development is higher than  $\sigma_{sII} = 243$  N/mm<sup>2</sup> for concrete classes B35 (which roughly

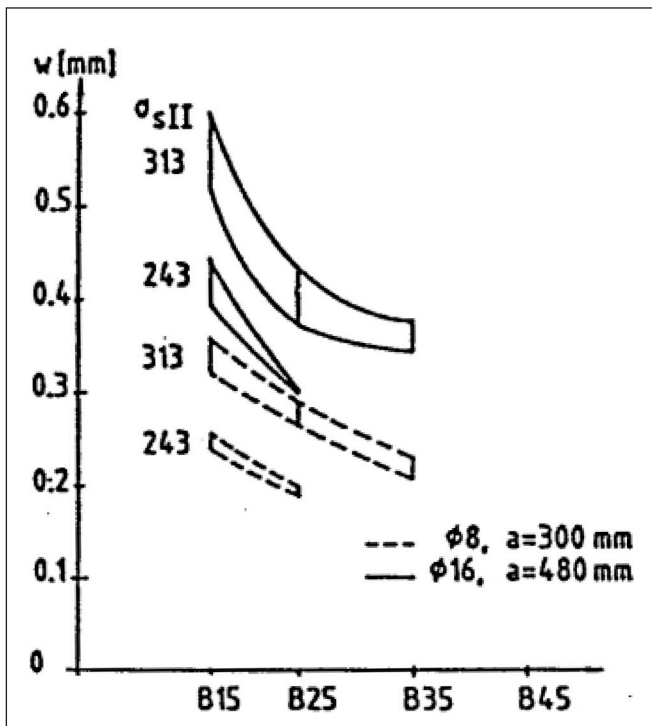


Figure 8: Influence of the concrete strength on the crack width, I.

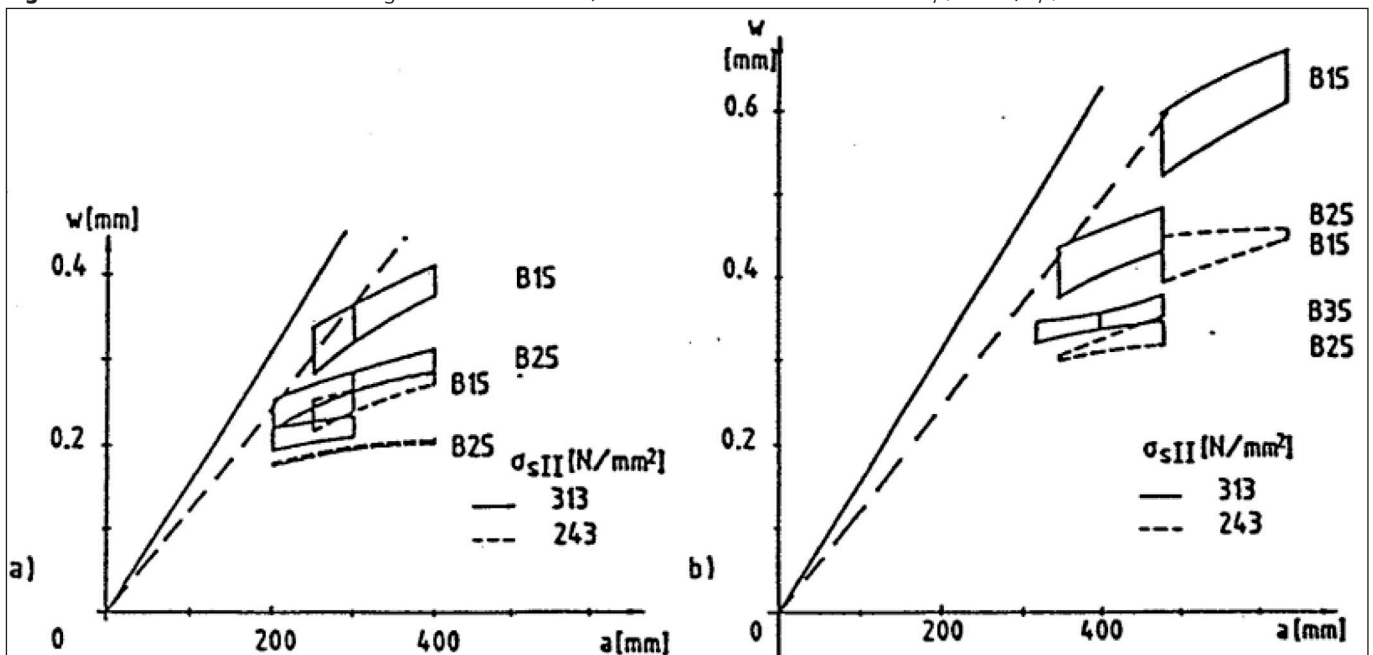
corresponds to C30) and B45 (which roughly corresponds to C35), and even higher than 313 N/mm<sup>2</sup> for concrete class B45, so these tension members remain crack-free at these steel stresses.

- An increase in concrete strength reduces the crack width disproportionately.

Figure 9 shows the influence of the concrete strength on the crack width as a function of the crack spacing and the steel stress in the crack,  $\sigma_{sII}$ .

The two straight lines represent the 'naked' elongation of the reinforcing bars. With increasing concrete strength, at constant crack spacing, the increase in the contribution of the concrete can be observed: the higher the concrete strength, the shorter is the transfer length, whereby it approaches the constant crack spacing and accordingly the concrete contribution increases.

Figure 9: Influence of the concrete strength on the crack width, II: tensile members reinforced with a) Ø8 mm, b) Ø16 mm rebars



## 4. CONCLUSIONS

The steel stress distribution between two primary cracks which occur at different load levels and at different distances from each other, is presented. The continuous crack formation is discussed where the stochastic distribution of the actual concrete tensile strength along the axis of the member in axial tension is considered.

Solving the differential equation of the bonded rebar a realistic local bond stress-slip relationship is taken into account where the hysteretic character of the relationship when the sign of local slip changes due to the occurrence of a new primary crack, is considered.

The calculations for Ø8 mm and Ø16 mm rebars and B 25 (which roughly corresponds to C20) concrete grade reveal that

- at the beginning the crack widths increase disproportionately with the crack spacing, but are independent of this above a certain limit distance, it is twice the transfer length for the tensile force in the reinforcement bar in the crack
- for smaller ( $a \leq 150$  mm) crack spacings, the crack widths calculated for Ø16 mm rebars are hardly wider than those for Ø8 mm rebars
- The ratio of the largest crack widths for Ø16 mm and Ø8 mm rebars is only about 1.65: 1, i.e. the largest (critical) crack widths do not depend linearly on the rebar diameter.
- The strong influence of the occurrence of the second primary crack and the crack spacing on the courses of steel stresses, bond stresses and slips is obvious.
- The contribution of the concrete increases as the distance between the cracks increases
- When the second crack occurs, the width of the first one decreases a bit, the more „closer“ the second crack is to the first one,
- If the crack spacing is only slightly greater than the transfer length belonging to the tensile force which caused the second primary crack, then the width of this second crack is at the beginning smaller than that of the first crack. However, as the tensile force increases, the later primary crack becomes wider than the first one.
- Neither the steel-, nor the concrete stresses have their

extreme (min. and max. resp.) at the middle of the crack distance. From this it follows that the crack spacing does not try to „halve“ itself regardless of the distribution of the concrete tensile strength.

- The „closer“ the cracks are to one another, the longer will be the zone with the smallest bond stresses, the flatter are the steel- and concrete stresses around their extreme values.
- The smaller is the concrete tensile strength in the cross section of the second crack, the greater is the likelihood of another crack occurring between the two.

These realistic courses of the steel stresses, slips and bond stresses should help to develop mechanically founded crack width calculation models.

## 5. ACKNOWLEDGEMENT

The author is extremely grateful to Professor Rehm, who has monitored and actively supported his scientific and professional work for more than 40 years.

## 6. REFERENCES

- Eligehausen, R., Popov, E.P., Bertero, V.U., (1983), „Local Bond Stress-Slip Relationships of Deformed Bars under Generalized Excitations“ *Report No. UCB/EERC-83/23*, University of California, Berkeley.
- Hawkins, N.M., Lin, I.J., Jeang, F. L., (1982) „Local bond strength of concrete for revised cyclic reversed loading“, In: *Bond in Concrete*, Applied Science Publishes, London, pp. 151-161.
- König, G., Fehling, E., (1988) „Zur Rissbreitenbeschränkung im Stahlbetonbau“, *Beton- und Stahlbetonbau* 83, Heft 6, pp. 161-167. <https://doi.org/10.1002/best.198800270>
- Krips, M., (1984) „Rissbreitenbeschränkung im Stahlbeton und Spannbeton“, Dissertation, Darmstadt.
- Martin, H., (1973), „Zusammenhang zwischen Oberflächenbeschaffenheit und Sprengwirkung von Bewehrungsstäben unter Kurzzeitbelastung“, *Schriftenreihe des DAfStb*, Heft 228.
- Morita, H., Kaku, T., (1975) „Cracking and deformation of r.c. prisms subjected to tension“, *Proceedings*, CEB-CIB-FIP-IASS-RILEM Symposium on Behavior in Service of Concrete Structures, University of Liège, 1975, V. 2, pp. 583-594.
- Noakowski, P., (1985), „Verbundorientierte, kontinuierliche Theorie zur Ermittlung der Rissbreite“, *Beton- und Stahlbetonbau*, Heft 7, pp. 185-190, and Heft 8, pp. 215-221. <https://doi.org/10.1002/best.198500410>
- Rehm, G., (1961), „Über die Grundlagen des Verbundes zwischen Stahl und Beton“, *Schriftenreihe des DAfStb*, Heft 138.
- Scott, R.H., Gill, P.A.T., (1987), „Short-term distribution of strain and bond stress along tension reinforcement“, *The Structural Engineer*, Vol. 65 B/ No. 2, S. 39-48
- Tassios, T.P., (1979), „Properties of bond between concrete and steel under load cycles idealizing seismic actions“, *Bulletin d'Information* No. 131, CEB, Paris S. 65-122.
- Windisch, A., Balázs, G., Szalai, K., Orosz, Á., „Local bond stresses – slip relationships for different deformed rebars“, *Research report* (in Hungarian) No. 232.019/8 TU Budapest, 133 p.
- Windisch, A., (1985), „A Modified Pull-out Test and a new evaluation for a more real local bond-slip relationship“, *Matériaux et Constructions*, Copy 3, S. 181-184. <https://doi.org/10.1007/BF02472967>
- Windisch, A., (1989), „Characteristic crack widths in tensile and flexural elements“, *Materials and Structures II*. (Zur Berechnung von kritischen Rissbreiten in Zugstäben und Biegebalken. *Werkstoff und Konstruktion II*.) Prof. Rehm 65. birthday, ibidem-Publisher. Stuttgart, pp. 241-261. (in German)
- Windisch, A. (2016), „Crack control: An advanced calculation model – Part I: Review of classic tests“, *Concrete Structures*, 2016, pp. 41-48,
- Windisch, A., (2017), „Crack control: An advanced calculation model - Part II: The model“, *Concrete Structures*, 2017, pp. 40-47.

**Andor Windisch PhD, Prof. h.c.** retired as Technical Director of Dywidag-Systems International in Munich, Germany. He made his MSc and PhD at Technical University of Budapest, Hungary, where he served 18 years and is now Honorary Professor. Since 1970 he is member of different commissions of FIP, CEB and *fib*. He is author of more than 180 technical papers. Andor.Windisch@web.de

# RADIATION SHIELDING STRUCTURES: CONCEPTS, BEHAVIOUR AND THE ROLE OF THE HEAVY-WEIGHT CONCRETE AS A SHIELDING MATERIAL - REVIEW



Suha Ismail Ahmed Ali - Éva Lublóy

<https://doi.org/10.32970/CS.2020.1.4>

The construction of radiation shielding buildings still developed. Application of ionizing radiations became necessary for different reasons, like electricity generation, industry, medical (therapy treatment), agriculture, and scientific research. Different countries all over the world moving toward energy saving, besides growing the demand for using radiation in several aspects. Nuclear power plants, healthcare buildings, industrial buildings, and aerospace are the main neutrons and gamma shielding buildings. Special design and building materials are required to enhance safety and reduce the risk of radiation emission. Radiation shielding, strength, fire resistance, and durability are the most important properties, cost-effective and environmentally friendly are coming next. Heavy-weight concrete (HWC) is used widely in neutron shielding materials due to its cost-effectiveness and worthy physical and mechanical properties. This paper aims to give an overview of nuclear buildings, their application, and behaviour under different radiations. Also to review the heavy-weight concrete and heavy aggregate and their important role in developing the neutrons shielding materials. Conclusions showed there are still some gaps in improving the heavy-weight concrete (HWC) properties.

**Keywords:** neutron shielding, heavy-weight concrete, heavy aggregates, Gamma rays

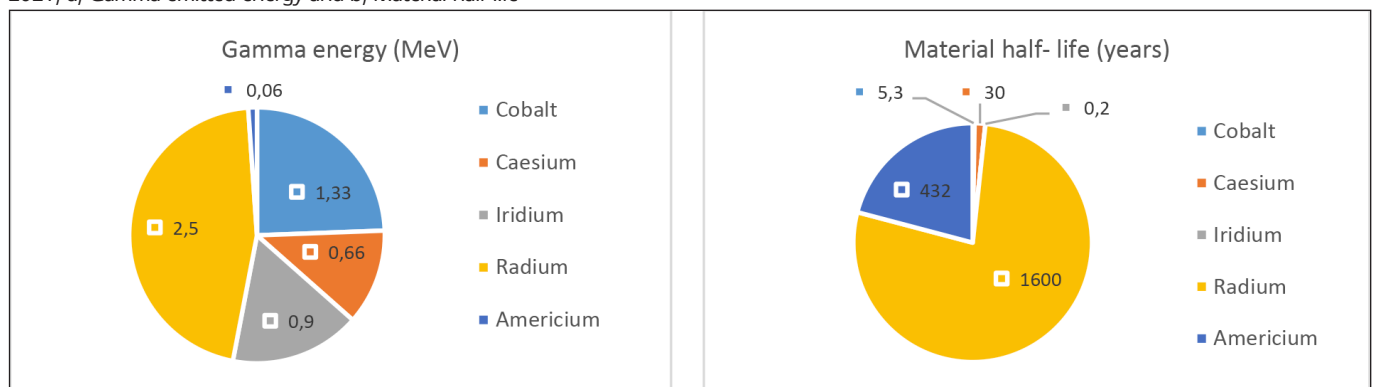
## 1. INTRODUCTION

Radiation is the emission of energy (wave) in space or an object. Radiation can be classified into ionizing radiation and non-ionizing radiation. Non-ionizing radiations are the radio, TV, ultraviolet, infrared, visible light, and power transmission, while ionizing radiation is the X-ray and gamma radiations. The application of ionization radiation is in nuclear power, medical diagnostics, cancer treatment, scientific research, and the aerospace industry. Nevertheless, structure elements of radioactive shielding structures must be shielding against high-energy neutron emission (Outline, 2018).

Application of Gamma/X-ray and neutron sources in nuclear, medical, and industrial sectors still developed. Reports showed there are 449 nuclear reactors in 30 countries and 60 nuclear power plants under construction in 15 countries in addition to more than 10.000 medical therapeutics over the world. Nuclear buildings or nuclear power plants are one of the most complex and dangerous structures. Special construction elements are used for shielding against ionization radiation (Jo, 2019; Kurtis et al., 2017).

Examples of the gamma-emitting radionuclides and their properties of emitted gamma energy and half- lifetime are shown in Fig. 1. Radium has the highest energy amount and

**Fig. 1:** Properties of (Cobalt  $^{60}\text{Co}_{27}$ , Caesium  $^{137}\text{Cs}_{55}$ , Iridium  $^{192}\text{Ir}_{77}$ , Radium  $^{226}\text{Ra}_{88}$ , and Americium  $^{241}\text{Am}_{95}$ ) radionuclides among Based on (Ban et al., 2021) a) Gamma emitted energy and b) Material half-life



a longer half-life. Americium has a lower energy amount and Cesium has a shorter half-life (Ban et al., 2021).

## 1.1 Application of neutron shielding structures with different neutron energy and shielding materials

Application of neutron shielding materials in different sectors are varied with the amount of neutron energy, the weight of the structure, safety, and economic issues. Fig. 2 illustrates the potential emitted energy in nuclear power plants, nuclear radiotherapy, hospitals, and aerospace. Concrete, metal, and polymers can be used in the construction of the walling elements (Zinkle, Busby, 2009).

In nuclear buildings, the emitted energy neutrons are relatively high that exceeding 2 MeV, so proper shielding is required to ensure the safety of the worker and environment. High density or heavy-weight concrete walls with some additives of moderator and polymers can slow the absorption of the high-energy neutrons. In medical structures, photo energy neutrons range between (25- 10 MeV) are used in the therapy treatment can hazard the patients and staff. Concrete, metal-based, and polymer-based can ensure effective protection for patients and workers (Sukegawa et al., 2014; Walsh, 2013).

Extraordinary shielding materials are required in the aerospace industrial sectors. Cosmic rays in aerospace contain high-energy neutrons and protons (>1 MeV to 1 GeV) and high atomic nuclei, so polymer composites are suitable for their shielding and lightweight properties (Zinkle and Busby, 2009; Sukegawa et al., 2014; Walsh, 2013).

## 1.2 Neutron penetration system

Neutrons interact with the material in three different phenomena, inelastic scattering, elastic scattering, and neutron absorption. Inelastic scattering occurred when a fast neutron exceeding 10 MeV interact with the nucleus. Elastic scattering occurs when neutrons with energy between 1 and 10 MeV lose their high energy neutrons and then the remained energy is kept inside the structure element. Thermal neutrons are slow energy neutrons thermalized by the nucleus during the absorption process, so no emission will occur (Fig. 3).

The concept of the process that neutrons work on exciting the nucleus then the liberation of gamma rays and alpha rays

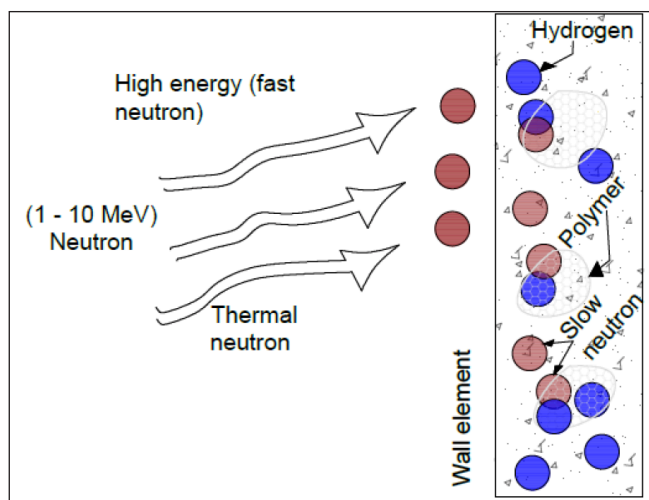


**Figure 3.** Neutron penetration system, based on (Abdulrahman et al., 2020; Jaeger et al., 1968)

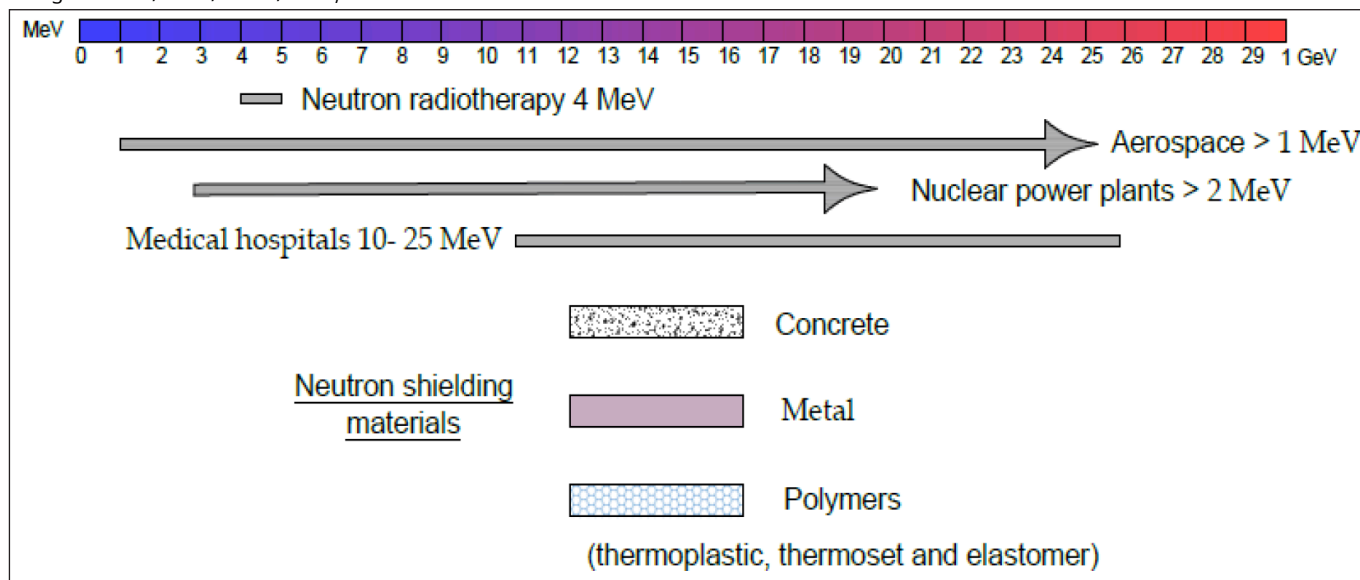
occurred. One of the traditional mechanisms works on decelerating the fast neutron to decrease the energy inside the medium. Slow neutrons need an absorbing element with a large cross-section. However, absorbed neutrons need alternative equal mass such as hydrogen (Abdulrahman et al., 2020; Jaeger et al., 1968).

## 1.3 Gamma ( $\gamma$ ) rays, X- rays, and neutrons radiations

Gamma ( $\gamma$ ) rays are high-frequency electromagnetic radiation. It has 100 keV energy amount and less than 10 pm wavelength. Gamma-ray is an indirect ionization source and it affects human cells. Gamma rays are weakened by interactions with electrons, hence concrete with high density can be used as a gamma- shielding material. Shielding against Gamma-ray can be achieved by using materials with a heavy atomic weight such as heavy-weight aggregates (Lessing, 2019).

Neutron radiation governed by the kinetic energy of the neutrons affects the nuclei of atoms. Neutrons are classified into thermal neutrons (lower than 1 eV), epithermal neutrons (between 1 eV and 0.1 MeV) and fast neutrons (above 0.1 MeV). Neutron shielding concrete is design to slow down fast neutrons and thermalize or capture thermal neutrons. It must be thermalized by the hydrogen atom in water and captured

**Figure 2.** Neutron shielding buildings according to the amount of energy and shielding materials based on (Zinkle and Busby, 2009; Sukegawa et al., 2014; Walsh, 2013)



by a boron atom (Jo, 2019). Concrete can be used as shielding materials for both gamma and neutron radiations. Protection against Gamma radiation depends on the density of materials while protection against neutrons (neutron energy/ speed) depends on the nuclei of the atom. The basic functions of the radiation shielding concrete are strength, durability, attenuation of gamma and neutron radiations, and thermal insulation (Piotrowski, 2020).

## 1.4 Radiation attenuation coefficient

The Beer-Lambert law is used in the calculation of the intensity of the radiation transmission. The thickness of the shielding material can be determined with an equation (Piotrowski, 2020):

$$I = I_0 e^{-\mu x}$$

where  $I_0$  is the radiation intensity before and after radiation transmission,  $\mu$  is the linear attenuation coefficient and  $x$  is the shielding thickness of the material. Linear attenuation coefficient proportion directly to the density and the atomic number of the material and inversely to the energy of the neutrons.

The effective atomic number can be calculated using the equation:

$$Z_{eff} = \frac{\sum \sigma_i f_i A_i \frac{\mu}{\rho}}{\sum \sigma_i f_i \frac{A_i}{Z_i} \left(\frac{\mu}{\rho}\right)_i}$$

where is  $f_i$  the ratio of the element number to the total element numbers in the material,  $A_i$  is the atomic weight and  $Z_i$  is the atomic number of the material.

## 2. HEAVY-WEIGHT CONCRETE (HWC) AS GAMMA/NEUTRON SHIELD

Concrete is one of the most used building materials all over the world. Examples of concrete structures are residential buildings, dams, bridges, power plants, and other infrastructures. Concrete is a mixture of cement, sand, stone (aggregate), and water. Concrete has high compressive strength and low tensile strength, that's why steel bar is added to develop the tensile strength (Brook, 1989). Heavy-weight concrete can be produced using a heavyweight aggregate. Heavy-weight concrete represents cost-effective, strength, attenuation radiation, and fire-resistance construction materials; it's useful for the construction of the nuclear building. Concrete with a high hydrogen atom is effective against neutron radiation, while concrete with a high water ratio is effective against both neutron and gamma radiations (Lessing, 2019).

### 2.1 Ingredients of concrete

Cement is the binding material in concrete; it represents 15 to 25 % of the total weight of the concrete. Water/ water-cement ratio are important parameters at the fresh and hardened phases of the concrete. Fresh concrete should have good workability and consistency properties, while hardened concrete should have sufficient compressive strength and durability. Aggregate represents the major part of concrete (about 70 –

80%). Fresh concrete must satisfy the workability and consistency properties while hardened concrete must have adequate strength, durability. The water to cement ratio is an important factor in the concrete mix, it could enhance the workability and reduce the performance of concrete. Other materials can be added to concrete to improve its performance; these materials are called admixtures (McArthur, Spalding, 2004).

### 2.2 Aggregates

Aggregate occupies the major part of concrete, (three to fourth) volume of concrete. The specific gravity of aggregates is the factor that controlling the unit weight of concrete. Some advantages of using aggregate are the economy, volume stability, density, and durability. The specific density of aggregate affects the unit weight and the strength of the concrete, while its absorption influences the durability of the concrete (Popovics, 1992).

Aggregates can be natural or manufactured, heavy or light-weight, crushed or naturally processed, inactive or reactive; and fine or coarse aggregates. The dividing line between fine and coarse aggregates is randomly chosen, but usually 4 mm site sieve (opening of 3/16 in (4.75 mm)) separates the two types.

Heavy-weight aggregates or minerals with a high specific gravity greater than 3.5, such as barite, magnetite, ilmenite, limonite, and goethite are mostly used, others are chromite, hematite, taconite, and galena, are not broadly used (Table 1). Ferrophosphorus and ferrosilicon could be used. Otherwise, steel and iron aggregates are available in the forms of shot, punching, and scrap (Popovics, 1992).

Some of the aggregate with high specific gravity, are magnetite, ilmenite, limonite, ferrophosphorus, or of steel shot, etc. The density of the concrete with mineral aggregates is over (200 lb/ft<sup>3</sup>) 3200 kg/m<sup>3</sup>, while the density of concrete with steel fibre aggregates can reach up to (400 lb/ft<sup>3</sup>) 6400 kg/m<sup>3</sup>. Concrete with heavy-weight aggregate can use as a shielding material, due to the combination of radiation absorption and good mechanical properties (Table 1).

*Chemically bound water content and the specific gravity of aggregates*

Hydrogen occurs in different forms in cementitious composition free water or chemically bounded (constitutive water) and embedded in the chemical structure of some aggregates; such as goethite (FeO (OH)) and limonite (2Fe2O3.3H2O). The content of free and embedded water content can be determined by thermogravimetric testing.

There are three types of specific gravity of aggregates (Leung, 2001): Bulk specific gravity, bulk specific gravity (saturated surface dry), and apparent specific gravity. Bulk specific gravity (saturated surface dry) can be determined using the equation:

$$G_{bssd} = \frac{B}{B - C}$$

where

A = weight of oven-dry aggregate sample in air  
B = weight of saturated surface-dry sample in air  
C = weight of saturated sample in water.

There are two states of moisture in aggregates; total moisture and surface moisture. Total moisture can be less than adsorp-

**Table 1:** Physical properties and radiation absorption factors of heavy-weight aggregates

Heavy-weight aggregate	Composition % by weight		Specific gravity (gm/cm <sup>3</sup> )		Concrete density lb/ft <sup>3</sup>	Radiation absorption factor cm <sup>2</sup> /g	
	Iron	Fixed water	Coarse	Fine		Fast neutrons	Gamma rays (3 MeV)
Limonite	58	9	3.75	3.80			
Goethite (hydrous iron ore)	55	11	3.45	3.70	180 - 200	0.0372	0.0362
Magnetite (iron mineral)	64	1	4.62	4.68	210 - 260	0.0258	0.0359
Barite (barium sulfate)	1-10	0	4.20	4.24	210 - 230		
	1	0	4.28	4.31		0.0236	0.0363
Ferro-phosphorus (slag)	70	0	6.30	6.28	255 - 330	0.0230	0.0359
Steel aggregate	99	0	7.78	-	290 - 380	0.0214	0.0359
Steel shot	98	0	-	7.50			

From Davis, *ACI Journal*, American Concrete Institute (Davis, 1962)

tion capacity in (oven and air dry) aggregates, less than or equal to the absorption capacity in (saturated) aggregates, or greater than absorption capacity in (wet) aggregates. The term saturated in aggregates means (surface saturated), because it considered only the quantity of water absorbed during 24- hr. So only the outside part of the aggregate is saturated (Leung, 2001).

## 2.3 Admixtures

Admixture can be added to the cement, water, and aggregate mixture to improve the workability, mechanical and shielding properties, and durability of the concrete. Admixtures can be categorized into chemical and mineral admixtures.

Chemical admixtures can be divided into surfactants, and set-controlling admixtures. Surfactants are long-chain organic molecules and they must be added in a small amount (< 1wt. %). Air- entraining agent, water-reducing admixture, and superplasticizer are some of the surfactants. The function of the air-entraining is to add small bubbles, so the defrost resistance can be improved. Water reducing surfactant work on releasing the inside captured water after diffusing charges into the cement and water paste. Superplasticizer is most effective on the water reduction prospect, and applicable on the production of high-strength and high-workability concrete. Set controlling admixtures are used for the purpose of retard or accelerate the hydration reaction on the cement and water mixture. It could be useful in reducing the degradation of concrete.

Minerals admixture are available in nature and can be added in a large amount compared to the chemical admixture about (> 10 wt. %). Some of the minerals admixtures are fly ash, blast furnace slag, and silica fume. Mineral admixtures have cementitious properties. It can be added to replace part of the cement in concrete. Consequently, the thermal behavior, ultimate strength, and durability will be developed in addition to the cost-effective benefit (Leung, 2001).

## 3. REVIEW AND ANALYSIS OF THE PAST FINDINGS

A review on the (Modern heavyweight concrete shielding: Principles, industrial applications, and future challenges) was handled by (Ban et al., 2021). The study introduced the future challenges and current limitations of research on the HWC as radioactive shielding material and the development of its

shielding capabilities. Recent studies showed that there is a direct proportion between the attenuation of gamma and neutrons radiation and the atomic (mass) number of the shielding material. There is some shortage of research on improving heavy-weight concrete by using natural or artificial heavy-weight aggregates or using more than one type of aggregates. No research on the effect of reducing the water/cement ratio on the attenuation coefficient, the lower reported ratio was 0.35. There is a scarcity of research on using the combination of using (nanoparticles, crack control, and elevating Z the atomic number to improve the resistance of the (HWC). No enough prior research on the shielding capabilities of the (HWC) on the elevated temperature up to 800 °C as well as the correlation between the thermal conductivity of the materials with the other shielding properties.

Akkurt et al. (2010) investigated the radiation shielding of the normal, Pumice, and barite aggregates, using the image processing techniques (IPT). The final results were compared to the calculated values using XCOM. Results showed that the linear attenuation coefficients increase with the density of the material. A good correlation was found to the calculated results, so (IPT) can be used as an alternative method for radiation shielding investigations. *Aslani et al.* analyzed the mechanical properties of the fibre-reinforced heavy-weight self-compacting concrete. Hooked end steel and polypropylene (PP) fiber (60, 65mm length and 0.75, 0.85 mm Dia.) were added as fibre, while magnetite was used as heavy aggregate (75- 100 %). The final results demonstrated the possibility of the production of heavyweight self-compacting concrete (HWSCC) with steel and (PP) fibres. Magnetite aggregates have higher water absorption than the normal aggregates, however, substitute the (NWA) with the (HWA) will reduce the compressive strength due to the crystallized microstructure of (HWA), high water absorption, and segregation. Adding 0.75 steel fibre and 0.25 (PP) will improve the compressive strength.

Aygün et al. (2021) developed new heavyweight (chromium ore) concrete for nuclear shielding radiations, based on the different type of minerals of (chromium ore, hematite (Fe<sub>2</sub>O<sub>3</sub>), titanium oxide (TiO<sub>2</sub>), limonite (FeO (OH) nH<sub>2</sub>O), and siderite (FeCO<sub>3</sub>) and compounds (galena (PbS), chromium oxide (Cr<sub>2</sub>O<sub>3</sub>) and manganese oxide (MnO<sub>2</sub>)). Experiments were used to investigate the mechanical and temperature resistance properties, while GEANT4 were used in the simulation of the mass attenuation coefficient and the effective atomic number. Results showed the developing of the compressive strength up to 30 MPa, and resistance under

**Table 2:** Results for some of the tested parameters of the reviewed literature

Author	Type of aggregates	Methods and Tested Parameters	Age	Strength (MPa)		Behaviors on elevated temperature		Linear attenuation coefficient (cm <sup>-1</sup> )/ Mass attenuation coefficient (cm <sup>2</sup> /g)
				Compressive	Flexural	Temp (°C)	Density kg/m <sup>3</sup>	
(Azreen <i>et al.</i> , 2018)	Steel fibre reinforced with different inner materials (silica sand, amang, and lead glass)	Experiments Mechanical properties, and Radiation absorption capabilities	28 days	(165.7, 157.5, and 170.1) at 28 days age	(30.7, 28.8, and 28.3) at 28 days age			Linear <sup>137</sup> Cs (0.155, 0.182, 0.175) at 0.662 MeV <sup>60</sup> Co (0.096, 0.112, 0.106) at 1.173 and 1.333 MeV
(Binici <i>et al.</i> , 2014)	Mortar Additives of colemanite (C <sub>0.25</sub> ), barite (B <sub>2.5</sub> ), ground basaltic pumice (P <sub>2.5</sub> ), and ground blast furnace slag (S <sub>2.5</sub> ) with different replacement.	Experiments - Mechanical Properties. - Radiological absorption capabilities	28 days	C (51.8), B (47.8), P (47.3) and S (51.3)	C (7.1), B (6.9), P (6.8) and S (7.3)			Linear C (0.08), B (0.25), P (0.1), and S (0.06) at 59.60 keV
			180 days	C (63.9), B (59.7), P (58.3) and S (64.4)	C (8.4), B (8.3), P (7.7) and S (8.4)			
(Demir <i>et al.</i> , 2011)	Barite (B), colemanite (K), and normal aggregate (N) 13 Mixtures Selected (B100, B85K15, N85K15, and N 100)	Experiments - Radiation transmission - Linear and mass attenuation coefficient				Room Temperature	(3451, 3208, 2157, and 2310)	Linear <sup>137</sup> Cs (0.261, 0.248, 0.185, and 0.187) at 0.663 MeV Mass (0.076, 0.077, 0.086 and 0.081) at 0.663 MeV
(Rasoul Abdar Esfahani <i>et al.</i> , 2021)	Ground granulated blast furnace slag (GGBFS) and copper slag (CS) with percentages of GGBFS (0–60%) and CS (0–100%) G30C50 and G60C100	Experiments Mechanical properties and Radiation absorption capabilities	28 days	43.2 and 32.4		Room temperature	2555 and 2845	<sup>137</sup> Cs (0.296 and 0.333) <sup>60</sup> Co (0.141 and 0.156)
								Thermal Conductivity (W.m <sup>-1</sup> )
(Beaucour <i>et al.</i> , 2020)	Dolomite (NWA) as reference concrete (REF), Barite aggregate (BAR), and Electric Arc Furnace (EAF) steel slag	Experiments Behaviour at high temperature (TGA/DSC), Thermal stability, thermal conductivity during heating, and mechanical properties	90 days	49, 47, and 65 MPa		20 °C	2401, 2766, and 2805	2.05, 1.34 and 1.51
				35, 40, and 49 MPa		150 °C	2600	1.75, 1.4, and 1.3
				36, 30, and 40 MPa		300 °C	2600	1.3, 1.0, and 0.9
				10, 25, and 39 MPa		450 °C	2500	1.5, 1.25, and 1.1

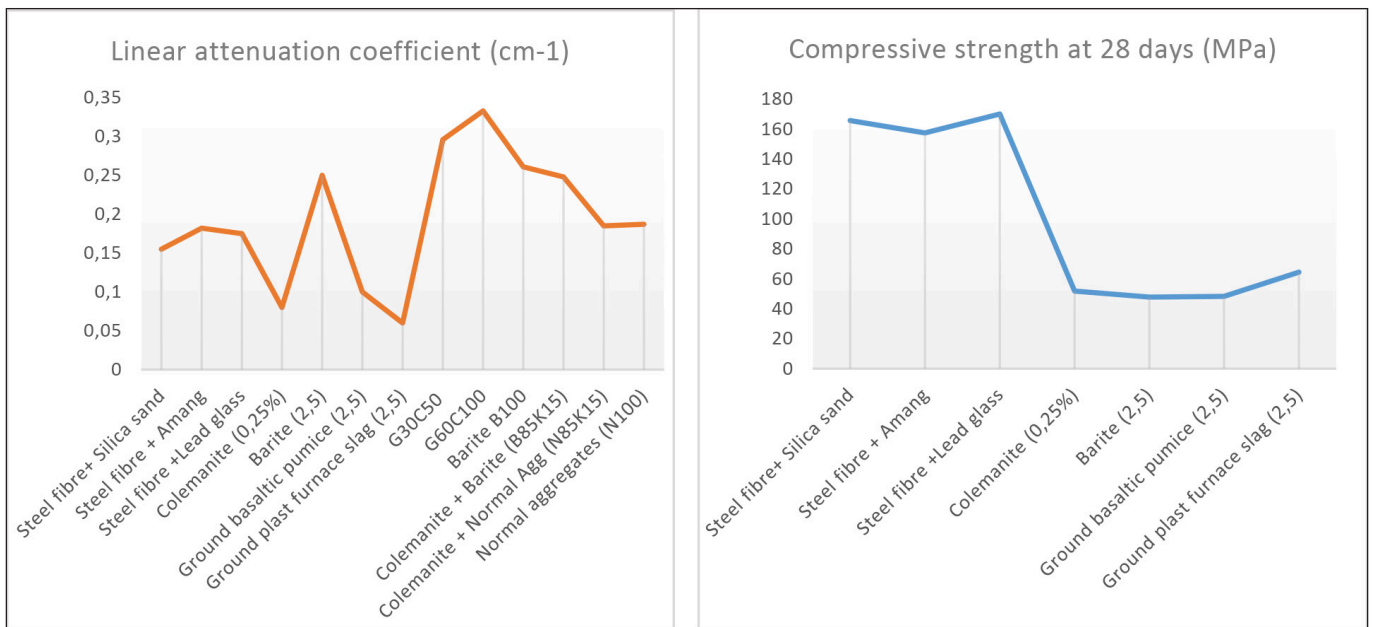


**Figure 4.** Values of the linear attenuation coefficient and the compressive strength of the reviewed literature

temperatures are up to the desired level. The study verified that concrete with aggregates and additives are better gamma and neutron shielding than the standard (HWC).

Azreen et al. (2018) tested the mechanical properties and the radiation absorption capabilities of the steel fibre-reinforced as ultra-high-performance concrete (UHPC) and the effect of adding, silica sand, amang, and lead glass. The tested samples showed compressive strength values higher than 155 MPa at 28 days. The compressive strength of the lead glass sample decrease for a long time. Amang is effective against Gamma rays due to its high density, but it has a radiological effect on the surroundings. Silica sand is most practical for nuclear buildings and cost-efficiency (Table 2).

Binici et al. (2014) investigated the mechanical and radioactivity shielding performance of mortars made with colemanite, barite, ground basaltic pumice, and ground blast furnace slag as additives to create special mortars. The final results showed that barite, colemanite, and blast furnace slag wastes are effective in gamma-ray shielding. The linear absorption coefficient decreased with increasing the colemanite percentage in the sample. Samples with blast furnace slag have low radioactive permeability (Table 2).

Demir et al. (2011) measured the radiation transmission of concrete with barite, colemanite, and normal aggregates using the beam transmission method for 0.663 MeV X-rays energy of <sup>137</sup>Cs radioactive isotope. Results showed the decrement of the linear attenuation coefficients with increasing the energy source. Barite is effective on 0.663 keV, while colemanite is effective for neutrons shielding because it contains boron (Table 2).

Rasoul Abdar Esfahani et al. (2021) which are mostly discarded in landfills. Alternatively, they can be used in concrete production to reduce the consumption of cement and natural aggregates. One of the applications that can benefit from heavy-weight aggregates such as CS, is concrete tailored for radiation shielding purposes. However, there was no prior study on effect of combined use of CS and GGBFS on radiation shielding capability of concrete. This study is aimed to address the effect of GGBFS and CS content on gamma-ray shielding and mechanical performance of high-density concrete. For this purpose, concrete mixes were prepared with different percentages of GGBFS (0–60% investigated the

mechanical and gamma-ray shielding properties and the environmental benefit of using the industrial waste of ground granulated blast furnace slag (GGBFS) and copper slag (CS) as aggregate for production (HWC). The concrete mix was designed with a combination of (GGBFS) and (CS) by a replacement of (0-60%) and (0-100%) respectively. Results verified that (GGBFS) and (CS) are suitable for the radiation shielding of structures. The optimum compressive strength was obtained by 30% (GGBFS) and 50% (CS), while the best radiation shielding capability was obtained with 60% (GGBFS) and 100% (CS) amount (Table 2).

Beaucour et al. (2020) studied the use of Electric Arc Furnace (EAF) and steel slag as heavyweight aggregates that could be suitable for radiation shielding. Likewise, his study compared the thermal behaviour of EAF to (barite and normal aggregates). Thermal stability of the three different aggregates was found in addition to the thermal conductivity. The final results showed the reduction of EAF strength under high temperatures. EAF slag aggregates have better thermal behaviour than barite aggregates (Table 2).

There is a strong correlation between the different parameters of the compressive strength, attenuation coefficient, density, and thermal conductivity/fire resistance. However, developing these parameters can ensure the best radiation shielding of the structure. Fig. 4 summarizes values of the compressive strength and attenuation coefficient for different testing materials. The steel fibre has a direct effect on improving the mechanical properties and it has less effective in increasing the linear attenuation while adding a replacement amount of mineral additives (mineral aggregates and steel aggregates) more effective on increasing the attenuation coefficient of the concrete.

## 4. CONCLUSIONS

The application of radiation shielding structures is developed all over the world. X-Rays and Gamma rays are utilized for different purposes in the nuclear, health, agriculture, and aerospace sectors. Proper design of radiation shielding structures is necessary to ensure safety for the people and the surroundings. Concrete, metal, and polymers are the main neutron shielding materials. Concrete with special properties

is a good solution for economic and sustainability purposes.

Previous research illustrated the shortage in the information and the development of heavy-weight concrete to be more applicable as a radiation shielding material. Heavy-weight aggregates and additives are two important key factors, because of their high density and their high atomic number in addition to their role in developing the strength and the linear attenuation coefficient of the concrete. Using heavyweight or natural/ artificial aggregates can decrease the thickness of the wall (cost-effectiveness). There are still gaps in improving the HWC by using natural or artificial heavyweight aggregate through improving the HWC mix design by the absolute volume approach (use more than one type of aggregate or even fiber). The literature reported some scarcity of research on the reduction of water/cement ratio to achieve high-density concrete, as well as the combination of using nano-particle, crack control, and elevating Z (atomic number) value to improve the resistance of the harmful radiation.

## 5. REFERENCES

- Akkurt, I. et al. (2010) 'Image processing technique ( IPT ) to determine radiation shielding', *Digital Signal Processing*. Elsevier Inc., 20(6), pp. 1592–1596. <https://doi.org/10.1016/j.dsp.2010.03.008>
- Aslani, F. et al. (2020) 'High-performance fibre-reinforced heavyweight self-compacting concrete : Analysis of fresh and mechanical properties', *Construction and Building Materials*. Elsevier Ltd, 232, p. 117230. <https://doi.org/10.1016/j.conbuildmat.2019.117230>.
- Aygün, B. et al. (2021) 'Progress in Nuclear Energy Development of new heavy concretes containing chrome-ore for nuclear radiation shielding applications', 133(December 2020). <https://doi.org/10.1016/j.pnu-cene.2021.103645>.
- Azreen, N. M. et al. (2018) 'Radiation shielding of ultra-high-performance concrete with silica sand, amang and lead glass', *Construction and Building Materials*. Elsevier Ltd, 172, pp. 370–377. <https://doi.org/10.1016/j.conbuildmat.2018.03.243>.
- Ban, C. C. et al. (2021) 'Modern Heavyweight Concrete Shielding: Principles, Industrial Applications, and Future Challenges; Review', *Journal of Building Engineering*. Elsevier Ltd, 39(February), p. 102290. <https://doi.org/10.1016/j.jobbe.2021.102290>.
- Beaucour, A. et al. (2020) 'Influence of elevated temperature on properties of radiation shielding concrete with electric arc furnace slag as coarse aggregate', *Construction and Building Materials*. Elsevier Ltd, 256, p. 119385. <https://doi.org/10.1016/j.conbuildmat.2020.119385>.
- Binici, H. et al. (2014) 'Mechanical and radioactivity shielding performances of mortars made with colemanite, barite, ground basaltic pumice and ground blast furnace slag', *Construction and Building Materials*. Elsevier Ltd, 50, pp. 177–183. <https://doi.org/10.1016/j.conbuildmat.2013.09.033>.
- Davis, (1962) *ACI Journal*, American Concrete Institute
- Demir, F. et al. (2011) 'Determination of radiation attenuation coefficients of heavyweight- and normal-weight concrete containing colemanite and barite for 0.663 MeV x-rays', 38, pp. 1274–1278. <https://doi.org/10.1016/j.anucene.2011.02.009>.
- Abdulrahman S. T, Ahmad Z., Thomas S., Rahman. A. A., 'Chapter 1 - Introduction to neutron-shielding materials', In Woodhead Publishing

- Series in Composites Science and Engineering, *Micro and Nanostructured Composite Materials for Neutron Shielding Applications*, Woodhead Publishing, 2020, pp. 1-23, ISBN 9780128194591, <https://doi.org/10.1016/B978-0-12-819459-1.00001-5>.
- McArthur H., Duncan Spalding (2004), '8 - CONCRETE', *Engineering Materials Science*, Woodhead Publishing, pp. 233-295, ISBN 9781898563112, <https://doi.org/10.1533/9781782420491.233>.
- Jaeger, R. G. et al. (1968) *Engineering Compendium on Radiation Shielding*, Vol. 21. Nuclear Engineering and Design, 1–531 pp. Available from: <http://linkinghub.elsevier.com/> <http://link.springer.com/10.1007/978-3-662-25858-3>.
- Brook K, M (1989), '37 - Concrete Construction', *Civil Engineer's Reference Book (Fourth Edition)*, Butterworth-Heinemann, pp. 37/1-37/36, ISBN 9780408012089. <https://doi.org/10.1016/B978-0-408-01208-9.50041-5>.
- Jo, D. (2019) '9.1 Introduction'. <https://doi.org/10.1016/B978-0-08-102616-8.00009-5>.
- Lessing, P. (2019) '9 - High-density and radiation shielding concrete', In Woodhead Publishing Series in Civil and Structural Engineering, Developments in the Formulation and Reinforcement of Concrete (Second Edition), Woodhead Publishing, pp. 193-228, ISBN 9780081026168. <https://doi.org/10.1016/B978-0-08-102616-8.00009-5>.
- Leung C.K.Y. (2001) 'Concrete as a Building Material', *Encyclopedia of Materials: Science and Technology*, Elsevier, pp. 1471-1479, ISBN 9780080431529. <https://doi.org/10.1016/B0-08-043152-6/00267-9>.
- Outline, C. (2018) 'Radioactive materials 13', pp. 357–371. <https://doi.org/10.1016/B978-0-12-813213-5.00013-4>.
- Piotrowski, T. (2020) *Shielding concrete with neutron attenuating and absorbing components, Micro and Nanostructured Composite Materials for Neutron Shielding Applications*. Elsevier Ltd. <https://doi.org/10.1016/B978-0-12-819459-1.00007-6>.
- Rasoul Abdar Esfahani, S. M. et al. (2021) 'Mechanical and gamma-ray shielding properties and environmental benefits of concrete incorporating GGBFS and copper slag', *Journal of Building Engineering*. Elsevier Ltd, 33(June 2020), p. 101615. <https://doi.org/10.1016/j.jobbe.2020.101615>.
- Popovics, Sándor (1992), '7 - Mineral Aggregates—General', *Concrete Materials (Second Edition)*, William Andrew Publishing, pp. 274-286, ISBN 9780815513087. <https://doi.org/10.1016/B978-0-8155-1308-7.50011-9>.
- Popovics, Sándor (1992), '14 - Lightweight and Heavyweight Aggregates', *Concrete Materials (Second Edition)*, William Andrew Publishing, pp. 512-532, ISBN 9780815513087. <https://doi.org/10.1016/B978-0-8155-1308-7.50018-1>.
- Steven J. Zinkle, Jeremy T. Busby (2009) *Structural materials for fission & fusion energy, Materials Today*, Volume 12, Issue 11, pp. 12-19, ISSN 1369-7021. [https://doi.org/10.1016/S1369-7021\(09\)70294-9](https://doi.org/10.1016/S1369-7021(09)70294-9).

### Suha Ismail Ahmed Ali

(Dec 1988), Ph.D. student (BME University, Hungary), MSc in architecture for health-healthcare design- (Sapienza University of Rome, Italy). P.G diploma in business administration (International University of Africa). BSc in civil engineering (University of Juba). Experience as a civil engineer, and lecturer (Sudan). Her main research field is healthcare (Hospitals) design, structure, construction cost estimation, and energy simulation modelling.

### Assoc. Prof. Éva Lublóy

Éva Lublóy (1976), Dr.-habil, PhD, Senior lecturer in structural engineering, at the Budapest University of Technology and Economics. Her main fields of interest are: fire design, behaviour of constructions materials at elevated temperature. Member of the Hungarian Group of *fib*. [lubloy.eva@epito.bme.hu](mailto:lubloy.eva@epito.bme.hu)

# PROPOSED SIMPLIFIED METHOD OF GEOPOLYMER CONCRETE MIX DESIGN



Ali Abdulhasan Khalaf - Katalin Kopecskó

<https://doi.org/10.32970/CS.2020.1.5>

*The research aims to determine the best combination of the controlling factors that govern geopolymer concrete's mechanical and physical properties by utilizing industrial waste. Therefore, a review on the controlling factors was conducted. Firstly, it is to identify the controlling factors, namely chemical composition, alkali activation solution, water content, and curing condition. Secondly, understanding the relationship between these controlling factors and the properties of geopolymer concrete. These factors are analysed to the mix proportion components. Finally, a new proportion method is proposed based on combining ACI 211 standard and recommended molar ratios of oxides involved in geopolymer synthesis. The effect of aggregate has been taken into account by applying the absolute volume method in mix design. Based on the results of the study, it is expected to determine the optimal mix proportions based on multi-responses.*

**Keywords:** geopolymer concrete, industrial waste, controlling factors

## 1. INTRODUCTION

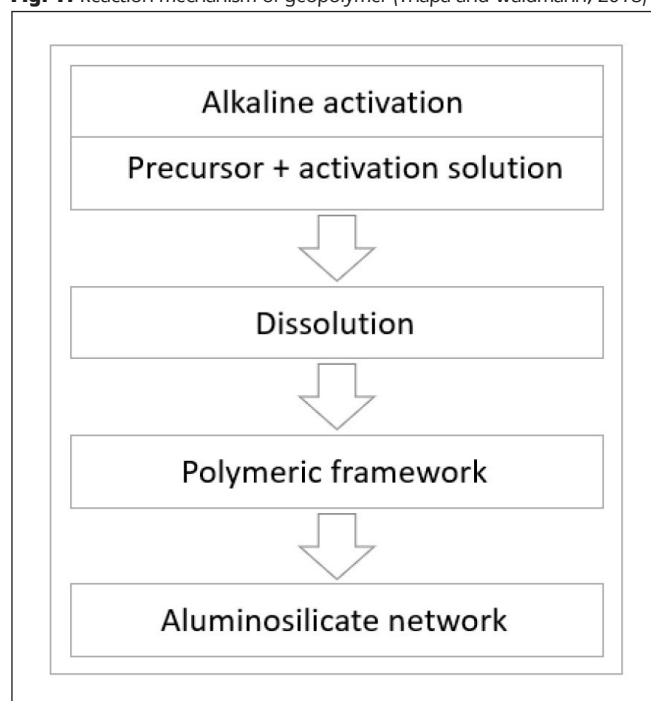
From an environmental point of view, the carbon-dioxide (CO<sub>2</sub>) emission has been being increased tremendously due to energy consumption, transportation, and industry. Even though cement plays a vital role in infrastructure construction, it involves an immense emission of carbon dioxide. Statistics showed that 1 ton production of cement produces about 1 ton of CO<sub>2</sub>. Therefore, geopolymers are used as an alternative way to reduce the emission of carbon-dioxide caused by cement processing (Davidovits, 1991; Davidovits, 1993). The patent of the geopolymer chemistry concept was introduced by Geopolymer Institute in 1979. This patent was the key to develop new binder materials. Consequently, the high-strength geopolymer cement was invented by Joseph Davidovits and James Sawyer in 1983 (Davidovits, 2002). The source of geopolymer binders can be either natural or synthetic aluminosilicate. The idea of geopolymerization is that the chemical reaction between aluminosilicate oxides and alkali polysilicates produces polymeric (Si-O-Al) bonds of amorphous to semi-crystalline three-dimensional silico-aluminate structures (Davidovits, 1991). Interestingly, it is found that most waste materials are sources of silica and alumina. As a result, these waste materials could be operated in geopolymerization reaction and being binder materials (Van Jaarsveld, Van Deventer and Lorenzen, 1998). In the case of natural sources used to produce geopolymers such as clay, high temperature is needed to calcine the clay, which is about 600 °C (Mlinárik and Kopecskó, 2013). On the contrary, geopolymer binders using waste materials are already calcined from other processes, so they do not need to be calcined (Merabtene et al., 2019; Tchakoute Kouamo et al., 2012). Therefore, utilising waste materials in the construction industry will improve both the sustainability and economics of infrastructure systems (Van Jaarsveld et al., 1998). The reaction

mechanism of geopolymer can be shown in Fig. 1 (Thapa and Waldmann, 2018).

## 2. TYPES OF INDUSTRIAL WASTE MATERIALS USED AS GEOPOLYMER BINDERS

Industrial waste based geopolymers do not have a unique chemical structure. Their properties are most dependent on their base material characteristics, namely: chemical compo-

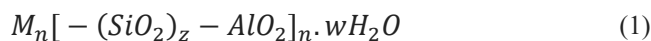
**Fig. 1:** Reaction mechanism of geopolymer (Thapa and Waldmann, 2018)



sition, the content of glassy phase, amount of soluble silicon and aluminium, particle size distribution, and presence of inert particles (Zhang et al., 2018). Therefore, it is crucial to identify the sources of base materials of geopolymer synthesis, which are under conducting a study. There are many types of waste and by-product materials that have been utilised in geopolymer synthesis, for example, fly ash, blast furnace slag, bottom ash, red mud, rice husk ash, bottom ash, palm oil fuel ash, waste paper sludge ash, tailing metals, silica waste, ceramic waste, etc., (Abdel-Ghani et al., 2018; Bakharev et al., 1999; Chawakitchareon, 2013; Chi, 2016; Ekaputri, Baihaqi and Aji, 2011; Ekaputri, Junaedi and Bayuaji, 2015; Erdogan, 2015; Hanjitsuwan et al., 2017; Junak et al., 2014; Karakoç et al., 2014; Karrech et al., 2019; Khater and Abd El Gawaad, 2016; Kim et al., 2014; Kopecký et al., 2019; Kovalchuk et al., 2007; Malkawi et al., 2016; Mucsi et al., 2020; Musaddiq Laskar and Talukdar, 2017; Monita et al., 2016; Ridzuan et al., 2014; Saeli et al., 2019; Sindhunata et al., 2006; Shoaie et al., 2019; Yankwa Djobo et al., 2016; Ye et al., 2016).

### 3. CHEMICAL COMPOSITION AND SYNTHESIS

The geopolymer reaction is achieved by the reaction of aluminate-silicate with the availability of alkali activator at low temperature. The following general formula below describes the chemical composition (1):



where  $M$  is an alkali cation;  $z$  is an integer;  $n$  is the degree of polymerisation and  $w$  is the molar amount of water (Davidovits, 2002). Table 1 shows an example of the chemical composition of slag and fly ash conducted using X-ray fluorescence (XRF) (Li et al., 2018). The chemistry matrix is a function of four variables, namely: Si/Al ratio, alkali activator type and concentration, curing temperature, and water content (Duxson et al., 2005; Duxson et al., 2007b).

#### 3.1 Influence of Si/Al ratio

The basic structure of geopolymers is the network structure of  $(SiO_4)$  tetrahedrons and  $(AlO_4)$  tetrahedrons, which are connected by mutual oxygen atoms. Si/Al ratio reflexes this structure and plays a vital role in geopolymer behaviour. The contribution of the Si/Al ratio comes from the base material of geopolymer. Although the Si-O-Si bonds are stronger than the Al-O-Si bonds, the geopolymer's high performance occurs at an intermediate Si/Al ratio at a certain range of alkalinity. This optimum Si/Al ratio differs for different base material geopolymers, and it is also dependent on processing conditions. It is found that some silicate would not participate in reactivity, such as silicate in quartz. In other words, the amorphous component is the reactive compound. Fur-

thermore, even some amorphous silicate could be prevented from being reacted (Ahmari, Zhang and Zhang 2012; Duxson et al., 2007a; Williams and Van Riessen, 2010; Zheng, Wang and Shi, 2010). Geopolymers with ground granulated blast furnace, GGBS, exhibit better performance at a low Si/Al ratio compared to low-calcium geopolymers (Kubba et al., 2018). The Si/Al ratio can be controlled by adding small silica fume content (Kovalchuk et al., 2007). Table 2 shows different optimum Si/Al ratios for different materials and the corresponding compressive strengths.

**Table 2:** Optimum Si/Al ratios for different geopolymers and their compressive strengths

Material	Si/Al ratio	Curing mode	Comp-res-sive strength (MPa)
MK <sup>1</sup> (Duxson, Mallicoat, et al. 2007)	1.9	Heat curing	78
RM <sup>2</sup> : FA <sup>3</sup> (Zhang, He, and Gambrell 2010)	3.2	Ambient curing	13
RM <sup>2</sup> : FA <sup>3</sup> : SF <sup>4</sup> (Singh, Aswath, and Ranganath 2018)	5.1	Heat curing	32
RM <sup>2</sup> : FA <sup>3</sup> : SF <sup>4</sup> (Singh et al. 2018)	4.0	Ambient curing	30

MK = metakaolin; RM = redmud; FA = fly ash; SF = silica fume

#### 3.2 Influence of alkali solution

Generally, hydroxide and silicate-based solutions can be used individually or proportionally mixed to synthesize geopolymers. The type and concentration of alkali solutions (hydroxide, silicate-based, and water) have an important impact on geopolymer performance (Chindaprasirt et al., 2007; Fernández-Jiménez and Palomo, 2003; Hardjito et al., 2004; Risdan-areni and Ekaputri, 2015; Tuyan et al., 2018).

Usually, sodium silicate,  $Na_2SiO_3$  ( $Na_2O + SiO_2 + H_2O$ ), is used as a silicate-based solution and could be proportionally mixed with either sodium hydroxide, NaOH, potassium hydroxide KOH, or both (Hardjito et al., 2004; N. Li et al., 2018). In the case of sodium silicate, the activator variables are defined by the silica modulus ( $M_s$ ) or  $Na_2O$  content. Silica modulus is measured in the molar ratio of  $SiO_2/Na_2O$ .  $Na_2O$  content is calculated as a percentage of the weight of raw material in dry condition (Silva et al., 2019). Increasing these variables for a particular value will decrease the porosity of mixtures. Accordingly, the density would be improved and producing maximum compressive strength values (Tuyan, Andiç-Çakir and Ramyar, 2018). Hydroxyl ions could be measured by molarity. The optimum concentration of NaOH is dependent on curing temperature. When the curing temperature is increased, the required optimum concentration of

**Table 1:** Chemical compositions of slag and fly ash (wt. %). LOI is the loss of ignition

Material	Oxide								
	SiO <sub>2</sub>	Al <sub>2</sub> O <sub>3</sub>	CaO	MgO	K <sub>2</sub> O	Fe <sub>2</sub> O <sub>3</sub>	Na <sub>2</sub> O	SO <sub>3</sub>	LOI
Slag	33.81	14.78	38.81	7.09	0.44	0.36	0.26	2.49	1.40
Fly Ash	54.22	31.18	1.24	0.47	1.34	2.36	0.49	0.35	3.25

NaOH increases (Ahmari et al., 2012).

In the case of geopolymers that have GGBS, NaOH concentration plays a vital role in altering the geopolymerization process and affecting the mechanical and physical properties. When NaOH concentration is low in alkali solution, calcium will be dissolved, contributing to the formation of CSH gel. This process yields homogenous and dense products because CSH works as a micro-aggregate. On the other hand, a high dosage of NaOH will be responsible for calcium hydroxide formation, which will prevent the formation of CSH gel. In this case, the variable parameters will be (low-calcium raw material / high-calcium raw material) by weight and  $\text{Na}_2\text{O}/\text{SiO}_2$  in the molar ratio (Kubba et al., 2018; Yip et al., 2005).

It should be noted that the unburnt carbon behaves as an inert particulate, which can increase the demand for activation solution due to absorption (Gunasekara et al., 2015). Recently, some geopolymers have been investigated with respect to mechanical activation as a partial and full replacement of chemical activation. They showed good response and developed high compressive strength values when used with activators (Y. Li et al., 2019)

### 3.3 Influence of curing mode

The curing temperature has a significant influence on optimising geopolymer properties because of related water evaporation. However, a very high curing temperature could be harmful and destabilise geopolymerization (Shoaei et al., 2019). In general, the heat-curing regime is mostly adopted in geopolymer applications. The heat-curing regime is expressed by two components. The first component is curing time, which is ranged from 4 hours to 96 hours with an optimum practical value of 24 hours. The other component is the temperature, which is started from the minimum value of 30 °C up to a maximum temperature of 90 °C.

Curing can be conducted by steam-curing, curing in covered moulds, or dry-curing. The type of curing affects the total porosity, the average pore diameter, and microstructural characteristics (Assi et al., 2016; Hardjito and Rangan, 2005; Jaydeep and Chakravarthy, 2013; Lloyd and Rangan, 2010; Kovalchuk et al., 2007). Interestingly, GGBS geopolymers can be optimised at a much lower curing temperature than low-calcium geopolymers (Kubba et al., 2018). It should be noted that there are some flexibilities in the heat-curing regime. First of all, the heat-curing can be postponed for up to five days with no degradation (Hardjito and Rangan, 2005). In precast concrete, sometimes it is needed to remove the moulds before the ending of curing time to use them in another casting. Therefore, the two-stage curing is valid. This flexibility is valuable in practical use when required to remove the moulds during the curing time (Hardjito and Rangan, 2005). However, full curing out-side the moulds is still controversial (Assi et al., 2016).

### 3.4 Influence of water content

The influence of water content is represented by a single parameter of which water-to-geopolymer solids ratio by mass, W/G.S ratio. This parameter has a tremendous effect on the compressive strength and workability of geopolymer concrete. The total water mass is equal to the summation of water in the sodium silicate solution, the water that is used to produce the sodium hydroxide solution, and the extra water, if any is needed, should be taken into account. On the other

hand, the geopolymer solids mass should contain the dry raw materials and the solids of the activator solution, for example, the solids of the sodium hydroxide solution and sodium silicate solution ( $\text{Na}_2\text{O}$  and  $\text{SiO}_2$ ) (Assi et al., 2016; Hardjito & Rangan, 2005). The increase of water-to-geopolymer solids ratio increases the workability of concrete. However, there is an optimum value of water-to-geopolymer solids ratio to achieve the maximum compressive strength at acceptable workability (Shoaei et al. 2019). This optimum value is affected by the type of raw materials and activator type (Assi et al., 2016; Kovalchuk et al., 2007; Shoaei et al., 2019; Shoaei et al., 2019).

## 4. GEOPOLYMER CONCRETE (GPC)

The main difference between geopolymer concrete (GPC) and conventional Portland cement based concrete is the binder, which in case of geopolymer concrete is including the raw material of geopolymer and the alkaline activator. However, the conventional methods that are used in the production of Portland cement concrete (PCC) can be utilised to produce geopolymer concrete. Fig. 2 shows a typical description of one cubic meter of the volume of Portland cement concrete and geopolymer concrete (Lloyd and Rangan, 2010; N. Li et al., 2019)

## 5. PROPOSED SIMPLIFIED METHOD OF GEOPOLYMER CONCRETE MIX DESIGN

A simplified mix design is proposed by combining ACI 211 (2009) standard and recommended molar ratios of oxides involved in geopolymer synthesis, where

- (i) the desired compressive strength is targeted, and
- (ii) the workability would be verified for the acceptable range based on absolute volume according to the standard (ACI 211, 2009).

The mix design is based on the similarity between the Portland cement concrete and geopolymer concrete mixtures and takes into account different properties of geopolymer concrete.

**Fig. 2:** Characterisation of Portland cement concrete (PCC) and geopolymer concrete (GPC) in 1 m<sup>3</sup> (N. Li et al. 2019)

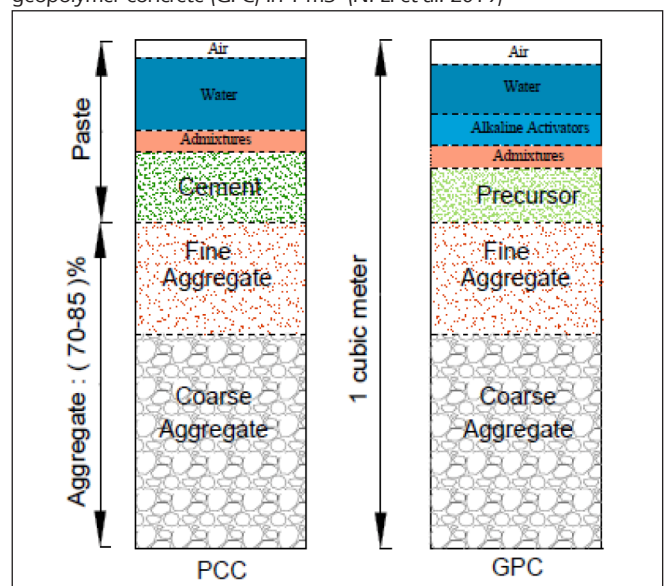


**Table 3:** Approximate mixing water and air content requirements for different slumps and maximum aggregate sizes for non-air-entrained PCC (ACI 211, 2009)

Slump	Water quantity in kg/m <sup>3</sup> for the nominal maximum aggregate size (mm)							
	9.5	12.5	19	25	37.5	50	75	100
25 – 50	207	199	190	179	166	154	130	113
75 – 100	228	216	205	193	181	169	145	124
150 – 175	243	228	216	202	190	178	160	-
Entrapped air (%)	3.0	2.5	2.0	1.5	1.0	0.5	0.3	0.2

## 5.1 Water content

According to ACI 211 (2009) standard, the maximum water content can be determined from the maximum size of aggregate, as is shown in *Table 3*.

## 5.2 Alkaline activator solution content

In case there is no extra water needed to be added to the mix, the water content is only provided from the alkaline activator solution. According to (Heath, Paine and McManus, 2014), the mix oxide molar ratios can be used to produce geopolymers in case of using sodium or potassium hydroxide and silicate (Na<sub>2</sub>O.nSiO<sub>2</sub> or K<sub>2</sub>O.nSiO<sub>2</sub>) activators as illustrated in *Table 4*, where M is Na or K. The alkaline solution will be selected in terms of molarity and concentration according to the chosen water content, see *Table 1* and *Table 4*. If the alkaline solution selection requires less water, the remaining amount of water will be added as extra water to the mixture.

**Table 4:** Mix oxide molar ratios of alkali activators

Oxide ratio	Molar ratio range
SiO <sub>2</sub> : Al <sub>2</sub> O <sub>3</sub>	3.5 – 4.5
*M <sub>2</sub> O : SiO <sub>2</sub>	0.20 – 0.28
H <sub>2</sub> O : *M <sub>2</sub> O	15.0 – 17.5
*M <sub>2</sub> O : Al <sub>2</sub> O <sub>3</sub>	0.80 – 1.20

Notation: \*M is stands for either Na or K

## 5.3 Water-to-geopolymer solids ratio

In conventional concrete, the compressive strength at the age of 28 days is considered to determine the water to cement ratio according to ACI 211 (2009) standard. Similarly, the ratio of the water-to-geopolymer solids can be selected from the standard water to cement ratio curve (*Fig. 3, Table 5*) (Pavithra et al., 2016; ACI 211, 2009)

**Table 5:** Relationship between water-cement ratio and compressive strength of Portland cement concrete, according to ACI 211 (2009) standard

Compressive strength at 28 days (MPa)	Water-cement ratio
41.0	0.41
35.0	0.48
28.0	0.57
21.0	0.68
14.0	0.82

## 5.4 Raw material content

After determining the water content and water-to-geopolymer solids ratio (W/GS), the geopolymer solids content (GS) can be calculated (2-5):

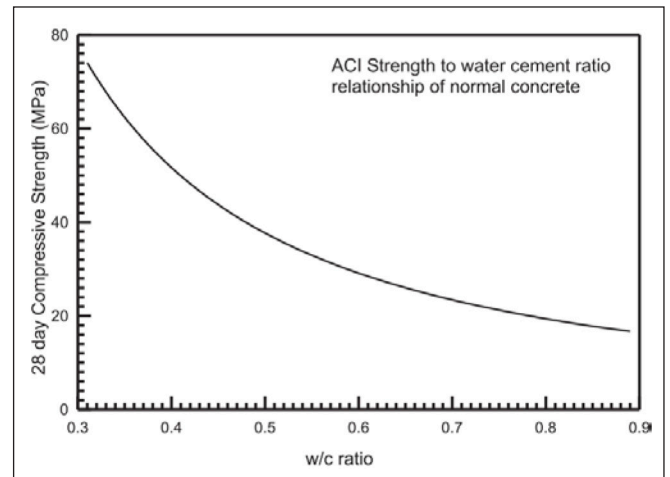


**Fig. 3:** Strength versus water to cement ratio curve (Pavithra et al., 2016)

$$GS = \frac{W_{content}}{W/GS} \quad (2)$$

$$GS_{SS} = m_{SS} * \% GS_{SS} \quad (3)$$

$$GS_{SH} = m_{SH} * \% GS_{SH} \quad (4)$$

$$GS = GS_B + GS_{SS} + GS_{SH} \quad (5)$$

, where GS is geopolymer solid content; GS<sub>SS</sub> is solid content of Na<sub>2</sub>SiO<sub>3</sub>; GS<sub>SH</sub> solid content of NaOH; m<sub>SS</sub> is the content of Na<sub>2</sub>SiO<sub>3</sub> solution; m<sub>SH</sub> is content of NaOH solution; GS<sub>B</sub> is raw material content.

## 5.5 Air content volume

The percentage of entrapped air in conventional concrete is illustrated in *Table 3*, depending on the maximum size of aggregate. However, for fly ash-based geopolymer, the air content was found greater than the conventional concrete for the same corresponding size of coarse aggregate based on trial mixes. For the maximum coarse aggregate size of 19 mm, the air content volume percent is assigned two, according to ACI 211 (2009). On the other hand, the air content volume percent of fly ash-based geopolymer was found 3.29 for maximum coarse aggregate size of 20 mm (Ferdous, Kayali and Khenane, 2013). This difference indicates that the entrapped air percent in geopolymer concrete would be greater than it is in conventional concrete. In this proposed method, the entrapped air content in geopolymer concrete will be taken equal to 3.29 V% based on the results of (Ferdous, Kayali and Khenane, 2013).

## 5.6 Addition of super-plasticiser

In fact, geopolymer concrete is stiffer and stickier than conventional concrete. Therefore, the same amount of water in

geopolymer concrete would produce decrease in workability. Workability can be increased either by increasing the water amount or adding super-plasticiser such as carboxylic ether polymer-based super-plasticiser or naphthalene-based super-plasticiser. Increasing the water amount has a much more negative effect on the strength of geopolymer concrete than adding super-plasticiser. Thus, the super-plasticiser addition is a better choice to increase the workability of geopolymer concrete. The super-plasticiser recommended dosage ranges from 0.8 to 1.5% of binder content (Ferdous et al., 2013; Pavithra et al., 2016; Reddy and Naqash, 2020).

## 5.7 Coarse aggregate volume

According to ACI 211 (2009) standard, the coarse aggregate volume can be selected depending on two criteria, namely the nominal maximum size of coarse aggregate and fineness modulus of fine aggregate, as is shown in *Table 6*. It should be noted that coarse aggregate volumes are based on oven-dry-rodded weights in accordance with ASTM C29 (ASTM:C29/C29M-09 2009, ACI 211 2009).

## 5.8 Fine aggregate content

Since all other ingredient volumes are determined, the remaining volume percentage represents the volume percentage of fine aggregate (ACI 211, 2009).

## 5.9 The moisture content of aggregate

The moisture of aggregate affects two parameters, namely weight of aggregate and content of mixing water. The adjustment of aggregate weight and mixing water content depends on the saturation degree of batched aggregate (ACI 211, 2009).

# 6. MIXING, CASTING AND COMPACTING OF GEOPOLYMER CONCRETE

One of the most distinctive characteristics of geopolymer concrete is the alkaline activator solution. The most used activator solutions are sodium hydroxide and sodium silicate. The sodium hydroxide solution is prepared by dissolution of sodium hydroxide pellets in distilled water. After that, the solution should be isolated from the atmosphere as much as possible to prevent the possible reaction with atmospheric carbonate for at least 24 hours. Sodium silicate solution can be provided by manufacturers in specific concentrations. Sodium silicate is usually used in combination with sodium hydroxide. In this case, the solution is prepared by dissolution of sodium silicate

**Table 6:** Coarse aggregate volume in 1 m<sup>3</sup> of PCC

Nominal max. aggregate size, mm	Fineness modulus of fine aggregate			
	2.40	2.60	2.80	3.00
9.5	0.50	0.48	0.46	0.44
12.5	0.59	0.57	0.55	0.53
19.0	0.66	0.64	0.62	0.60
25.0	0.71	0.69	0.67	0.65
37.5	0.75	0.73	0.71	0.69
50.0	0.78	0.76	0.74	0.72

in sodium hydroxide to obtain the required concentration. The solution should be prepared at least 24 hours before it is used in mixing to allow the necessary equilibrium (Ahmari et al., 2012; Duxson et al., 2005; Duxson et al. 2007b).

The addition of amorphous silica with sodium hydroxide can replace the use of sodium silicate since the alkali activator is the most expensive component in geopolymer concrete (Heath et al., 2014; Pavithra et al., 2016). After the activator solution is being ready to use, the raw material and aggregate should be mixed dry for at least three minutes. Then the alkaline liquid should be added after it is mixed with the super-plasticiser and the extra water if it is needed just prior to mixing. The wet mixing time should last for four minutes at least. The fresh concrete can be handled and formed up to 120 minutes after mixing (Hardjito and Rangan, 2005). Based on our experience, we were not able to mix geopolymer concrete, when first the dry material (precursor and aggregate) is mixed, then thereafter the alkali activator solution was added, similarly to the mixing method in case of PCC. In case of geopolymer mortar or concrete first the liquid gel (alkali activator solution + precursor + super-plasticiser) formation is achieved, then the aggregate is added and mixed (Kopeckó et al., 2017). It is essential to make trial mix before starting the main experiments.

The compaction of geopolymer concrete is as same as it is in conventional concrete (Hardjito and Rangan, 2005).

# 7. CONCLUSIONS

The following conclusions and future work can be stated:

- The controlling factors (chemical composition, alkali activation solution, water content, and curing condition) of geopolymer are sensitive to the source material.
- Heat curing limits the use of geopolymer concrete in practical applications. For this reason, the use of geopolymer concrete is primarily limited to the precast concrete application.
- The cost of geopolymer concrete synthesis with sodium silicate is relatively high.
- Herein a new simplified geopolymer concrete (GPC) mix design is proposed based on the Portland cement concrete (PCC) mix design (ACI 211, 2009) with the combination of the recommended molar ratios of oxides involved in geopolymer synthesis. This simplified method will allow us to optimize the controlling factors of geopolymer concrete to produce optimum compressive strength with acceptable workability. This process will be conducted by utilizing the common factors between PCC and GPC, namely water and aggregate.
- In future work, it is essential to investigate the possible replacement of sodium silicate by amorphous silica such as silica fume, rice husk ash, or ground waste glass in the activator solution to reduce the cost of production.

# ACKNOWLEDGEMENT

*Stipendium Hungaricum* Scholarship Programme is highly acknowledged for supporting the PhD study and research work.

# 8. REFERENCES

- Abdel-Ghani, Nour T., Hamdy A. Elsayed, and Sara AbdelMoied. 2018. "Geopolymer Synthesis by the Alkali-Activation of Blastfurnace Steel Slag and Its Fire-Resistance." *HBRC Journal* 14(2):159-64. <https://doi.org/10.1016/j.hbrj.2016.06.001>

- ACI 211, Committee. 2009. Standard Practice for Selecting Proportions for Normal, Heavy-Weight, and Mass Concrete.
- Ahmari, Saeed, Lianyang Zhang, and Jinhong Zhang. 2012. "Effects of Activator Type/Concentration and Curing Temperature on Alkali-Activated Binder Based on Copper Mine Tailings." *Journal of Materials Science* 47(16):5933-45. <https://doi.org/10.1007/s10853-012-6497-9>
- Ambrus, M., Papné Halyag, N., Czupy, I., Szalay, D. and Mucsi, G. 2020. "Mechanical and structural properties of biomass-geopolymer composites." *Geosciences and Engineering: a publication of the University of Miskolc*, Vol. 8:12 pp. pp. 47-60.
- Assi, Lateef N., Edward Deaver, Mohamed K. Elbatanouny, and Paul Ziehl. 2016. "Investigation of Early Compressive Strength of Fly Ash-Based Geopolymer Concrete." *Construction and Building Materials* 112:807-15. <https://doi.org/10.1016/j.conbuildmat.2016.03.008>
- ASTM C29 / C29M-17a, Standard Test Method for Bulk Density ("Unit Weight") and Voids in Aggregate, ASTM International, West Conshohocken, PA, 2017, www.astm.org [https://doi.org/10.1520/C0029\\_C0029M-17A](https://doi.org/10.1520/C0029_C0029M-17A)
- Bakharev, Tatiana, Jay Gnananandan Sanjayan, and Yi Bing Cheng. 1999. "Alkali Activation of Australian Slag Cements." *Cement and Concrete Research* 29(1):113-20. [https://doi.org/10.1016/S0008-8846\(98\)00170-7](https://doi.org/10.1016/S0008-8846(98)00170-7)
- Chawakitchareon, Petchporn. 2013. "American Transactions on Engineering & Applied Sciences Geopolymer Mortar Production Using Silica Waste as Raw Material." 2(1):3-13.
- Chi, Maochih. 2016. "Synthesis and Characterisation of Mortars with Circulating Fluidized Bed Combustion Fly Ash and Ground Granulated Blast-Furnace Slag." *Construction and Building Materials* 123:565-73. <https://doi.org/10.1016/j.conbuildmat.2016.07.071>
- Chindaprasirt, P., T. Chareerat, and V. Sirivivatnanon. 2007. "Workability and Strength of Coarse High Calcium Fly Ash Geopolymer." *Cement and Concrete Composites* 29(3):224-29. <https://doi.org/10.1016/j.cemconcomp.2006.11.002>
- Davidovits, J. 1993. "Geopolymer Cements To Minimise Carbon-Dioxide Greenhouse-Warming." *Ceramic Transaction* 37(1):165-82.
- Davidovits, J. 1991. "Geopolymers - Inorganic Polymeric New Materials." *Journal of Thermal Analysis* 37(8):1633-56. <https://doi.org/10.1007/BF01912193>
- Davidovits, J. 2002. "30 Years of Successes and Failures in Geopolymer Applications . Market Trends and Potential Breakthroughs ." *Geopolymer 2002 Conference* 1-16. <https://doi.org/10.1017/CBO9781107415324.004>
- Duxson, P., A. Fernández-Jiménez, J. L. Provis, G. C. Lukey, A. Palomo, and J. S. J. Van Deventer. 2007. "Geopolymer Technology: The Current State of the Art." *Journal of Materials Science* 42(9):2917-33. <https://doi.org/10.1007/s10853-006-0637-z>
- Duxson, P., S. W. Mallicoat, G. C. Lukey, W. M. Kriven, and J. S. J. van Deventer. 2007. "The Effect of Alkali and Si/Al Ratio on the Development of Mechanical Properties of Metakaolin-Based Geopolymers." *Colloids and Surfaces A: Physicochemical and Engineering Aspects* 292(1):8-20. <https://doi.org/10.1016/j.colsurfa.2006.05.044>
- Duxson, Peter, John L. Provis, Grant C. Lukey, Seth W. Mallicoat, Waltraud M. Kriven, and Jannie S. J. Van Deventer. 2005. "Understanding the Relationship between Geopolymer Composition, Microstructure and Mechanical Properties." *Colloids and Surfaces A: Physicochemical and Engineering Aspects* 269(1-3):47-58. <https://doi.org/10.1016/j.colsurfa.2005.06.060>
- Erdogan, S. T. 2015. "Properties of Ground Perlite Geopolymer Mortars." *Journal of Materials in Civil Engineering* 27(7). [https://doi.org/10.1061/\(ASCE\)MT.1943-5533.0001172](https://doi.org/10.1061/(ASCE)MT.1943-5533.0001172)
- Ekaputri, J. J., Baihaqi, A., and Aji, P. 2011. "Mechanical Properties of Volcanic Ash Based Concrete," *Proc. Int. Semin. Appl. Technol. Sci. Arts*, pp. 224-229.
- Ekaputri, J. J., Junaedi, S. and Bayuaji, R. 2015. "Light Weight Geopolymer Paste Made with Sidoarjo Mud (Lusi)," *Materials Science Forum*, Volume 803, pp. 63-74.
- Ferdous, M. W., O. Kayali, and A. Khennane. 2013. "A Detailed Procedure of Mix Design for Fly Ash Based Geopolymer Concrete." *Proceedings of the 4th Asia-Pacific Conference on FRP in Structures, APFIS 2013 (December)*:11-13.
- Fernández-Jiménez, A., and A. Palomo. 2003. "Characterisation of Fly Ashes. Potential Reactivity as Alkaline Cements." *Fuel* 82(18):2259-65. [https://doi.org/10.1016/S0016-2361\(03\)00194-7](https://doi.org/10.1016/S0016-2361(03)00194-7)
- Gunasekara, Chamila, David W. Law, Sujeeva Setunge, and Jay G. Sanjayan. 2015. "Zeta Potential, Gel Formation and Compressive Strength of Low Calcium Fly Ash Geopolymers." *Construction and Building Materials* 95:592-99. <https://doi.org/10.1016/j.conbuildmat.2015.07.175>
- Hanjitsuwan, Sakonwan, Tanakorn Phoo-ngernkham, and Nattapong Damrongwiriyanupap. 2017. "Comparative Study Using Portland Cement and Calcium Carbide Residue as a Promoter in Bottom Ash Geopolymer Mortar." *Construction and Building Materials* 133:128-34. <https://doi.org/10.1016/j.conbuildmat.2016.12.046>
- Hardjito, Djwantoro, and B. Vijaya Rangan. 2005. Development and Properties of Low-Calcium Fly Ash-Based Geopolymer Concrete. <https://doi.org/10.1080/13287982.2005.11464946>
- Hardjito, Djwantoro, Steenie E. Wallah, Dody M. J. Sumajouw, and B. Vijaya Rangan. 2004. "On the Development of Fly Ash-Based Geopolymer Concrete." *ACI Materials Journal* 101(6):467-72. <https://doi.org/10.14359/13485>
- Heath, Andrew, Kevin Paine, and Marcelle McManus. 2014. "Minimising the Global Warming Potential of Clay Based Geopolymers." *Journal of Cleaner Production* 78:75-83. <https://doi.org/10.1016/j.jclepro.2014.04.046>
- Jaydeep, S., and B. J. Chakravarthy. 2013. "Study On Fly Ash Based Geopolymer Concrete Using Admixtures." *International Journal of Engineering Trends and Technology* 4(10):4614-17.
- Junak, Jozef, Nadezda Stevulova, and Marcela Ondova. 2014. "Concrete Samples Prepared with Different Types of Wastes." *Pollack Periodica* 9(SUPPL. 1):95-104. <https://doi.org/10.1556/Pollack.9.2014.S.10>
- Karakoç, Mehmet Burhan, Ibrahim Türkmen, Müslüm Murat Maraş, Fatih Kantarci, Ramazan Demirboğa, and M. Uur Toprak. 2014. "Mechanical Properties and Setting Time of Ferrocchrome Slag Based Geopolymer Paste and Mortar." *Construction and Building Materials* 72:283-92. <https://doi.org/10.1016/j.conbuildmat.2014.09.021>
- Karrech, A., M. Dong, M. Elchalakani, and M. A. Shahin. 2019. "Sustainable Geopolymer Using Lithium Concentrate Residues." *Construction and Building Materials* 228:116740. <https://doi.org/10.1016/j.conbuildmat.2019.116740>
- Khater, H. M., and H. A. Abd El Gawaad. 2016. "Characterisation of Alkali Activated Geopolymer Mortar Doped with MWCNT." *Construction and Building Materials* 102:329-37. <https://doi.org/10.1016/j.conbuildmat.2015.10.121>
- Kim, Yun Yong, Byung Jae Lee, Velu Saraswathy, and Seung Jun Kwon. 2014. "Strength and Durability Performance of Alkali-Activated Rice Husk Ash Geopolymer Mortar." *Scientific World Journal* 2014. <https://doi.org/10.1155/2014/209584> PMID:25506063 PMCID:PMC4258323
- Kopecskó, Katalin, Hajdu, Mátyás, and Balázs, György L. 2019. "Alkali-Activated Binders Based on Fly Ash and GGBS." Pp. 2167-74 in *Concrete Innovations in Materials, Design and Structures*, Derkowski W., Gwozdiewicz P., Hojdy L., Krajewski P., Pantak M. (szerk.), fib.
- Kovalchuk, G., A. Fernández-Jiménez, and A. Palomo. 2007. "Alkali-Activated Fly Ash: Effect of Thermal Curing Conditions on Mechanical and Microstructural Development - Part II." *Fuel* 86(3):315-22. <https://doi.org/10.1016/j.fuel.2006.07.010>
- Kubba, Ziyad, Ghasan Fahim Huseien, Abdul Rahman Mohd Sam, Kwok Wei Shah, Mohammad Ali Asaad, Mohammad Ismail, Mahmood Md Tahir, and Jahangir Mirza. 2018. "Impact of Curing Temperatures and Alkaline Activators on Compressive Strength and Porosity of Ternary Blended Geopolymer Mortars." *Case Studies in Construction Materials* 9:e00205. <https://doi.org/10.1016/j.cscm.2018.e00205>
- Li, Ning, Caijun Shi, Zuhua Zhang, Hao Wang, and Yiwei Liu. 2019. "A Review on Mixture Design Methods for Geopolymer Concrete." *Composites Part B: Engineering* 178(April):107490. <https://doi.org/10.1016/j.compositesb.2019.107490>
- Li, Ning, Caijun Shi, Zuhua Zhang, Deju Zhu, Hyeon Jong Hwang, Yuhan Zhu, and Tengjiao Sun. 2018. "A Mixture Proportioning Method for the Development of Performance-Based Alkali-Activated Slag-Based Concrete." *Cement and Concrete Composites* 93(July):163-74. <https://doi.org/10.1016/j.cemconcomp.2018.07.009>
- Li, Yuancheng, Xiaobo Min, Yong Ke, Degang Liu, and Chongjian Tang. 2019. "Preparation of Red Mud-Based Geopolymer Materials from MSWI Fly Ash and Red Mud by Mechanical Activation." *Waste Management* 83:202-8. <https://doi.org/10.1016/j.wasman.2018.11.019> PMID:30514467
- Lloyd, N. A., and B. V. Rangan. 2010. "Geopolymer Concrete with Fly Ash." Pp. 1493-1504 in *2nd International Conference on Sustainable Construction Materials and Technologies*. Vol. 7.
- Malkawi, Ahmad B., Muhd Fadhil Nuruddin, Amir Fauzi, Hashem Almatarneh, and Bashar S. Mohammed. 2016. "Effects of Alkaline Solution on Properties of the HCFA Geopolymer Mortars." *Procedia Engineering* 148:710-17. <https://doi.org/10.1016/j.proeng.2016.06.581>
- Merabtene, Meriem, Larbi Kacimi, and Pierre Clastres. 2019. "Elaboration of Geopolymer Binders from Poor Kaolin and Dam Sludge Waste." *Heliyon* 5(6):e01938. <https://doi.org/10.1016/j.heliyon.2019.e01938> PMID:31249896 PMCID:PMC6584774
- Mlinárik, L. and Kopecskó, K. 2013. "Impact of metakaolin - a new supplementary material - on the hydration mechanism of cements." *Acta-Technica Napocensis - Civil Engineering & Architecture* 56:2 pp. 100-110. Paper: 9, 11 p. (2013), viewed 21 December 2020, [https://constructii.utcluj.ro/ActaCivilEng/download/atn/ATN2013\(2\)\\_9.pdf](https://constructii.utcluj.ro/ActaCivilEng/download/atn/ATN2013(2)_9.pdf)
- Mucsi, G., Szabó, R., Halyag, N., Ambrus, M., Kocserha, I., Géber, R., Máda, F., Kristály, F., Mórićz, F., Rácz, Á., Bohács, K., Gregus, É., Csák, Cs., Marinkás, Gy., Debreczeni, Á. and Molnár, J. 2020. "Summarizing recent achievements of the silicate waste research group." *Geosciences and Engineering: a publication of the University of Miskolc*, Vol. 8:12 pp. 15-32.
- Musaddiq Laskar, Sulaem, and Sudip Talukdar. 2017. "Development of Ultrafine Slag-Based Geopolymer Mortar for Use as Repairing Mortar." *Journal of Materials in Civil Engineering* 29(5). [https://doi.org/10.1061/\(ASCE\)MT.1943-5533.0001824](https://doi.org/10.1061/(ASCE)MT.1943-5533.0001824)

- Olivia, Monita, Chrisfela Wulandari, Iskandar R. Sitompul, Lita Darmayanti, and Zulfikar Djauhari. 2016. "Study of Fly Ash (FA) and Palm Oil Fuel Ash (POFA) Geopolymer Mortar Resistance in Acidic Peat Environment." *Materials Science Forum* 841 (January):126-32. <https://doi.org/10.4028/www.scientific.net/MSF.841.126>
- Pavithra, P., M. Srinivasula Reddy, Pasla Dinakar, B. Hanumantha Rao, B. K. Satpathy, and A. N. Mohanty. 2016. "A Mix Design Procedure for Geopolymer Concrete with Fly Ash." *Journal of Cleaner Production* 133(May):117-25. <https://doi.org/10.1016/j.jclepro.2016.05.041>
- Reddy, Panga Narasimha, and Javed Ahmed Naqash. 2020. "Effectiveness of Polycarboxylate Ether on Early Strength Development of Alccofine Concrete." *Pollack Periodica* 15(1):79-90. <https://doi.org/10.1556/606.2020.15.1.8>
- Ridzuan, A. R. M., A. A. Khairulniza, M. A. Fadzil, J. Nurliza, A. M. A. Fauzi, and W. M. F. W. Yusoff. 2014. "Alkaline Activators Concentration Effect to Strength of Waste Paper Sludge Fly Ash-Based Geopolymer Mortar." in the International Civil and Infrastructure Engineering Conference 2013. [https://doi.org/10.1007/978-981-4585-02-6\\_15](https://doi.org/10.1007/978-981-4585-02-6_15)
- Risdanareni, P. and Ekaputri, J. J. 2015. "The Influence of Alkali Activator Concentration to Mechanical Properties of Geopolymer Concrete with Trass as a Filler." *Materials Science Forum*, Volume 803, pp. 125-134.
- Saeli, Manfredi, David M. Tobaldi, Maria Paula Seabra, and João A. Labrincha. 2019. "Mix Design and Mechanical Performance of Geopolymeric Binders and Mortars Using Biomass Fly Ash and Alkaline Effluent from Paper-Pulp Industry." *Journal of Cleaner Production* 208:1188-97. <https://doi.org/10.1016/j.jclepro.2018.10.213>
- Shoaei, Parham, Hamid Reza Musaei, Farinaz Mirlohi, S. Narimani zamanabadi, Farshad Ameri, and Nasrollah Bahrami. 2019. "Waste Ceramic Powder-Based Geopolymer Mortars: Effect of Curing Temperature and Alkaline Solution-to-Binder Ratio." *Construction and Building Materials* 227:116686. <https://doi.org/10.1016/j.conbuildmat.2019.116686>
- Silva, Guido, David Castañeda, Suyeon Kim, Alvaro Castañeda, Bruno Bertolotti, Luis Ortega-San-Martin, Javier Nakamatsu, and Rafael Aguilar. 2019. "Analysis of the Production Conditions of Geopolymer Matrices from Natural Pozzolana and Fired Clay Brick Wastes." *Construction and Building Materials* 215:633-43. <https://doi.org/10.1016/j.conbuildmat.2019.04.247>
- Singh, Smita, M. U. Aswath, and R. V. Ranganath. 2018. "Effect of Mechanical Activation of Red Mud on the Strength of Geopolymer Binder." *Construction and Building Materials* 177:91-101. <https://doi.org/10.1016/j.conbuildmat.2018.05.096>
- Tchakoute Kouamo, H., A. Elimbi, J. A. Mbey, C. J. Ngally Sabouang, and D. Njopwouo. 2012. "The Effect of Adding Alumina-Oxide to Metakaolin and Volcanic Ash on Geopolymer Products: A Comparative Study." *Construction and Building Materials* 35:960-69. <https://doi.org/10.1016/j.conbuildmat.2012.04.023>
- Thapa, V. B. and Waldmann, D. 2018. "A Short Review on Alkali-Activated Binders and Geopolymer Binders." Pp. 576-91 in *Vielfalt Im Massivbau - Festschrift Zum 65. Geburtstag von Prof. Dr. Ing. Jürgen Schnell*, Pahn M., Thiele C., Glock C. Berlin, Germany: Ernst & Sohn.
- Tuyan, Murat, Özge Andıç-Çakır, and Kambiz Ramyar. 2018. "Effect of Alkali Activator Concentration and Curing Condition on Strength and Microstructure of Waste Clay Brick Powder-Based Geopolymer." *Composites Part B: Engineering* 135(November 2016):242-52. <https://doi.org/10.1016/j.compositesb.2017.10.013>
- Van Jaarsveld, J. G. S., J. S. J. Van Deventer, and L. Lorenzen. 1998. "Factors Affecting the Immobilisation of Metals in Geopolymerized Flyash." *Metallurgical and Materials Transactions B: Process Metallurgy and Materials Processing Science* 29(1):283-91. <https://doi.org/10.1007/s11663-998-0032-z>
- Williams, Ross P., and Arie Van Riessen. 2010. "Determination of the Reactive Component of Fly Ashes for Geopolymer Production Using XRF and XRD." *Fuel* 89(12):3683-92. <https://doi.org/10.1016/j.fuel.2010.07.031>
- Yankwa Djobo, Jean Noël, Antoine Elimbi, Hervé Kouamo Tchakouté, and Sanjay Kumar. 2016. "Mechanical Properties and Durability of Volcanic Ash Based Geopolymer Mortars." *Construction and Building Materials* 124:606-14. <https://doi.org/10.1016/j.conbuildmat.2016.07.141>
- Ye, Nan, Jiakuan Yang, Sha Liang, Yong Hu, Jingping Hu, Bo Xiao, and Qifei Huang. 2016. "Synthesis and Strength Optimisation of One-Part Geopolymer Based on Red Mud." *Construction and Building Materials* 111:317-25. <https://doi.org/10.1016/j.conbuildmat.2016.02.099>
- Yip, C. K., G. C. Lukey, and J. S. J. Van Deventer. 2005. "The Coexistence of Geopolymeric Gel and Calcium Silicate Hydrate at the Early Stage of Alkaline Activation." *Cement and Concrete Research* 35(9):1688-97. <https://doi.org/10.1016/j.cemconres.2004.10.042>
- Zhang, Guoping, Jian He, and Robert P. Gambrell. 2010. "Synthesis, Characterisation, and Mechanical Properties of Red Mud-Based Geopolymers." *Transportation Research Record* (2167):1-9. <https://doi.org/10.3141/2167-01>
- Zhang, Peng, Yuanxun Zheng, Kejin Wang, and Jinping Zhang. 2018. "A Review on Properties of Fresh and Hardened Geopolymer Mortar." *Composites Part B: Engineering* 152(June):79-95. <https://doi.org/10.1016/j.compositesb.2018.06.031>
- Zheng, Lei, Wei Wang, and Yunchun Shi. 2010. "The Effects of Alkaline Dosage and Si/Al Ratio on the Immobilisation of Heavy Metals in Municipal Solid Waste Incineration Fly Ash-Based Geopolymer." *Chemosphere* 79(6):665-71. <https://doi.org/10.1016/j.chemosphere.2010.02.018> PMID:20304461

**Ali Abdulhasan Khalaf** finished his bachelor (2007) in Civil Engineering at Faculty of Engineering College, University of Basrah in Iraq and finished his master studies (2014) Master of Science in Engineering at Civil/ Environmental & Chemical Department, Faculty of Engineering School, Youngstown State University, Ohio, USA. Fields of study: Structures, construction materials and geotechnics. Since 2019 PhD student at Faculty of Civil Engineering, Budapest University of Technology and Economics. Research areas: geopolymers, cement-based materials, steel.

**Katalin Kopeckó** is associate professor at the Budapest University of Technology and Economics in Hungary. Graduated in Chemical Engineering (1990) and has postgraduate studies in Concrete Technology (2004). She has PhD degree since 2006. She teaches Chemistry for Civil Engineers (BSc); Material Science for Civil Engineers (MSc); and Alkali activated materials in Civil Engineering (PhD) subjects. Her research fields are: deterioration processes of construction materials, durability of concrete and other materials, cement hydration, diagnostics, mineralogical and microstructural analyses, X-ray diffraction (XRD), thermal analyses (TG/DTG/DTA), scanning electron microscopy (SEM). She is a member of the Hungarian Group of *fib* and of the Technical Committee MSZT/MB 102 (Cement and Lime) in the Hungarian Standards Institution.

## fib BULLETIN NO. 91

**Title:** Floating concrete structures

**Year:** 2019

**Pages:** 99

**Format approx.** DIN A4 (210x297 mm)

**ISBN:** 978-2-88394-133-5

### Abstract:

This bulletin is the first document prepared by TG 1.2 “Concrete structures in marine environments”. This theme is considered important for Commission 1, since in the future several applications are forecast in marine environments.

Floating concrete structures allow the use of marine spaces with important developments for urban areas, industrial plants, infrastructures and energy production. In this bulletin a series of applications, projects and conceptual ideas are presented. This should be considered as a document representing the potentialities and the innovations on the use of structural concrete in marine environmental.

The floating structure presented in the bulletin should be of inspiration for new application that will be developed in the nearly future, representing a challenge not only for structural designers, but also for administrations, construction companies and industrial entities.

The use of structural concrete is becoming essential in these kinds of applications, in terms of cost, durability and sustainability.

As Commission 1 chair, I'm very grateful to Tor Ole Olsen and to all members of WP 1.2.1 “Floating concrete structures” for having produced this document that I consider very interesting not only for the *fib* members, but also for concrete community.

## fib BULLETIN NO. 92

**Title:** Serviceability Limit State of Concrete Structures

**Year:** 2019

**Pages:** 209

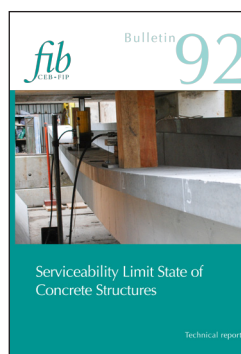
**Format approx.** DIN A4 (210x297 mm)

**ISBN:** 978-2-88394-135-9

### Abstract:

Serviceability limit states are essential for appropriate function and durability of concrete structures. The attention is paid especially to the stress limitation, crack width analysis and deflection analysis. The document provides supplementary information to the *fib* Model Code 2010 (MC2010), where a limited space did not allow for a detailed description of individual procedures. The principles used in MC2010 in chapter 7.6 are explained in detail within this document.

The stress analysis is focused on stresses in concrete and steel including the stress redistribution



due to the long-term load and cracking of reinforced concrete and prestressed concrete elements. Crack width analysis explains the mechanism of cracking under mechanical loading and due to deformation restraint. Cracks in prestressed concrete elements are also discussed. Deflection analyses with different levels of accuracy are described including the

shear effects.

Examples illustrate the practical application of rules defined in the MC2010 of individual serviceability limit states. Simplified and more general methods are used.

An important part of the bulletin shows the development and extension of the serviceability limit states after publishing of the MC2010 and alternative approaches. Special attention is paid to deflections of prestressed concrete beams, shear effects on deflection, slenderness limits and influence of the concrete cover. The final part deals with an application of numerical simulations.

## fib BULLETIN NO. 93

**Title:** Birth Certificate and Through-Life Management Documentation

**Year:** 2020

**Pages:** 90

**Format approx.** DIN A4 (210x297 mm)

**ISBN:** 978-2-88394-137-3

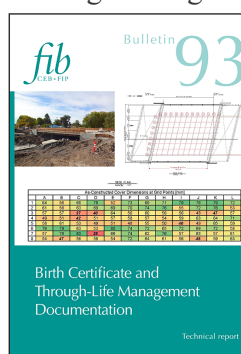
**DOI:** doi.org/10.35789/fib.BULL.0093

### Abstract:

While it is generally accepted by owners and users that vehicles such as airplanes or cars must be subjected to a pre-defined maintenance plan during their lifetime, this is less obvious in public opinion for engineering structures and buildings. This may

be related to the general feeling that “moving objects” should be more sensitive to aging and deterioration than “structures anchored in ground”! This may also relate to the fact that detailed maintenance manuals, which are considered obligatory by insurance companies, are generally for aircraft, boats and cars, but not systematically for civil engineering structures, except for iconic or major projects.

The performance-based approach to the durability design and assessment of concrete structures is also becoming increasingly popular in the construction sector. In recent years, numerous studies have been carried out worldwide in order to better assess the expected properties related to the durability of concrete. This has led to the standardization of test protocols, but also to a better understanding of the



main parameters impacting the overall durability of concrete. Documentation related to durability indicators will then become increasingly necessary for the accurate implementation of a performance-based approach that enables the promotion of sustainable materials.

Durability models have a strong need for relevant in-field data feedback in order to define accurate inputs for modelling both during the design process (gathered from previous projects) and during the follow-up process to allow for re-calibration of inputs and re-assessment of durability expectations by the models if judged necessary.

A framework for data collection was therefore considered extremely important by the fib Commission 8: Durability, and is the objective of this fib Technical report "Birth-certificate and Through-Life Management Documentation". It is indeed very important to collect relevant data within a comprehensive and standardized format, as now proposed by this fib Bulletin. Thanks to its pre-defined format, compatible with the general fib framework, "Birth-certificate and Through-Life Management Documentation" will definitively be useful to owners for the maintenance plan and intervention strategies of their assets.

This operational technical report will also be very useful for designers, as it should encourage the collection of relevant information in databases to be used for future projects where a realistic assessment of expected properties is considered through largely similar concrete mix designs under given exposure conditions.

The Commission, which deals with durability aspects, hopes that this Bulletin will provide users a valuable tool and perspective on service life management issues.

## **fib BULLETIN NO. 94**

**Title:** Precast concrete bridge continuity over piers

**Year:** 2020

**Pages:** 44

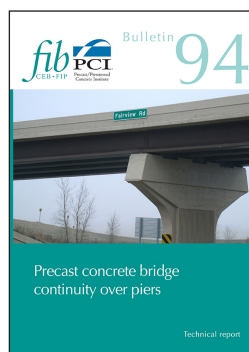
Format approx. DIN A4 (210x297 mm)

**ISBN:** 978-2-88394-139-7

**DOI:** doi.org/10.35789/fib.BULL.0094

### **Abstract:**

Concrete bridges are an important part of today's road infrastructure. An important part of those concrete bridges is to a large extent prefabricated. Precast concrete enables all the advantages of an industrialized process to be fully utilized. Contemporary concrete mixtures are used to realize high-strength bridge girders and piers that exactly meet the requirements set, both structurally and aesthetically, with a small ecological footprint. Sustainable and



durable! On the construction site, there is no need for complex formwork, the execution time is drastically reduced and where road, water and rail traffic on or under the bridge has to be temporarily interrupted, it is only minimally inconvenienced during the execution of the project.

There is a wide variety of prefabricated bridges. In 2004, the fib commission on prefabrication already published the Bulletin 29 *Precast concrete bridges* which, in addition to the history of prefabricated bridges, also gave an overview of the different bridge types and structural systems. This document elaborates on one specific structural system: the continuous bridge. Task Group 6.5 „Precast concrete bridges” discusses in detail how to achieve continuity over the piers with precast elements. This bulletin bundles the experiences of experts in the field of bridge design so that less experienced designers would be able to identify the points of attention and make a correct design. In addition to the theoretical considerations, the principles are tested against three realizations in the USA and Europe.

Commission 6 thanks the Co-Conveners Maher Tadros and Hugo Corres and all active members of the Task Group for sharing their knowledge and experience and for the successful realization of this bulletin.

## **fib BULLETIN NO. 95**

**Title:** Fibre Reinforced Concrete: From Design to Structural Applications.

Proceedings of the ACI-fib-RILEM International Workshop - FRC2018

**Year:** 2020

**Pages:** 539

Format approx. DIN A4 (210x297 mm)

**ISBN:** 978-2-88394-141-0

### **Abstract:**

The first international FRC workshop supported by RILEM and ACI was held in Bergamo (Italy) in 2004. At that time, a lack of specific building codes and standards was identified as the main inhibitor to the application of this technology in engineering practice. The workshop aim was placed on the identification of applications, guidelines, and research needs in order for this advanced technology to be transferred to professional practice.

The second international FRC workshop, held in Montreal (Canada) in 2014, was the first ACI-fib joint technical event. Many of the objectives identified in 2004 had been achieved by various groups of researchers who shared a common interest in extending the application of FRC materials into the realm of structural engineering and design. The aim of the workshop was to provide the State-of-the-Art on the recent progress that had been made in term of specifications and actual



applications for buildings, underground structures, and bridge projects worldwide.

The rapid development of codes, the introduction of new materials and the growing interest of the construction industry suggested presenting this forum at closer intervals. In this context, the third international FRC workshop was held in Desenzano (Italy), four years after Montreal. In this first ACI-*fib*-RILEM joint technical event, the maturity gained through the recent technological developments and large-scale applications were used to show the acceptability of the concrete design using various fibre compositions.

The growing interests of civil infrastructure owners in ultra-high-performance fibre-reinforced concrete (UHPFRC) and synthetic fibres in structural applications bring new challenges in terms of concrete technology and design recommendations. In such a short period of time, we have witnessed the proliferation of the use of fibres as structural reinforcement in various applications such as industrial floors, elevated slabs, precast tunnel lining sections, foundations, as well as bridge decks. We are now moving towards addressing many durability-based design requirements by the use of fibres, as well as the general serviceability-based design. However, the possibility of having a residual tensile strength after cracking of the concrete matrix requires a new conceptual approach for a proper design of FRC structural elements.

With such a perspective in mind, the aim of FRC2018 workshop was to provide the State-of-the-Art on the recent progress in terms of specifications development, actual applications, and to expose users and researchers to the challenges in the design and construction of a wide variety of structural applications.

Considering that at the time of the first workshop, in 2004, no structural codes were available on FRC, we have to recognize the enormous work done by researchers all over the world, who have presented at many FRC events, and convinced code bodies to include FRC among the reliable alternatives for structural applications. This will allow engineers to increasingly utilize FRC with confidence for designing safe and durable structures.

Many presentations also clearly showed that FRC is a promising material for efficient rehabilitation of existing infrastructure in a broad spectrum of repair applications. These cases range from sustained gravity loads to harsh environmental conditions and seismic applications, which are some of the broadest ranges of applications in Civil Engineering.

The workshop was attended by researchers, designers, owner and government representatives as well as participants from the construction and fibre industries. The presence of people with different expertise provided a unique opportunity to share knowledge and promote collaborative efforts. These interactions are essential for the common goal of making better and sustainable constructions in the near future.

The workshop was attended by about 150

participants coming from 30 countries. Researchers from all the continents participated in the workshop, including 24 Ph.D. students, who brought their enthusiasm in FRC structural applications.

For this reason, the workshop Co-chairs sincerely thank all the enterprises that sponsored this event. They also extend their appreciation for the support provided by the industry over the last 30 years which allowed research centers to study FRC materials and their properties, and develop applications to making its use more routine and accepted throughout the world. Their important contribution has been essential for moving the knowledge base forward.

Finally, we appreciate the enormous support received from all three sponsoring organizations of ACI, *fib* and Rilem and look forward to paving the path for future collaborations in various areas of common interest so that the developmental work and implementation of new specifications and design procedures can be expedited internationally.

## *fib* BULLETIN NO. 96

**Title: Guidelines for Submerged Floating Tube Bridges.**

Guide to good practice

**Year: 2020**

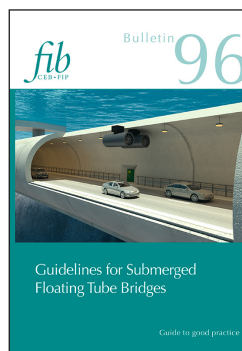
**Pages: 119**

Format approx. DIN A4 (210x297 mm)

**ISBN: 978-2-88394-143-4**

### **Abstract:**

This bulletin is a guidelines document for “Submerged Floating Tube Bridges”, that represents an innovation in Marine Concrete Structures. This theme is considered important for Commission 1 since in the future several applications are forecast in marine environments.



Submerged Floating Tube Bridges are a solution that can be proposed to solve different problems in passing water constrains as lakes and fiords, reducing the impact and allowing several economic advantages.

The guidelines certainly will boost the application of Submerged Floating Tube Bridges since the document is useful not only for designers but also for construction companies, owners and public administrations.

As guidelines, the bulletin gives wide information on the design, construction and management of these structures, allowing all the users to be confident in promoting the use of Submerged Floating Tube Bridges.

As Commission 1 Chair, I'm very grateful to Arianna Minoretti and to all members of WP 1.2.2 "Submerged Floating Tube Bridges", for having produced this document that I consider very interesting not only for the *fib* members but also for the concrete community.



 **A-HÍD**

**CREATE THE FUTURE**

A-Híd Zrt. | 1138 Budapest, Karikás Frigyes u. 20. | [www.ahid.hu](http://www.ahid.hu)

National Competitiveness and Excellence Program, Subprogram B: National Program for Materials Science and Technology  
Hungarian Research Grant NVKP\_16-1-2016-0019

**“Development of concrete products with improved resistance to chemical corrosion, fire or freeze-thaw”.**

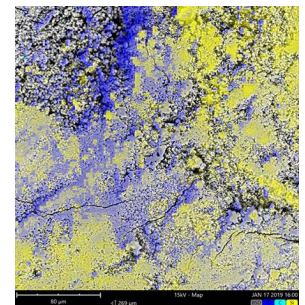
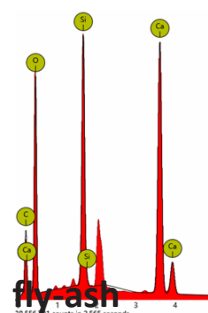
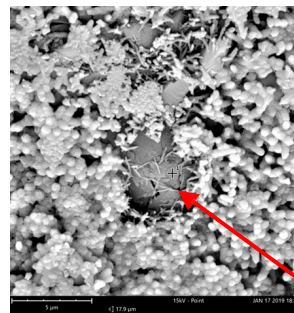
Procurement of laboratory equipment within the framework of the tender entitled

**Project supervisor: Prof. György L. Balázs**

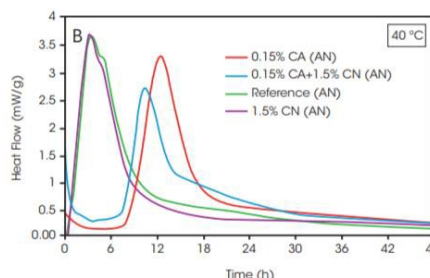
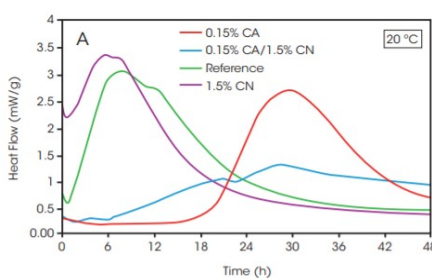
Project sub-theme responsables: Dr. Éva Lublóy, Dr. Salem G. Nehme, Dr. Katalin Kopecskó

## MATERIAL SCIENTIFIC STUDIES FROM NANO-LEVEL TO MACRO-LEVEL

- 1. PHENOM XL Scanning Electron Microscope (SEM) with elemental analysis of EDS**  
(energy dispersive X-ray spectroscopy) for small and large (max. 100 mm x 100 mm) samples



- 2. TAM Air 3+3 channel microcalorimeter, with 125 ml ampoules, application range: from cement paste to concrete**



- 3. Zetasizer Nano ZS – Measurement of Zeta potential with titrator (variable pH range)**  
3,8 nm – 100 μm, particle size distribution in range 0,3 nm – 10 μm

